Nano-scale surface analysis of ultra-thin silicon oxide layers hetero-epitaxially grown on a rutile titanium dioxide with improvement of water hydrophilicity

by

LE TRAN UYEN TU

Submitted to

Japan Advanced Institute of Science and Technology

In partial fulfillment of the requirements

For the degree of

Doctor of Philosophy

Supervisors: Professor Dr. Masahiko Tomitori

School of Materials Science

Japan Advanced Institute of Science and Technology

December, 2013

Referee in Chief:

Professor Masahiko Tomitori

Japan Advanced Institute of Science and Technology

Referees:

Professor Tatsuya Shimoda

Japan Advanced Institute of Science and Technology

Professor Goro Mizutani

Japan Advanced Institute of Science and Technology

Professor Susumu Horita

Japan Advanced Institute of Science and Technology

Professor Toshiaki Taniike

Japan Advanced Institute of Science and Technology

Professor Hiroshi Onishi

Kobe University

ACKNOWLEDGEMENTS

First and foremost, I wish to express my deepest appreciation to my Ph.D. supervisor, Prof. Masahiko Tomitori. With his enthusiasm, inspiration, and great efforts, he continuously teaches, advises and supports me during my working periods under his supervision. His advice and encouragement regarding this research are invaluable to me.

I would like to thank my internal committee members, Prof. Tatsuya Shimoda, Prof. Goro Mizutani, Prof. Susumu Horita, and Prof. Toshiaki Taniike from School of Materials Science, JAIST. My special thanks go to Prof. Hiroshi Onishi from Kobe University as an external committee. I thank all of them for their time and consideration in serving on my thesis committee.

Also my great respect and thankfulness address to Prof. Tatsuya Shimoda and his lab members, especially Mr. Kazuhiko Fukada, for welcoming and supporting me to complete my minor research and Mr. Hirose Daisuke for kindly helping in simulation.

I also wish to acknowledge Japanese and Vietnamese Professors who have supported me with fundamental and advanced knowledge about a modern science, nano science and technology.

Special thanks go to my lab members, Assist. Prof. Akira Sasahara, Mrs. Hashimoto Miho, Miss. Tatsumi Hitomi, Mr. Tetsuya Yoshi, Mr. Amer Hassan Mahmoud, Mr. Makoto Nogami, Mr. Tomoaki Miyagi and so on for their camaraderie throughout my graduate school experience, especially for all of the hours of interesting we have shared.

I am thankful to the following organizations, The Ministry of Education and Training of Vietnam, Japan Advanced Institute of Science and Technology, and Hue University of Sciences, for their financial support during my study in Japan.

Finally, my deepest thanks are to my parents, my family and relative for their selfless love, understanding, and support me all the time. I thank my husband and my lovely son very much for their love, patience, and support.

Last but not least, thank you for all you have done for me.

JAIST, Nomi, Ishikawa, Japan

December 2013

Le Tran Uyen Tu

Contents

Chapter 1

INTRODUCTION

1.1 Historical background

In the current material science and technology, metal oxides play key roles because of their variety and unique features suitable for electronic devices and catalysts. A variety of the properties of metal oxides originate from their compositional diversity and complexity. Thus, scientific insights into their features are fundamentally needed to improve the performance of the devices and catalysts utilizing the metal oxides in many fields. In particular, surface scientific approach is crucial to study atomic phenomena on metal oxide surfaces. The obtained knowledge is useful for applications to catalysis, gas sensors, photo-electrolysis, and transparent semiconducting films. The phenomena on metal oxide surfaces, however, are less understood than those on metal surfaces. The real surfaces of metal oxides are easily deviated from the stoichiometry of bulk, exhibiting high surface reactivity. In addition, since most of their features are deeply linked to the insulating properties of metal oxides, the conventional surface analytical techniques utilizing electron beam or ion beam incident on the surface cannot fully be applied owing to electric charges induced on it with the beam. Further difficulty in understanding of metal

oxide lies in their dynamic nature. Hence, there are still many issues on metal oxides under debate.

Among a tremendous number of metal oxides, titanium dioxide (TiO_2) has been widely known as one of fascinating materials with expansive applications in industries at low-cost and environmentally friendly, commonly found in minerals, and a research target as a model system of metal oxides in surface science. In particular, a rutile TiO_2(110) surface is regarded as a standard model in surface science, because a large-size single crystal wafer of high quality is commercially available with the most stable crystalline plane of (110), and it has been well characterized using a wide-range of surface analytical techniques through surface cleaning procedures. The cleaning procedures including the cycles of Argon ion sputtering and annealing in ultra-high vacuum (UHV) reduce the TiO_2, providing a semiconducting nature. Consequently, the charging problem is not a significant obstacle to carry out the conventional surface analysis on it. Up to now, x-ray photoelectron spectroscopy (XPS), low energy electron diffraction (LEED), Auger electron spectroscopy (AES), low energy ion scattering (LEIS), electron stimulated desorption technique (ESD), and static secondary ion mass spectrometry (SIMS) have often been applied to analyze the rutile TiO_2(110) surface. Those analyses showed the chemical composition and states of them, including the relaxation and reconstruction as well as molecular adsorption on them, such as hydrogen, oxygen, water molecules, and others [1-8].

Furthermore, scanning tunneling microscopy (STM) has greatly contributed to reveal their features on a nanoscale: in 1995 Onishi et al. reported the atomic-scale STM images

of a rutile TiO_2(110)-(1×1) surface. The STM images successfully depicted unoccupied surface states localized on individual fivefold (5f) coordinated Ti^{4+} atoms [1], which were forming regular ridges along the [001] direction, depicted as bright rows in STM images. This report indicated that there were bright spots on dark rows, corresponding to bridging oxygen rows [9]. Several years later Wendt et al. showed that an oxygen vacancy was depicted darker than a hydroxyl group on the bridging oxygen rows in the STM images [10]. The results were further confirmed by the density-of-state (DOS) on the TiO_2(110)-(1×1) surface calculated by Diebold et al. [11]. Subsequently, Xu et al. recognized using STM that the phase transition from the (1×1) to the (1×2) structure could be caused by oxygen desorption, while the oxygen diffusion from bulk to surface led to the transformation from the (1×2) to the (1×1) structure [12]. It is noted that the STM usually depicts the Ti rows clearly, which have the high density of empty states, and thus, tunneling electrons pass from an STM tip into them, although the bridging oxygen rows with the low density are observed just as dark rows in a stable manner on the STM imaging.

Meanwhile, frequency modulation atomic force microscopy (FM-AFM) was developed, the principle of which is similar to the STM but utilizes the force between a tip and a sample, and successfully demonstrated to observe insulating sample surfaces with atomic resolution. The FM-AFM was able to visualize bright rows composed of the topmost oxygen atoms, i.e., the bridging oxygen rows, along the [001] direction on the rutile TiO_2(110)-(1×1) surface, and dark single oxygen vacancies in their rows [13-16].

The atomistic pictures of the rutile TiO_2(110)-(1×1) surface prepared in UHV have progressively been constructed experimentally.

Here it should be mentioned that theoretical studies have significantly contributed to understand the features of TiO_2(110)-(1×1) surface. Many of them provided overviews on the atomic and electronic structures involving surface defects and the relaxation as well as the adsorption of hydrogen, oxygen, and water molecules on it, and reconstruction phases [17-19]; those were stimulated by experimental studies accumulated on it. Moreover, the mechanism of empirical phenomena such as the interaction with aqueous solution on it was also examined [20, 21].

Conversely, fully oxidized TiO_2 surfaces have not been examined thoroughly, while a large number of researches were conducted for reduced TiO_2 surfaces annealed in UHV. Noted that the reduced TiO_2 surface can be partially restored to the chemical stoichiometry through annealing procedures in oxygen gas, leaving the electric conductivity in bulk [22]. Meanwhile, for the first time, in 2005, Nakamura et al. investigated the smoothness and stability of the rutile (100) and (110) surfaces, which were oxidized thoroughly by annealing in air after doping with Nb oxide at 0.05 wt%, which provided the conductivity [22]. AFM and LEED were used to observe the morphology and the order of its surface structure. The AFM images showed clear terrace and step structures over a wide scanning region with a shape intense (1×1) LEED pattern. The authors concluded that the air-annealed TiO_2 surfaces were stable enough in aqueous solution, contrary to the instability of surfaces prepared by the ion sputtering and annealing in UHV. A similar conclusion was

obtained by observing a TiO_2(100) surface annealed in air with the FM-AFM operated in water, reported by Sasahara et al. in 2010 [23]. At present we have attained to a new stage of surface analysis for insulating materials with atomic resolution by the FM-AFM.

From a viewpoint of application, one of the most prominent features of TiO_2 is a photocatalyst, which splits water into hydrogen and oxygen under sunlight and produces electric energy, and decomposes hydrocarbons over the surface. The photo-catalytic activity of rutile TiO_2(110) surface have remarkably been investigated [11, 24-26]; many of the studies indicated that the surface reactivity was related to the vacancies in the bridging oxygen rows. Fujishima et al. shed light on two types of photo-induced phenomena on a TiO_2 surface in their review paper [24]: one is the photo-catalysis, and the other is super-hydrophilicity under ultraviolet (UV) light; completely spreading of a water droplet over the surface with a contact angle of ~0° under UV light. This was explained as follows: when UV light incident on the TiO_2 surface can generate a lot of pairs of an electron and a hole, the electrons react with molecular oxygen to produce super-oxide radical anion (O_2^-), and the holes react with water to produce hydroxyl (OH^+) radicals. The two types of reactive radicals work together to decompose and remove organic compounds covering the surface with help of water, resulting in the super-hydrophilicity. On the other hand, Yates et al. pointed out that the second order recombination of an electron-hole pair was dominant to the photo-desorption rate of organic compounds [25]. An exciton produced by absorption of a photon is followed by charge separation of an electron-hole

pair. The charge transport to the surfaces led by two processes induces desirable reduction and oxidation reactions at the surface, resulting in O_2^- and hydroxyl radicals.

The photo-induced hydrophilicity was historically discovered at a laboratory of TOTO Ltd. in 1995. They explained it in a different way: the photo-generated electrons tend to reduce the Ti^{4+} cations at the surface to Ti^{3+} state, and the holes oxidize the O^{-2} anions to O^- state, leading to ejection of oxygen atoms by weakened chemical bond of TiO_2 at the surface, and to formation of oxygen vacancies. Water (H_2O) molecules can then be decomposed into H and OH at the oxygen vacancies, and OH groups are adsorbed at the vacancies, which tend to make the surface hydrophilic through hydrogen bonding between the OH groups and water molecules around them [11, 26, 27]. Hence, the TiO_2 prepared by sputtering and annealing processes in UHV, inducing oxygen vacancies, likely exhibits the super-hydrophilicity. To the contrary, an air-annealed TiO_2 surface showed less hydrophilicity when the stoichiometry of surfaces is maintained with less oxygen vacancies, i.e., terminated mostly with oxygen atoms [23].

On the one hand, the photo-induced super-hydrophilicity of TiO_2 rapidly vanishes when the surface is stored in dark [28-31]. To overcome this drawback, TiO_2-based hyrdophilicity without UV light irradiation has been explored: the treatment of TiO_2 by air plasma [31], or mixing SiO_2 to TiO_2 is promising to extend the lifetime of the hydrophilicity in dark, which is previously activated with UV light irradiation [31-33]. The mixing of SiO_2 can also provide the hardness and durability to the TiO_2 surfaces, which are beneficial for self-cleaning and anti-fog coating of mirrors used in the open air. The

layers of SiO_2 on TiO_2 substrates have been fabricated using a range of different techniques, including sol-gel dip coating, evaporation-induced self-assembly using dip-coating, electrochemical deposition, and ion milling [31-33]. In sol-gel method, several successive studies agreed with the conclusion obtained by Machida et al. that the super-hydrophilicity of TiO_2 system was improved by adding SiO_2 into TiO_2 films. This might be attributed to suppression of the phase transformation from anatase to rutile structure or of the size-growth of particle during annealing process [34]. On the other hand, Guan et al. recognized that the minor formation of complex oxides as the bond Ti-O-Si changed the surface acidity. This means that the electron pair acceptor accelerating in the topmost layer due to Ti-O-Si formation increased the number of hydroxyl groups on the surface, resulting in maintaining the hydrophilicity [35, 36]. In addition, the bonding energy of Si-OH are known to be more stable than Ti-OH. These results coincided with results reported by Nakamura and others [36-38]. Nevertheless, most of the techniques could not avoid film inhomogeneity on a nano-scale to clarify the reason why adding SiO_2 enhanced the super-hydrophilicity. Barranco et al. at first analyzed surface compositions of a SiO_2 layer on a TiO_2(110) surface prepared by evaporation in UHV from silicon monooxide powder [38]. The chemical shift of Si-O component was estimated through the XPS spectra of Si. Abad et al. evaluated the deposition of Si onto the TiO_2(110)-(1×2) surface using AES and STM. The positive shift of the Si XPS peak with the increase of the Si coverage was attributed to the formation of less oxidized species SiO_x ($1<x<2$). However, no ordered structure was observed for the SiO_x layer by STM. In 2010, the group in our laboratory investigated a

SiO_x layer grown on a single crystal rutile TiO_2(100) substrate using a vapor phase method; during annealing process in air, the TiO_2 substrate was being stored in a quartz container, which acted as a Si-O source [39]. The results analyzed by LEED, XPS and FM-AFM indicated that the SiO layer was hetero-epitaxially grown on the TiO_2 substrate in an atomically well-ordered manner, resulting in the surface phase transition from (1×1) to (3×4) of the LEED pattern. It is notable that the vapor phase hetero-epitaxial growth of silicon oxide on the TiO_2(100) surface can form a well-ordered surface structure, and seems to be a promising approach for understanding of the SiO_2/TiO_2 system with the ordered surface structure.

To summarize the historical background mentioned above, the atom-scale surface analysis of metal oxides, in particular, rutile TiO_2, has rapidly developed, and TiO_2 has attracted much interest because of a model system of metal oxides and of its prominent photo-induced chemical reactivity. The hybrid metal oxide systems, such as TiO_2-SiO_2, has inspiring potential to open novel applications of materials, but there are many unsettled issues on the metal oxides from a viewpoint of material science; it is keenly expected to reveal the mechanism of their fascinating phenomena fully using surface analytical methods by combining with sample preparation methods to prepare well-defined surfaces of metal oxides.

1.2 Motivation.

To date, well-characterized TiO_2 surfaces have been obtained by preparation methods involving the processes in UHV, and various informative studies were reported on photocatalytic reaction and adsorbed molecules on the TiO_2 surfaces. Nevertheless, understanding of superior properties of TiO_2 in practical use has not yet been sufficient because of the difference between the surfaces well characterized in UHV and the surfaces in practical use as well as its polymorphism, complex native defects and extrinsic impurities. To clarify the properties in practical use, it is indispensable to prepare the most suitable surface of a sample well-defined for the purpose, to characterize it, and to discuss the phenomena found under control experiments.

In this study the rutile TiO_2(110) surfaces are focused, and the sample is annealed in air at about 1000 °C as the surface preparation method. It is noted that a sapphire container was utilized for the first time as an annealing environment in air, which is expected to steadily oxidize the surfaces to decrease the number of vacancies in the bridging oxygen rows as well as to remove extrinsic impurities as oxidized evaporants from the environments. An ideal stoichiometric rutile TiO_2(110) surface has been subject to debate, which should contain simultaneously two kinds of titanium atoms in different states as well as oxygen atoms, on which bridging oxygen anion occupy in the topmost. Because of under-saturated coordination of bridging oxygen, atoms from these rows are through to be removed relatively easily by thermal excitation. The induced point defects affect the overall chemistry of surface through the oxygen vacancies, resulting in the super-hydrophilicity.

Moreover, a disagreement arose for the adsorption of the water molecules on the rutile (110) face, which is still a matter of controversy [40, 41]: some authors found spontaneous dissociation, while others agreed with molecular adsorption mechanism. Thus, further experimental researches focusing on mechanism of adsorbed water on the rutile TiO_2(110) are necessary as a background for more understanding of wettability on composite systems based on TiO_2 substrates.

Here, referring to Sasahara's discovery of the silicon oxide ultra-thin layer grown on the rutile TiO_2(100) surface by annealing in air stored in a quartz container [39], two annealing procedures are adopted for the control experiment on the rutile TiO_2(110) surface as a model system: annealed in the quartz container as a SiO vapor source and in a sapphire container with no vapor. Since the silicon oxide layer was hetero-epitaxially grown on the rutile TiO_2(100) surface, the growth on the rutile TiO_2(110) surface is examined using XPS, LEED, and FM-AFM operated in water. This is also a first step to confirm whether the method to grow a single crystal oxide layer on a crystal can be extended to other system or not.

One of representative benefits of this system prepared in this study is to reveal the mechanism of the super-hydrophilicity of SiO_2/TiO_2; it is still in dispute. To my knowledge, there have been few reports on not only experimental but also theoretical results to approach it, plausibly due to the absence of a method to prepare a well-ordered surface of SiO_2/TiO_2 to give a decisive clue for it. The change in water wettability on the surfaces is characterized through water contact angle measurements, and the correlation

among the contact angle, the morphology and chemical composition is discussed. An atomistic model of the grown layer to explain the change in the water wettability is proposed. This possibly leads to revealing the photo-induced super-hydrophilicity of TiO_2 and related material systems.

1.3 Outline.

This thesis describes the work done in my PhD course at School of Materials Science, Japan Advanced Institute of Science and Technology. It consists of six chapters, and the contents of the thesis is as follows:

Chapter 1: **Introduction**. The historical background of studies of TiO_2 and SiO_2/TiO_2 composite system is concisely described as well as the motivation from my standpoint with future prospect of this study, and the outline of this thesis.

Chapter 2: **Rutile titanium dioxide and silicon dioxides**. The atomic structures and prominent properties as well as the interaction of TiO_2 and SiO_2 surfaces with aqueous solution are described. The properties of SiO_2/TiO_2 composite systems are also discussed.

Chapter 3: **Experimental procedures**. The experimental procedures of sample preparation as well as the analytical methodology used in this study are described.

Chapter 4: **Structural and compositional analysis of silicon oxide layers on rutile TiO_2(110)**. The surface composition and atomic arrangement of silicon oxide layers grown on the rutile TiO_2(110) surfaces are described. An atomistic model of the silicon oxide layer grown on a rutile TiO_2(110) surface is proposed.

Chapter 5: **Water wettability of silicon oxide layers on rutile TiO_2(110)**. The water wettability of an intrinsic rutile TiO_2(110) surface and the hydrophobic-hydrophilic conversion of silicon oxide layers on the TiO_2(110) are described together with the effect of UV irradiation on the water wettability.

Chapter 6: **Summary**. The general summary of this study is given, followed by an outlook at the future prospect and unsettled issues of super-hydrophilicity of TiO_2 systems and the applications of hetero-epitaxial growth of silicon oxide on TiO_2 surface.

References

[1] H. Onishi et al., Bull. Chem. Soc. JPN., 68, 1995, 2447.

[2] A. N. Shultz et al., Sur. Sci., 339, 1995, 114.

[3] S. Suzuki, K. I. Fukui, H. Onishi, Y. Iwasawa, Phys. Rev. Let., 84, 2000, 10.

[4] J. M. Pan et al., J. Vac. Sci. Techno. A., 10, 1992, 4.

[5] G. Charlton et al., Phys. Rev. Let., 78, 1997, 3.

[6] P. Karmakar, G. F. Liu, J.A. Yarmoff, Phys. Rev. B, 76, 2007, 193410.

[7] M. B. Hugenschmidt, L. Gamble, C. T. Campbell, Sur. Sci., 302, 1994, 329.

[8] S. Fischer et al., J. Vac. Sci. Technol. B, 14, 1996, 961.

[9] E. Asiri, R. Souda, Sol. Sta. Com., 129, 2004, 15.

[10] Wendt et al., Sur. Sci., 598, 2005, 226.

[11] U. Diebold, Surf. Sci. Rep. 48, 2003, 53.

[12] C. Xu, X. Lai, G. W. Zajac, D. W. Goodman, Phys. Rev. B., 56, 1997, 20.

[13] K. I. Fukui, H. Onishi, Y. Iwasawa, Phys. Rev. Let., 79, 1997, 21.

[14] C. L. Pang, H. Raza, S.A. Haycock, G. Thornton, Appl. Sur. Sci., 157, 2000, 233.

[15] M. Ashino et al., Appl. Sur. Sci., 157, 2000, 212.

[16] A. Yurtsever, Y. Sugimoto, M. Abe, S. Morita, Nanotechnol., 21, 2010, 165702.

[17] K. O. Ng, D. Vanderbilt, Phys. Rev., 56, 1997, 16.

[18] A. T. Paxton, L. T. Nga, Phys. Rev., 57, 1998, 3.

[19] M. Ramamoorthy, D. Vanderbilt, Phys. Rev. B, 49, 1994, 23.

[20] L. Vernon, S. D. Kenny, R. Smith, E. Sanville, Phys. Rev. B, 83, 2011, 075412.

[21] A. A. Skelton, T. R. Walsh, Mole. Sci., 33, 2007, 379.

[22] R. Nakamura et al., J. Phys. Chem. B, 109, 2005, 5.

[23] A. Sasahara and M. Tomitori, J. Vac. Sci. Technol. B, 28, 2010, 3.

[24] A. Fujishima, T. N. Rao, D. A. Tryk, J. Photo-chem. Photo-bio. C, Rev., 1, 2000, 1.

[25] J. T. Yates, Sur. Sci., 603, 2009, 1605.

[26] M. A. Henderson, Langmuir, 12, 1996, 5093.

[27] T. Zubkov, J. T. Yates et al., J. Phys. Chem. B, 109, 2005, 15454.

[28] J. M. White, J. Szanyi, M. A. Henderson, *J*. Phys. Chem. B, 107, 2003, 9029.

[29] N. Ohtsu, N. Masahashi, Y. Mizukoshi, K. Wagatsuma, Langmuir, 25, 2009,11586.

[30] N. Ishida, D. Fujita, J. Vac. Sci. Technol. A, 30, 2012, 051402.

[31] M. Machida, K. Norimoto, T. Watanabe, K. Hashimoto, A. Fujishima, J. Mater. Sci., 34, 1999, 2569.

[32] K. Gan, B. Lu, Y. Yin, Sur. & Coat. Tech., 173, 2003, 219.

[33] M. Jarn, Q. Xu, M. Linden, Langmuir, 26, 13, 2010, 11330-11336.

[34] M. Machida, K. Norimoto, T. Watanabe, J. Mater. Sci., 34, 1999, 2569.

[35] K. Guan, B. Lu, Y. Yin, Sur. Coat. Technol., 173, 2003, 219.

[36] K. Guan, H. Xu, B. Le, Trans. Nonferrous Met. Soc. China, 14, 2004, 2.

[37] M. Nakamura, M. Kobayashi, N. Kuzuya, T. Komatsu, T. Mochizuka, Thin solid films, 502, 2006, 121.

[38] A. Barranco, F. Yubero, J. A. Mejı´as, J. P. Espino´s, A. R. Gonza´lez-Elipe, Surf. Sci., 482-485, 2001, 680.

[39] A. Sasahara, C. L. Pang, M. Tomitori, J. Phys. Chem. C, 114, 2010, 20189.

[40] M. Menetrey, A. Markovits, C. Minot, Surf. Sci., 524, 2003, 49.

[41] A. S. Barnard, P. Zapol, L. A. Curtiss, J. Chem. Theory Comput., 1, 2005, 107.

CHAPTER 2

RUTILE TITANIUM DIOXIDE AND SILICON DIOXIDE

During the last decades, there has been a shift in target systems that surface scientists enthusiastically investigated: whereas the initial focus was predominantly on metals and semiconductors, there is an upward trend on metal-oxide surfaces. A driving force for metal-oxide surfaces, in general, has come from their variety and unique features, which open many important applications [1-3]. Progressive insights into their surface properties on the fundamental level will help to improve the material characteristics and device performance of metal oxides in many fields.

Among metal oxides, titanium dioxide (TiO_2) has fascinating properties as a photo-catalyst to typically dissociate water, and has intensively been explored as a model of oxides with rapidly increasing interest and applications [4-5]. On one hand, the combination with other oxides such as silicon dioxide (SiO_2) on it has expanded their applications by providing novel features; the heterogeneous oxide films have a wide range of benefits and complexities, which should be revealed in regard to fundamental physics and chemistry, for applications such as self-cleaning, anti-fogging, and photo induced super hydrophilic properties [6-7]. Those applications have widely been used in practice, especially for the automobile's exterior rear view mirrors. However, general understanding of the properties is still controversial, because the surfaces and interfaces of SiO_2/TiO_2 composite systems used for the application are complicated in terms of their atomic structure and electronic states. To reveal their properties, well-ordered heterogeneous oxide films should be prepared and analyzed from atomistic point of view.

In general, the inherent compositional and structural inhomogeneity of oxide surfaces makes the issue extremely difficult in identifying the essential properties for their functions. In addition, the insulating or semi-insulating properties often refuse the use of electron beam techniques for characterization. This problem can be overcome using scanning probe microscopy (SPM) with a fine needle probe (tip) that is scanned over a surface. The use of tunneling current passing or force working between the probe and a sample, or light through an aperture in the probe allows us to observe the topography and to measure the properties of the fascinating oxide surfaces and interfaces.

2.1 Rutile titanium dioxide – TiO_2

Titanium dioxide was discovered in 1791 when chemist William Gregor examined sand from the local river. He used a magnet to extract ilmenite ($FeTiO_3$), from which he removed iron by treatment with hydrochloric acid. The residue was the impure oxide of a new element. In 1795, German M. H. Klaproth also independently discovered titanium dioxide [8, 9]. Since then, titanium dioxide has attracted much interest in many research groups due to its fascinating and unique characteristics, opening novel industrial application. Titanium dioxide is used as heterogeneous catalysis [1, 4], as photocatalyst [5] for waste water treatment, in biocompatible implants [10], in solar cells for the production of hydrogen and electric energy [4, 5], in gas sensors, and for optical coating.

Titanium dioxide minerals are found in three different crystalline forms; rutile, anatase, and brookite. Brookite transforms into rutile at low temperature [1]. Consequently, only rutile and anatase have been studied and play a role in applications of TiO_2. Rutile, the thermodynamically most stable phase, is focused in this study. The bulk structure of rutile

with tetragonal unit cell is shown in Fig. 2.1 [11]. Although the structures of rutile and anatase appear very different, their building blocks, distorted TiO_6 octahedra, are similar, where each Ti^{4+} ion is surrounded by an octahedron of six O^{2-} ions [1, 11-15]. In the rutile structure, each octahedron is in contact with ten neighbor octahedra; two by edges and eight by corners. The chains of edge-sharing octahedral lie along the [001] direction, and adjacent octahedral on different chains share corner [15]. The octahedron in rutile is not regular, showing a slight orthorhombic distortion.

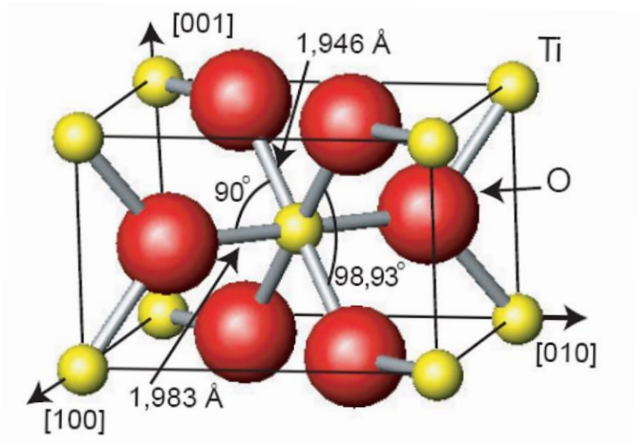

Figure 2.1. The primitive unit cell of bulk rutile TiO_2 [11].

The bond lengths between Ti and O atoms are 1.946 Å and 1.983 Å for the four-fold symmetric and two-fold symmetric bonds, respectively. In the crystal, the octahedra are stacked with their long axis alternating by 90°, resulting in three-fold coordinated O atoms [15]. Stoichiometric rutile TiO_2 is a transparent yellow non-conducting crystal, which turns black blue upon reduction of the bulk [12]. On the other hand, the bulk contains defects that might migrate to the surface, which should also be considered.

The fully oxidized compound, rutile TiO_2 has a wide band-gap of ~3 eV and therefore it is an insulator at room temperature. Fig. 2.2 shows the theoretically calculated density of states (DOS) of the oxygen 2p and the Ti 3d orbitals arising from the non-negligible covalent

character in TiO_2 [16, 17]. The valence band is based predominantly on O 2p orbitals, while the conduction band is Ti 3d based [16].

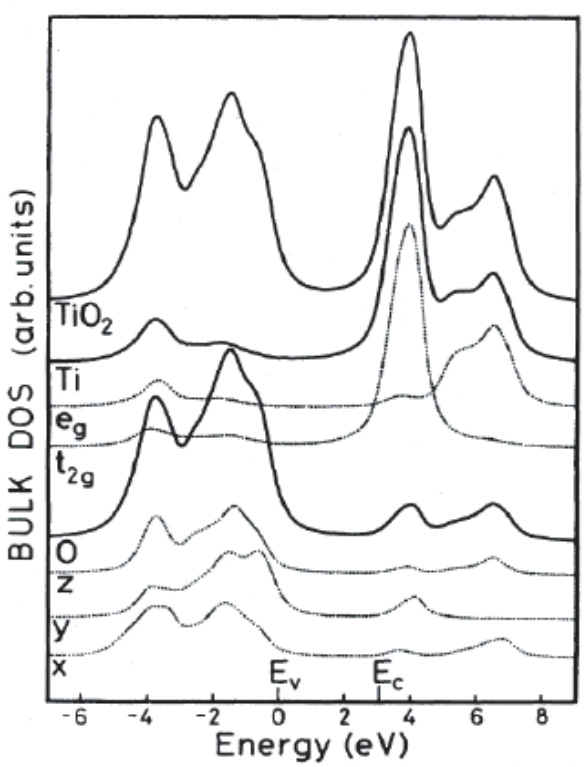

Figure 2.2. The density of states (DOS) of bulk TiO_2. The DOS is decomposed into partial Ti and O density of states, and their respective sub-bands with different symmetry [16].

However, under UHV condition the oxide is reduced mildly so that oxygen vacancies are present, donor states appear in the band gap region and the electrical conductivity increases dramatically [18, 19]. The optical properties depend strongly on the density of oxygen vacancies as well. A fully oxidized crystal is transparent, but with increasing concentration of oxygen vacancy it gradually becomes yellow, light blue, dark blue and finally completely black. Although these changes are dramatic and clearly visible, the change in composition associated with them is very small [19].

2.2 Properties of TiO_2 surface

2.2.1 Geometric structure of rutile TiO_2(110) surface

On the surfaces of TiO_2 the octahedral is truncated in various ways, giving rise to patterns of atomic coordination at surfaces differing from that in the bulk. Among the low-index surfaces, rutile has three main crystal faces: (110), (100), and (001). The (110) and (100) surfaces are quite stable and are thus considered to be important for practical applications [20]. The (110) surface, as shown in Fig. 2.3, is the most stable with the surface energy of 30.7 and 15.6 meV/(a.u.^{2}) for unrelaxed and relaxed, respectively. This is evidenced by the fact that it has the least number of dandling bonds on the surface [20]. The stability of this surface can also be explained using an auto-compensation concept, which was applied to metal oxide surfaces by La Femina [21].

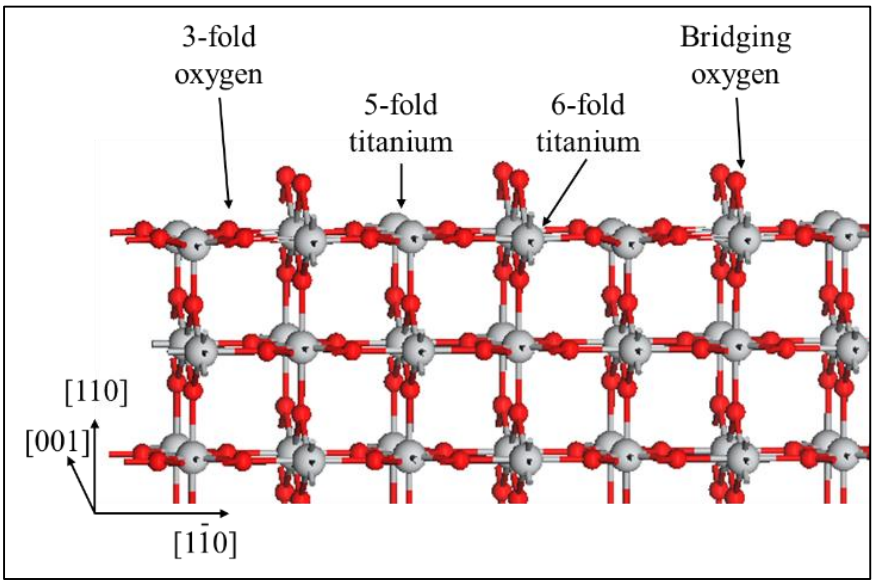

Figure 2.3. Ball and stick model of rutile TiO_2(110)-(1×1) surface. Grey and red spheres are titanium and oxygen atoms, respectively.

The electrons transferred from the bonds of the Ti cations are just compensated with the charge in the dangling bonds of the O anions. To realize the neutral planes of the oxide, the number of Ti to O bonds broken on the top plane is the same with that of O to Ti bonds broken on the bottom plane.

Geometrically the rutile TiO_2(110) surface comprises both Ti atoms and O atoms with two different kinds of coordination. In the surface plane the rows of five-fold coordinated (5f) Ti atoms are alternately placed with the rows of six-fold coordinated (6f) Ti atoms, which are separated by rows of O atoms. All rows run in the [001] direction. The former Ti atoms are exposed to the surface, while the latter are covered with the row of two-fold coordinated O atoms positioned at bridge sites, named the bridging oxygen rows (see Fig. 2.3). The size of a (1×1) unit cell at the surface is 2.96 Å in the [001] direction and 6.5 Å in the [110] direction [22].

When an oxide crystal is broken at a surface, the top layer accommodates the surface atoms by relaxing their positions into a more energetically favorable atomic arrangement. On the TiO_2(110) surface the two different types of Ti atoms move in opposite directions. Ti (5f) atoms move inwards, i.e., towards the bulk, by 0.16 Å, while Ti (6f) atoms move outward by 0.12 Å. This gives rise to a rumpling of the in-plane layer with an amplitude of 0.3 Å. When the bridging oxygen atoms above the Ti (6f) relax inwards by as much as 0.27 Å, the (3f) oxygen atoms move either upwards or laterally towards the (5f) neighboring Ti atoms. The second layer relaxes in the same directions, but the relaxations are significantly less [12, 22].

2.2.2 Preparation of surface

For investigation, an appropriate method to prepare a TiO_2 surface is chosen from several recipes. The widely used process in UHV condition is repetition of Ar^+ sputtering and annealing in UHV with different temperatures above 600 °C [12-22], exhibiting pale or deep blue in color, resulting in the reduced (1×1) or (1×2) reconstructed surfaces for rutile TiO_2(110). C. D. Pang and others suggested a model for the (1×2) structure, featured with added rows along the [001] direction, in which the termination is of a completely reduced (1×1) surface, as depicted in Fig. 2.4. In this model, two rows of fivefold coordinated Ti atoms in outer, and fourfold coordinated Ti atoms in the center are added, which involves narrow rows with missing bridging oxygen that are effectively part of the upper terrace. Lateral relaxations were also included.

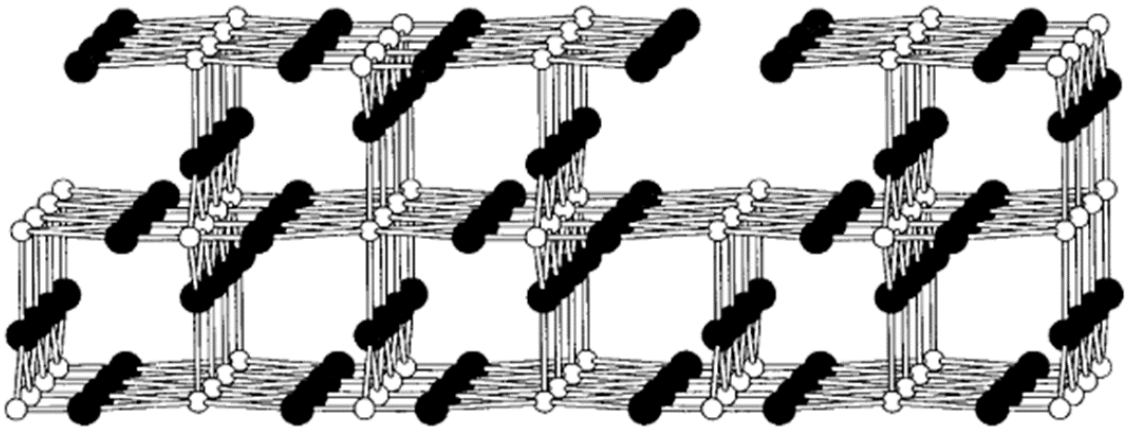

Figure 2.4. Ball and stick model of reduced rutile TiO_2(110)-(1×2) surface. White and black spheres are titanium and oxygen atoms, respectively [36].

Annealing in air [23] or chemical etching [24, 25] is usually applied as a pre-treatment prior to the preparation in UHV to improve the cleanness and flatness of a TiO_2 substrate. Etching

solutions, sulfuric acid (H_2SO_4) or hydrofluoric acid (HF), are frequently used to completely remove metal contaminations. The substrate annealed in oxygen gas after the sputtering exhibits nearly stoichiometric surface, evidenced by sharp Ti 2p X-ray photoemission spectroscopy (XPS) peaks with no indication of reduced Ti states [26]. Annealing in air can make fully oxidized stoichiometric TiO_2 surface [27]. Comprehensive understanding of fully oxidizied stoichiometric TiO_2, however, has not been achieved to nano-scale characterization.

2.2.3 Experimental analysis on TiO_2 (110) surface

In order to understand the geometric structure, electronic states, and surface chemistry of TiO_2, considerable research effort has been directed to single crystal surfaces of TiO_2 as model systems from a scientific point of view. So far, the research in this field is wide-ranging with activity extending from synthesis of novel TiO_2 to fundamental characterization aiming at comprehensive surface chemistry at the atomic scale. TiO_2 has been analyzed with a wide variety of surface-sensitive techniques, such as x-ray photoelectron spectroscopy (XPS), low energy electron diffraction (LEED), Auger electron spectroscopy, low energy ion scattering (LEIS), near-edge x-ray absorption fine structure, and static secondary ion mass spectrometry, which all show sputtering-induced changes in the composition and chemical state [11,12, 19, 24]. Pan et al. introduced a change of stoichiometry caused by the formation of oxygen vacancy during XPS analysis. While symmetric sharp Ti 2p peaks correspond to only the Ti^{4+} component on a nearly perfect surface, the shoulder in lower binding energy side of XPS spectra ascribed to Ti^{3+} and Ti^{2+} was observed in slightly oxygen deficient surface, with a

(1×1) LEED pattern was obtain. The Ti^{4+} component and the surface ordered structure vanish for a highly oxygen deficient surface; no spot of LEED pattern was observed on it [26].

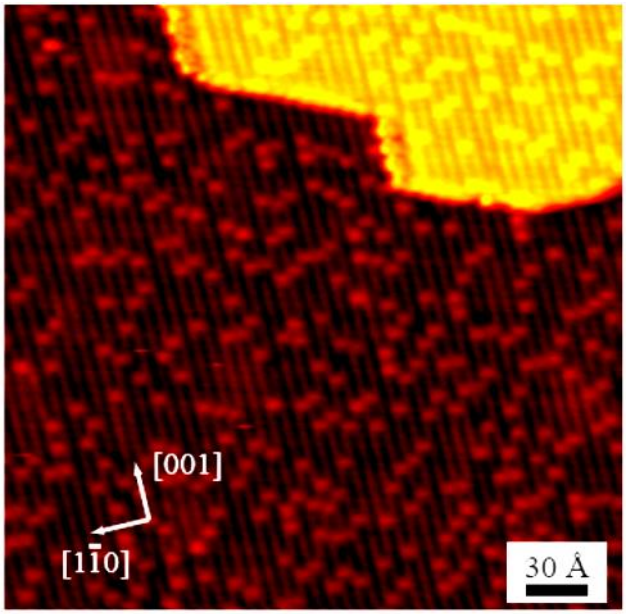

Figure 2.5. STM image of rutile TiO_2(110)-(1×1) surface. The bright lines are Ti rows separated by darker bridging oxygen rows with oxygen vacancies, which are imaged as bright protrusions [33].

These results is fully consistent with that reported by Karmakar et al. for cluster formation induced by sputtering [28]. Moreover, the TiO_2(110) morphologies with different preparation processes have been confirmed experimentally using various quantitative probes for surface crystallography. Initially, the reduced TiO_2(110) surface was imaged with STM for the first time in 1990 [29], and the atomic resolution of the surface was obtained in 1994 [30]. Interpretation of the STM data took a little longer, and it was in 1996 when the final interpretation was found [31]. When the TiO_2(110) surface is imaged with STM, it is stably possible to work at a positively biased sample, since a negatively biased sample often causes the tip to crash into the surface, ruining resolution. When biased positively, electrons tunnel

from an STM tip into the empty surface states of the sample. These states are located primarily on the Ti atoms and the in-plane Ti(5f) atoms appear protruding in the STM images.

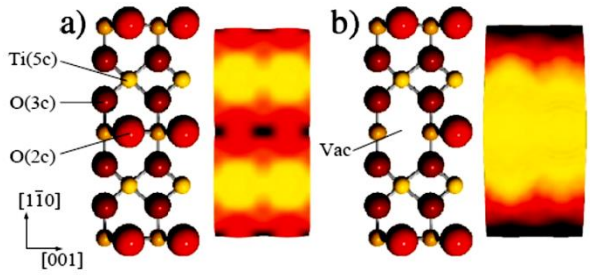

Figure 2.6. TiO_2 surface structures and simulated STM images of (a) the stoichiometric TiO_2 surface illustrating how the Ti(5f) appears as protruding, (b) a missing oxygen atom in a bridging oxygen row, giving rise to a protrusion on the bridging oxygen row in the STM image [33].

Due to a low local density of state (LDOS) at the Fermi level of oxygen atoms, they are imaged as depressions with STM, despite the fact that they protrude in the atomic structure, so that the bright rows in the STM images correspond to the rows of Ti(5f) atoms in the [001] direction. For a long period time, it was difficult to distinguish whether protrusions appearing on the bridging oxygen rows in STM images are missing oxygen atoms or hydroxyls (OH groups). This issue was not clarified until Suzuki et al. discovered hydroxyls based on an experiment that TiO_2(110) surface was exposed to atomic hydrogen [32]. In agreement with results by Diebold et al. [31], Schaub et al. have shown that both defects look much the same in STM images, but that the two can be distinguished from each other in size of bright spots in dark rows [32, 33]. Fig. 2.5 shows a typical STM image of the surface with bridging oxygen vacancies clearly present. Simulated STM images in Fig. 2.6 illustrate the difference between (a) the stoichiometric surface and (b) a bridging oxygen vacancy. Along with STM, AFM has

been known with a promising ability in visualizing reactions on metal oxide surfaces even in the presence of reactant gas and for natural insulation of fully oxidized surfaces. In general, if it is difficult for STM to distinguish between geometric and electronic structures on oxygen rows due to less electron tunneling, non-contact (NC)-AFM utilizing the interaction force between an AFM tip and a sample can visualize rows of the topmost oxygen atoms, such as bridging oxygen rows running in the [001] direction and also single oxygen vacancies in their rows on the (1×1) phase [34, 37-39]. By this way, the atomic-scale AFM images of reconstruction TiO_2(110)-(1×2) surfaces were observed, which gave a sufficient evidence to determine the correctness of several theoretical models, such as a missing row model originally proposed by Molle and Wu, a Ti_2O_3 added row model by Onishi et al., or modified added row models by Pang el al. [32-37]. In addition, AFM images recently visualized in atmospheric conditions have provided a great deal of nano-scale information of interaction between aqueous solution and TiO_2 surfaces [27, 40, 41]. However, the atomic resolution of AFM images of fully oxidized TiO_2(110) surfaces in air until now has not been performed thoroughly.

2.2.4 Adsorption on TiO_2(110) surfaces

With the wide variety of technological applications utilizing the properties of TiO_2, it is no wonder that extensive studies have been performed on the interaction of gases and aqueous solutions with the surfaces of TiO_2. The adsorption, dissociation and/or reactions of atoms and molecules on the TiO_2(110) surface are of fundamental importance to understand surface chemistry that governs the exciting technological applications. Extensive experimental and

theoretical works have been done on the system, and those works have been excellently reviewed by Henrich and Cox, and Diebold [1, 12]. This section is primarily based on these reviews, where some of the interesting features of adsorption of small molecules on TiO_2(110) were focused to give a better background. That said, despite wide-range and numerous studies of absorption on TiO_2(110) surface, the adsorption chemistry on this surface has been not well understood. Different experimental groups dispute, and the discrepancies between experiment and theory are not negligible.

Chemisorption on the TiO_2(110) surface is much affected by the ionic nature of the crystal. Ti cations on the surface are coordinatively unsaturated, and act as Lewis acids (electron pair acceptor) that may interact with electron donors like H_2O. Bridging oxygen atoms are basic sites and interact with electron acceptors like H^+ creating bridging hydroxyls (-OH groups). Most studies show that the stoichiometric (110) surface is relatively inert, as is expected from the lowest-energy surface of the TiO_2 surfaces [1]. The primary adsorption sites on the non-stoichiometric surface are the bridging oxygen vacancies, where especially dissociative adsorption is found. The main problem with the study of these interactions is the inherently low concentration of these vacancies, which makes the signal from the vacancies small when utilizing space averaging surface science techniques. The vacancies are hot spots with respect to adsorbates, because two electrons are left in non-bonding 3d states on the neighboring coordinatively unsaturated Ti atoms. This makes electronic interactions favorable in a large number of cases. Some features relating to atomic interaction between hydrogen, oxygen or water molecules and individual surface atoms are reviewed as follows.

2.2.4.1 Hydrogen adsorbed on TiO_2(110) surface.

The adsorption sites and characteristics of hydrogen on the TiO_2(110) surface are still unresolved. Molecular hydrogen does not stick to the stoichiometric surface at room temperature. When dosing molecular hydrogen on the reduced surface, several experimental studies proposed the dissociative adsorption of two hydrogen atoms in the bridging oxygen vacancies each bound to a five-fold coordinated Ti atom as a hydride (Ti(III)-H) [42, 43], while others found no change in the surface-defects states upon exposure to hydrogen molecules [44]. Very few theoretical studies have been made, falling short for the problem whether hydrogen molecules bind more strongly to both the bridging oxygen atoms or to the acidic cation sites on the stoichiometric surface than in the vacancies [45, 46].

Dosing atomic hydrogen also brings about unresolved matters. Suzuki claimed that by dosing atomic hydrogen cracked over a hot filament in front of the sample, around 25% of the bridging oxygen atoms are hydrogenated to form hydroxyls [43], while Wöll in similar experiments found 100% hydroxyls on the surface by means of helium scattering [47]. Fujino carried out low energy ion scattering and recoiling spectroscopy experiments in the combined mode of coaxial impact-collision ion scattering spectroscopy and time-of flight elastic recoil detection. This analysis indicated one monolayer of hydrogen atoms on vacuum-annealed TiO_2(110)-(1x1). The hydrogen atoms were assigned to surface hydroxyls, created through the vacancy sites by dissociative adsorption of water molecules during thermal annealing [48]. An interesting problem with hydrogen on the TiO_2(110) surface is the fact that hydrogen is able to diffuse into and out of the bulk. The hydrogen atoms have been shown to diffuse

preferentially along the bulk crystal channels, while some diffusion have been found along the (110) surface normal [49, 50].

2.2.4.2 Oxygen adsorbed on TiO_2 (110) surface.

Hereafter, oxygen chemistry on the TiO_2(110) surface is reviewed briefly. It was previously assumed that the entire interaction between oxygen molecules and the surface was through a simple dissociative filling of a vacancy:

$$V_O + O_A \rightarrow O_L, \qquad (2.1)$$

where V_O is the bridging oxygen vacancy, O_A the adsorbed oxygen atom and O_L a bridging oxygen atom in the lattice structure [42]. At low temperatures (~100 K) Henderson et al. showed that three oxygen molecules adsorb to each vacancy present on the surface [19]. They argued that all three molecules were bound as O^-_2 species in and around the vacancy. One molecule in the vacancy dissociates to fill the vacancy, while the other two molecules desorb at 410 K. The rest oxygen atom dissociated from the molecule was unaccounted for in Ref. 19, while the same group in Ref. 51 suggested that the single atom most probably diffuses into the bulk. When exposing a vacuum annealed surface to 2.4 L O_2 at 120 K (the favorable condition for adsorption of oxygen molecules at vacancy sites), a significant temperature programmed desorption (TPD) peak was found at 410 K. This peak disappeared if the oxygen dosing is done in two steps with an initial exposure of 0.8 L O_2 at 120 K followed by annealing to 200 K and then exposure to the remaining 1.6 L at 120 K to give a total of 2.4 L O_2. This would indicate that further molecular adsorption is blocked by annealing the surface with

oxygen molecules adsorbed in the vacancies. Lu et al. [52, 53] found two low temperature oxygen species, with distinctly different photo-desorption patterns; one channel (α) which undergoes slow photo-desorption and can be photo-activated to oxidize CO to CO_2, and a fast channel (β). The α state is populated at 105 K, and it is thermally converted into the β state above 200 K, indicating that either the β state is more strongly bound to the surface than the α state or the α state is not entropically stable above 200 K. Population of the β state is maximized between 250-300 K.

2.2.4.3 Water adsorbed on TiO_2 (110) surface.

Accompanying with hydrogen and oxygen, the interactions with water are important to understand, because water, either liquid or vapor, is almost always present in photo-catalytic reactions. In the past decades, much of the work has been targeted at the question of whether water is adsorbed molecularly or dissociatively. Santerler, in 1992, reported that water adsorption on TiO_2(110) surface depends on its geometric arrangements [54]. On the surface with appreciable amounts of oxygen vacancies, water molecules tend to adsorb on the bridging rows. The water molecules, consequently, may interact with its neighboring atoms and dissociate to form bridging hydroxyl groups. On the other hand, if the surface has almost no oxygen vacancies, water adsorbs preferentially and dissociates to OH and H on Ti (5f) cation rows, resulting in terminal hydroxyl group. Nevertheless, Henderson, using high-resolution electron energy loss spectroscopy (HREELS) and TPD study, concluded that the adsorption of water on TiO_2(110) is molecular on the stoichiometric surface and dissociative on the reduced surface, which is conventionally produced by heat treatment, forming oxygen

defects [55, 56]. The reason of molecular water forming on the stoichiometric surfaces is that the distance between each bridging oxygen sites and biding sites of water (five-coordinate Ti^{4+} site) is too large to form hydrogen bonding interactions with water that might facilitate O-H bond dissociation. Taking adsorbed water in oxygen vacancy sites, Henrich et al. detected using UPS that surface hydroxyl groups were present after adsorption of H_2O on a slightly reduced TiO_2(110) surface at 300 K [57]. Several other studies have confirmed the existence of hydroxyl groups on reduced surfaces [22, 24, 26, 32, 33, 39, 42, 48, 51] and the consensus among them is that H_2O adsorbs in the bridging oxygen vacancy, where one of the hydrogen atoms is transferred onto the neighboring bridging oxygen atom. Isotopic labelling studies have shown that the hydrogen atoms loose the original adsorption site in the dissociation process, indicating that they readily diffuse along the bridging oxygen rows [55].

2.3 Silicon dioxides

Silicon dioxide is a commonly found material in minerals with many polycrystalline forms as well as a vitreous glassy state. From a technological point of view, silicon dioxide is one of the most useful wide band gap materials. SiO_2 plays a crucial role in silicon based electronic devices as well as in the glass and ceramic industry. Most common forms of silica, including α- and β-quartz, β-tridymite, α- and β-crystobalite, keatite, coesite, and stishovite are composed of silicon atoms bonded in a covalent manner to oxygen atoms [58, 59]. With the exception of stishovite, all these polycrystals phases have local structures of fourfold tetrahedral bonding for Si and twofold bridging bonding for O. The tetrahedra link together corner to corner and different rotations determine the different forms of the silicon dioxide.

In α-quartz, which is thermodynamically the most stable form at room temperature, the SiO_4 tetrahedra form interlinked helical chains; there are two slightly different Si-O distances (1.59 Å and 1.61 Å) and the angle Si-O-Si is 144°.

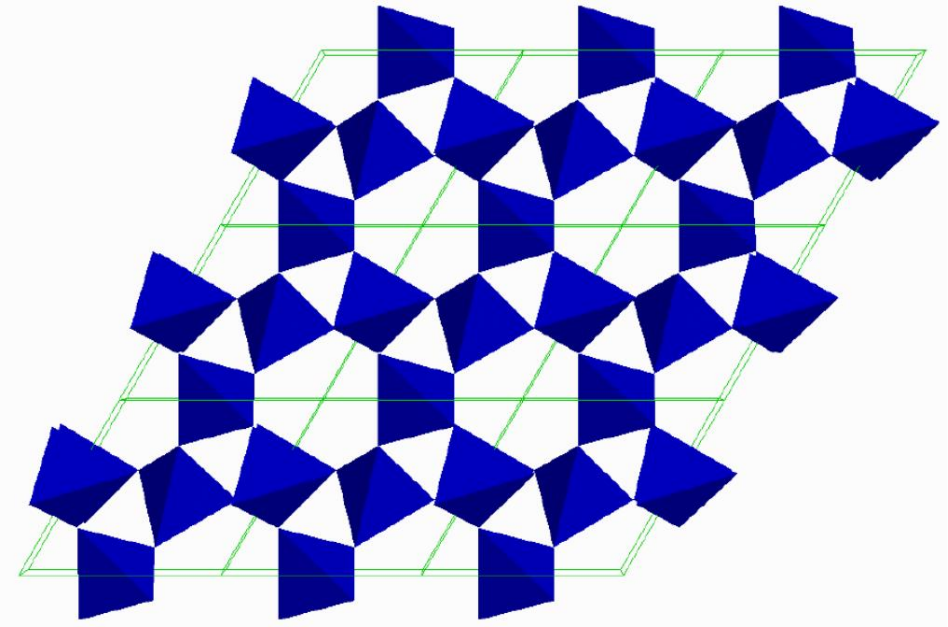

Figure 2.7. The crystal structure of α-quartz, c-axis projection [58].

The helices in any one crystal can be either right-handed or left-handed so that individual crystals have non-superimposable mirror images [59]. The structure of α-quartz crystal is illustrated in Fig. 2.7. Meanwhile, for stishovite formed under high pressures at high temperatures, each Si atom is six-fold coordinated in the form of a distorted SiO_6 octahedron and each O atom is threefold bonded in the center of a planar triangle [58-59], depicted in Fig. 2.8, the same with the rutile structure. The density of stishovite is 4.287 g/cm^3, while α-quartz, the densest among the low pressure forms, has a density of 2.648 g/cm^3. The difference of density can be ascribed to the increase in coordination. Using first principle orthogonalized linear combination of atomic orbital methods, Li and Ching elucidated the linear correlations

between the band gaps and the average Si-O bond lengths as well as Si-O-Si angles [60]. Accordingly, because of increased coordination number corresponding to a reduced band gap in stishovite, it has more covalent bonding character than the 4:2 bonded polymorphs and has a quite different electronic structure [61].

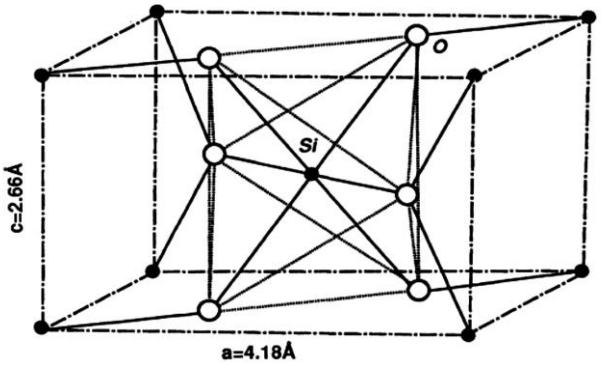

Figure 2.8. The structure of unit cell of stishovite, illustrating the octrahedral coordination of silicon atom [61].

The surface aspect of silicon dioxide, on the other hand, presents a somewhat different structural problem. One of surface structures have been suggested in Ref. 62. The requirements are that O satisfies two bonds and Si satisfies four bonds. Newman constructed numerous models and came to the conclusion that in real possibility for the surface structure of silicon dioxide, the oxygen atoms form the surface layer by double bonding with the silicon atoms below them. It should be noted that the substructure is quartz and the single bond lengths are longer than in the tetrahedra substructures. The various bond lengths and orientations of the surface bond structures directly depend on the substructure tetrahedra orientations and, thus, the particular form of the silicon dioxide. Because of the dependence of the bond orientations of the surface structure on the substructure form, one would expect

that surface reactivity involving the oxygen atoms would be temperature dependent as the temperature dependence of the bulk form. The temperature dependence and relationship between the crystalline forms of silicon dioxide are as follows [58]:

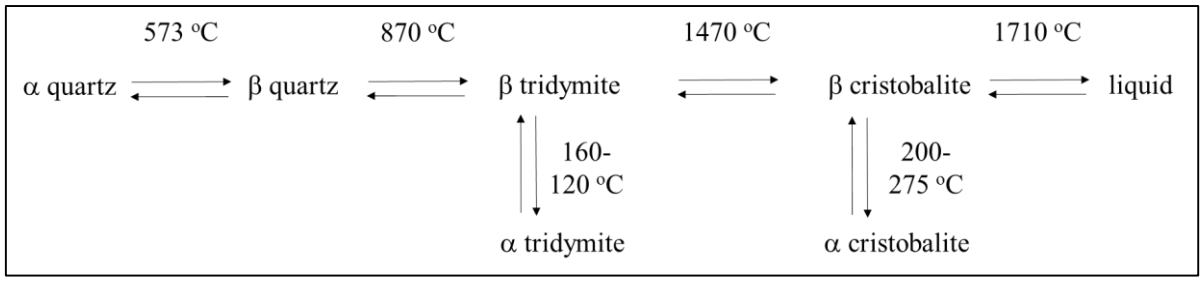

Figure 2.9. The crystalline forms of silicon dioxide dependence on temperature [58].

Here the surface structure of α-quartz, most commonly colorless, transparent and crystalline stable in atmosphere condition, has been extensively discussed for understanding its water wettability. In general, the structure terminates at the surface in either siloxane groups with the oxygen on the surface, or silanol groups with hydroxyls [58].

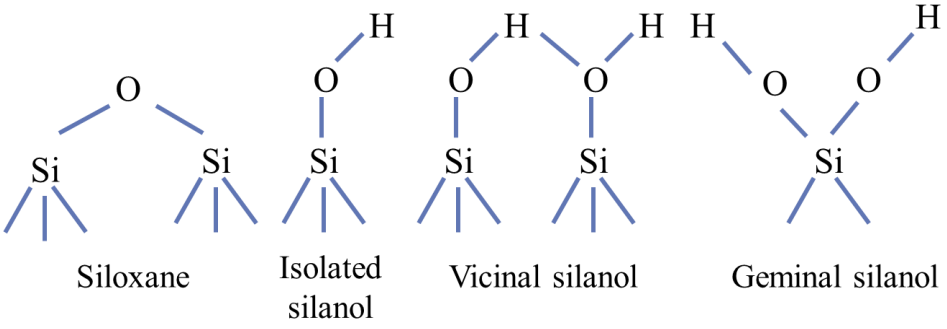

Figure 2.10. The structure of siloxane, isolated silanol, vicical silanol, and germinal silanol groups, which occupy the topmost layer of silicon dioxide [62].

There are three possibilities of silanol formation as shown in Fig. 2.10; the first one is an isolated group when the surface silicon atom has three bonds into the bulk and a bound with a single hydroxyl group, and the second one is bridged silanol groups, formed by hydrogen bonding of two adjacent single groups of different silicon atoms due to close distance. The third type of silanol consists of two hydroxyl groups attached to the same silicon atom, called germinal silanol [62]. Even various theoretical and empirical studies have been tried, but no consensus can be found concerning the existence of germinal hydroxyl groups.

In addition, the hydrophobic/hydrophilic conversion was discussed in terms of the structural alteration of surface arrangement dependent on treatment temperature. At room temperature, crystalline silicon dioxide surfaces which are fully hydroxylated through one of three forms of silanol groups display the hydrophilicity due to the characteristic of hydroxyl groups. On the other hand, the quartz surfaces present hydrophobicity (or less hydrophilicity) after annealing up to 673 K. This conversion has been likely induced by dehydration and dehydroxylation processes under high temperature up to 1373 K [59, 61, 62]. While the number of physisorbed water molecules decreases as a function of increasing temperature in dehydration, the condensation of hydroxyl groups forms siloxane bonds that exhibit hydrophobicity in dehydroxylation. Agzamkhodzhaev et al. showed that the dehydroxylated surface of silica can be completely recovered to be terminated with silanol groups with water at room temperature, but it needs several years [62]. Further study of correlation between structural arrangement and its wettability should be carried out to fully understand the hydroxyl termination of SiO_2 crystals as well as SiO_2 layers.

2.4 TiO_2-SiO_2 composite systems.

So far, TiO_2 has been known as one of metal oxides showing interesting photoinduced reactions, called photocatalytic reactions. Two kinds of photo-induced reactions, that is, strong oxidation reaction and high hydrophilicity are widely known under UV light irradiation onto titanium oxide surfaces. The former is caused by several active oxygen species, such as O_2^- (superoxide) or OH^+ (hydroxyl radical), formed by redox reaction with electrons and holes generated by UV light irradiation. The latter is considered that trapping of adsorbed water at the oxygen defects, which are caused by reduction of TiO_2 matrices, result in formation of hydrophilic domains. The oxidation reactions have received much attention from the standpoint of environmental applications, such as self-cleaning and anti-bacterial coatings, and have been extensively investigated [5]. In spite of its potential into wide application fields, the investigation on photo-induced super-hydrophilic properties of TiO_2 surfaces has been studied only in recent decades since super hydrophilic phenomenon was accidently discovered in TOTO Inc. laboratory in 1995 [5]. However, the super-hydrophilicity showing a water contact angle of zero does not persist in time in the absence of UV light radiation, which limits the field of its application because in real conditions surfaces are not permanently exposed to UV light. Therefore, enhancing and persisting the super-hydrophicity of TiO_2 surfaces using various additives have recently become more attractive. Silicon dioxide with its notable hardness and chemical stability has been one of the most popular candidates for research of mixed oxide systems with TiO_2 for improving its super-hydrophilicity. Machida et al. have first reported that the addition of 10-30 mol% of SiO_2 in sol-gel process into a TiO_2 film yielded optimum photo-induced super-hydrophilicity, which maintained for a certain time in the dark [63]. This was explained as SiO_2 less than 30 mol% has a suppress effect on

the transformation of anatase to rutile and on the crystal growth in annealing process. This is consistent with that in several successive studies of photo-induced hydrophilic on SiO_2/TiO_2 systems. Subsequently, SiO_2-TiO_2 composite films have been produced using various techniques including sol-gel [63], spin-coating [64], electron-beam evaporation [66], chemical vapor deposition [67, 68], and flame hydrolysis [69] processes in order to understand the intrinsic correlation of surface chemical and electronic properties, and super-hydrophilicity. Another interpretation for the enhancement and durability of super-hidrophilicity by adding SiO_2 to TiO_2 has been proposed by K. Guan et al. [64]. Due to minor formation of complex oxides with the bonds of Ti-O-Si formed from single oxides of SiO_2 and TiO_2 particles, the surface acidity can be improved, resulting in stronger surface hydroxyl groups to maintain the hydrophilicty. Tanabe et al. showed that silicon can enter the TiO_2 lattice as a minor component, because Si^{4+} cations retain their fourfold coordination, $SiO_4^{+4/3}$ unit are formed with the charge difference as +4/3, as depicted in Fig. 2.10. Lewis acidity is thus assumed to appear owing to an excess of localized positive charge. Similarly, when titanium can enter the SiO_2 network as a minor component, because Ti^{4+} cations retain their sixfold coordination, TiO_6^{2-} units are formed [70]. Bronsted acidity is thus assumed to appear because these units may be compensated by two protons to keep the electric neutrality. Moreover, the decreasing of grain size in composite films, which was formed in sol-gel solution by dip coating method, was also helpful in increasing hydrophilic property due to the increased quantum effect of TiO_2 [64]. The super-hydrophilic mechanism of SiO_2-TiO_2 system related to chemistry and electronic properties of the surface was further discussed in terms of the hydrophilic property of SiO_2 overlayers films on TiO_2 and SiO_2/TiO_2 mixing films [65].

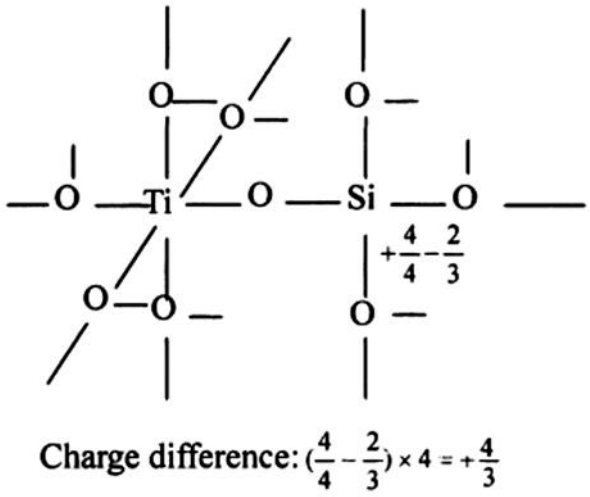

Figure 2.10. Schematic model of SiO_2-TiO_2 structure and charge difference [64].

It was concluded that the super-hydrophilicity of SiO_2 overlayer on TiO_2 can be attributed to enlargement of charge space layer at the interface between TiO_2 and SiO_2 layers, while the super-hydrophilicity of TiO_2 surface was determined by the number of oxygen vacancies of SiO_2/TiO_2 mixing films due to enhancing surface acidity. The surface acidity was thought to take the form of more stable surface hydroxyl groups. The stable hydroxyl groups on the surface of SiO_2/TiO_2 multilayer films is beneficial in maintaining the hydrophilicity, which can explain the reason why the contact angle increases slowly and remains low for a long time in dark place. Later in another publication [66], it was reported that the wettability of either TiO_2 or SiO_2 surfaces is mainly governed by hydroxyls density. The number of hydroxyl groups per unit area reduced in dehydroxylation processes in high temperature treatment. Therein UV light irradiation has no effect on silica surface, but remarkably removed organic contamination from titania surfaces. This has been entirely attributed to photocatalytic decomposition. A simple model incorporating van der Waals and Lewis type acid-base interfacial interaction was proposed to interpret the wettability difference between

SiO_2 and TiO_2 surfaces [66]. Accordingly, it can be described that under intensive heat treatment, the number of siloxanes per unit area (on account of the number of OH per unit area before dehydroxylation) should be higher on titania, because the Lifshitz-van der Waals component of surface free energy of titania is much more than that of silica. Hence silica surfaces show notable change from super-hydrophilic to hydrophobic with intensive heat treatment. Otherwise, silica with a higher band gap compared to titania should be inert with UV light irradiation. This conclusion has been independently confirmed by Nakamura et al. [67]. In their research, using TEM, XPS, FT-IR and TOF-SIMS measurements, they noticed that SiO_2/TiO_2 double layer films showed super-hydrophilicity due to the presence of stable Si-OH on the top layer. This characteristics can be restored by the photo-catalytic activity of anatase TiO_2 underneath layer, and maintained by the high hardness and chemical stability of the porous SiO_2 top layer.

While up to now most of the techniques cannot control film homogeneity on a nano-scale, Sasahara et al. examined the atomic structure of silicon oxide ultra-thin layer on TiO_2 (100) surfaces using silicon oxide vapor phase deposition method [72]. Barranco et al. first time performed XPS analysis of a SiO_2 layer on TiO_2(110) prepared by evaporation from SiO powder in 2001 [68]. An increase of the Si 2p binding energy by 1.3 eV and a decrease of the Si Auger parameter by 0.9 eV were observed with the increase of the amount of SiO_2. This likely indicated the changes in the electronic properties of Si atoms at the first monolayer in contact with TiO_2 substrate produced variations in the initial and final state energies of the Si atoms, leading to observed energy shifts. By comparing with the results on a SiO_2 layer on Al_2O_3(0001), perturbation of electronic state of Si at the SiO_2/TiO_2 interface was concluded. Continuously, Abad et al. examined the deposition of Si onto TiO_2(110)-(1×2) surfaces by

using several techniques including Auger electron spectroscopy (AES) and STM in 2006 [71]. The Si LVV Auger peak appeared at 75 eV when the Si was less than 0.5ML, which indicated the formation of SiO_2 at room temperature. The positive shift of the Si peak with the increase of the Si coverage was attributed to the formation of less oxidized species SiO_x ($1 < x < 2$). Nevertheless, no ordered structure for the SiO_x layer was observed by STM, and the subsequent annealing of the SiO_x layer at 723 K induced the aggregation of the SiO_x. Recently, the epitaxial growth of silicon oxide on a single crystal rutile TiO_2(100) was conducted by annealing it in air, while it was being stored in a quartz case; the case acted as a Si-O vapor source [72]. The deposition amount of Si on the surface increased with annealing time, characterized by X-ray photoemission spectroscopy (XPS), and a low energy electron diffraction (LEED) pattern of (3×4) was observed at the coverage of a few molecular thickness of Si-O. Frequency modulation–atomic force microscopy (FM-AFM) observation in pure water showed that the (3×4) surface consists of atomically flat terraces. Those results indicated the hetero-epitaxial growth of thin-films of silicon oxide on the TiO_2(100) surface. It opened the direction to reveal the atomic structure understanding of SiO_2-TiO_2 systems. Further study of the atomic structure of the ultra-thin layers of silicon oxide on the TiO_2(110) surface is needed to fully understand the OH termination of the silicon oxide top-layer and to reveal the super-hydrophilicity of the surface of SiO_2-TiO_2 system from a scientific point of view.

References

[1] V. E. Henrich, P. A. Cox, Cambridge, Cambridge University Press, 1994.

[2] H. H. Kung, Elsevier, Amsterdam, 1989.

[3] U. Diebold, S. C. Li, and M. Schmid, Annu. Rev. Phys. Chem., 61, 2010, 129.

[4] L. A. Linsebigler, G. Lu, T. J. Yales, Chem. Rev., 95, 1995, 735.

[5] A. Fujishima, et al, Journal of Photochemistry and Photobiology C: Photochemistry Rev., 1, 2000, 1.

[6] M. Machida, K. Norimoto, T. Watanabe, K. Hashimoto, A. Fujishima, J. Mater. Sci., 34, 1999, 2569.

[7] M. Jarn, Q. Xu, M. Linden, Langmuir, 26, 2010, 11330.

[8] P. van der Krogt, "Elementymology & Elements Multidict",, http://www.vanderkrogt.net/elements/elem/ti.html.

[9] M.Winter, "WebElements: The Periodic Table on the WWW",, http://www.webelements.com/webelement/scholar/elements/titanium/history.html.

[10] B. Kasemo and J. Gold, Adv. Dent. Res., 13, 1999, 8.

[11] K. M. Glassford and J. R. Chelikowsky, Phys. Rev. B, 46, 1992, 1284.

[12] U. Diebold, Surf. Sci. Rep., 48, 2003, 53.

[13] J. Burdett, Inorg. Chem., 24, 1985, 2244.

[14] A. Fahmi, C. Minot, B. Silvi, and M. Causa, Phys. Rev. B, 47, 1993, 11717.

[15] M. Ramamoorthy, D. Vanderbilt, and R. King-Smith, Phys. Rev. B, 49, 1994, 16721.

[16] S. Munnix and M. Schmeits, Phys. Rev. B, 30, 1984, 2207.

[17] A. Fujishima, X. Zhang, and D. A. Tryk, Surf. Sci. Rep., 63, 2008, 515.

[18] W. S. Epling, C. H. F. Peden, M. A. Henderson, and U. Diebold, Surf. Sci., 333, 1998, 412.

[19] M. A. Henderson, W. S. Epling, C. L. Perkins, and C. H. F. Peden, J. Phys. Chem., 103, 1999, 5328.

[20] M. Ramamoorthy, D. Vanderbilt, R.D. King-Smith, Phys. Rev. B, 49, 1994, 16721.

[21] U. Diebold et al., Surf. Sci., 411, 1998, 137.

[22] M. Ramamoorthy, R. D. King-Smith, and D. Vanderbilt, Phys. Rev. B, 49, 1994, 7709.

[23] H. Onishi et al., Bull. Chem. Soc. JPN., 68, 1995, 2447.

[24] A. N. Shultz et al., Sur. Sci., 339, 1995, 114.

[25] Y. Yamamoto et al., J.J. Appl. Phys., 44, 2005, 511.

[26] J. M. Pan et al., J. Vac. Sci. Techno. A.,10, 1992, 2470.

[27] A. Sasahara and M. Tomitori, J. Vac. Sci. Technol. B, 28, 2010, 3.

[28] P. Karmakar, G. F. Liu, J.A. Yarmoff, Phys. Rev. B, 76, 2007, 193410

[29] G. S. Rohrer, V. E. Henrich, and D. A. Bonnell, Sci., 250, 1990, 1239.

[30] D. Novak, E. Garfunkel, and T. Gustafsson, Phys. Rev. B, 50, 1994, 5000.

[31] U. Diebold, J. F. Anderson, K.-O. Ng, and D. Vanderbilt, Phys. Rev. Let., 77, 1996, 1322.

[32] S. Wendt et al., Sur. Sci., 598, 2005, 226.

[33] R. Schaub, R. Thostrup, N. Lopez, E. Lægsgaard, I. Stensgaard, J. K. Nørskov, and F. Besenbacher, Phys. Rev. Let., 81, 2001, 6104.

[34] K. I. Fukui, H. Onishi, Y. Iwasawa, Phys. Rev. Let., 79, 1997, 21.

[35] M. Ashino et al., Appl. Sur. Sci., 157, 2000, 212.

[36] C. L. Pang, H. Raza, S.A. Haycock, G. Thornton, Appl. Sur. Sci., 157, 2000, 233.

[37] M. Ashino et al., Phys. Rev. Let., 86, 2001, 19.

[38] C. L. Pang, A. Sasahara, H. Onishi, Q. Chen, G. Thornton, Phys. Rev. B, 74, 2006, 073411.

[39] G. H. Enevoldsen et al., Phys. Rev. B, 76, 2007, 205415.

[40] R. Nakamura et al., J. Phys. Chem. B, 109, 2005, 1648.

[41] A. Sasahara, S. I. Kitamura, H. Uetsuka, H. Onishi, J. Phys. Chem. B., 108, 2004, 15735.

[42] W. Göpel, G. Rocker, and R. Feierabend, Phys. Rev. B, 28, 1983, 3427.

[43] S. Suzuki, K. Fukui, H. Onishi, and Y. Iwasawa, Phys. Rev. Let., 84, 2000, 2156.

[44] V. E. Henrich and R. L. Kurtz, Phys. Rev. B, 23, 1981, 6280.

[45] J. Leconte, A. Markovits, M. K. Skalli, C. Minot, and A. Belmajdoub, Surf. Sci., 497, 2002, 194.

[46] M. Menetrey, A. Markovits, and C. Minot, Surf. Sci., 524, 2003, 49.

[47] K. A. Fosser, R. G. Nuzzo, P. S. Bagus, and C. Wöll, J. Chem. Phys., 118, 2003, 5115.

[48] T. Fujino, M. Katayama, K. Inudzuka, T. Okuno, K. Oura, and T. Hirao, Appl. Phys. Let., 79, 2001, 2716.

[49] O. W. Johnson, S. H. Paek, and J. W. DefordJ. Appl. Phys., 46, 1975, 1026.

[50] J. B. Bates, J. C. Wang, and R. A. Perkins, Phys. Rev. B, 19, 1979, 4130.

[51] W. S. Epling, C. H. F. Peden, M. A. Henderson, and U. Diebold, Surf. Sci., 333, 1998, 412.

[52] G. Q. Lu, A. Linsebigler, and J. T. Yates, J. Chem. Phys., 102, 1995, 3005.

[53] G. Q. Lu, A. Linsebigler, and J. T. Yates, J. Chem. Phys., 102, 1995, 4657.

[54] D. J. Santeler, J. Vac. Sci. Technol. A, 10, 1992, 4.

[55] M. A. Henderson, Langmuir, 12, 1996, 5093.

[56] M. A. Henderson, Surf. Sci. Rep., 46, 2002, 1.

[57] V. E. Henrich, G. Dresselhaus, and H. J. Zeiger, Sol. Sta. Comm., 24, 1997, 623.

[58] A. P. Legrand, John Wiley, New York, 1998.

[59] Harrison, W. A., Proceedings of the International Topical Conference on the Physics of SiO_2 and its Interfaces, edited by S. T. Pantelides, Pergaman, New York, 1978, 105.

[60] Y. P. Li and W. Y. Ching, Phys. Rev. B, 31, 1985, 2172.

[61] N. R. Keskar, Phys. Rev. B., 44, 1991, 4081.

[62] E. F. Vansant et al, Elsevier, Amsterdam, the Netherlands, 1997.

[63] M. Machida, K. Norimoto, T. Watanabe, J. Mater. Sci., 34, 1999, 2569.

[64] K. Guan, B. Lu, Y. Yin, Sur.Coat. Technol., 173, 2003, 219.

[65] K. Guan, H. Xu, B. Le, Nonferrous Met. Soc. China, 14, 2004, 2.

[66] A. Kanta, R. Seved, J. Ralston, Langmuir, 21, 2005, 2400.

[67] M. Nakamura, M. Kobayashi, N. Kuzuya, T. Komatsu, T. Mochizuka, Thin solid films, 502, 2006, 121.

[68] A. Barranco, F. Yubero, J. A. Mejı´as, J. P. Espino´s, A. R. Gonza´lez-Elipe, Surf. Sci., 482-485, 2001, 680.

[69] A. Trioli, M. Righettoni, S. E. Pratsinis, Langmuir, 25, 2009, 12578.

[70] S. Permpoon, G. Berthome, B. Baroux, J. C. Joud, M. Langlet, J. Mater. Sci., 41, 2006, 7650.

[71] J. Abad, C. Rogero, J. Me´ndez, M. F. Lo´pez, J. A. Martı´n-Gago, E. Roma´n, Surf. Sci., 600, 2006, 2696.

[72] A. Sasahara, C. L. Pang, M. Tomitori, J. Phys. Chem. C, 114, 2010, 20189.

CHAPTER 3

EXPERIMENTAL PROCEDURES

3.1 Sample preparation: vapor phase deposition of silicon oxides on TiO_2(110)

To fabricate epitaxially-grown thin films with well-ordered surface structures, physical vapor phase atomic layer epitaxy was developed by Sunlota in the late 1970's as a new coating technique [1]. Atomic layer epitaxy is a method for fabricating a thin film of single crystal, in general, composed of two components grown alternatively by one atomic layer. The source materials are supplied as atomic vapors of the components or as molecular vapors of volatile compound of them. Each component is alternatively supplied on the substrate with an interval time for completing the growth of one layer of each component, followed by pumping down the vapor of component. The atoms or molecules of the component in vapor phase are supplied until all available sites on the surface are occupied with them, that is, until one complete monolayer is formed. A condition necessary to the atomic layer growth is that the binding energy of the monolayer chemisorbed on the original surface is higher than that of the overlayer on the monolayer [1, 2]. The temperature of the substrate is a primary parameter to control the quality of the films. It is adjusted low enough to keep the monolayer remaining on the surface until the reaction with the following reactants takes place, but high enough to re-evaporate adsorbates on the top of the monolayer. As the difference in binding energy of each component on the monolayer from that on the subsequent layers becomes larger, the self-controlling of the process works well [2]. The epitaxy process has been generally distinguished into two types according to the chemical composition difference between substrate and deposited crystal. Homo-epitaxy when a crystalline film is grown on a substrate

of the same material, and hetero-epitaxy when the chemical component of the crystalline film is different from that of the subsurface [3].

The samples in this study were prepared from rutile TiO_2(110) wafers of a size of 20 × 22 × 0.3 mm with one side mirror-polished (Shinkosha) in following steps:

- Cleaning processes included ultrasonic washing in acetone for 5 min, etching in a HF (10 %) solution for 20 min, and rinsing in Milli-Q water. In some cases described later, a UV ozone cleaner (NL-UV253, Nippon Laser & Electronics Lab) was used to remove hydrocarbon contaminants on the substrate by reaction with ozone generated by UV light.

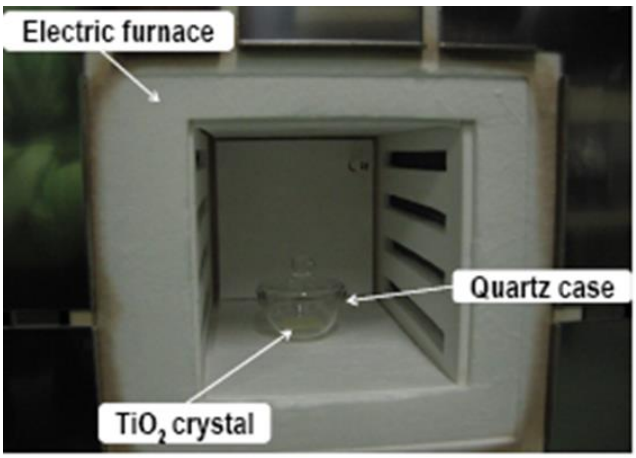

Fig. 3.1: Photo of an electronic furnace to anneal TiO_2(110) stored in a fused quartz container.

- In annealing processes, the TiO_2 substrate was stored in a sapphire container with a sapphire lid, or in a fused quartz container with a fused quartz lid, and subsequently the container was annealed at 1000 °C in an electric furnace (Muffle Furnace Model FO100, Yamato Scientific Co.,Ltd.) in air. The heater power was 1 kW and the maximum temperature was 1150 °C in a rise time from room temperature (RT) of about 60 minutes using a ceramic

fiber insulator of alumina and silica; the temperature was controlled to keep constant using a proportional-integral-differential (PID) feedback circuit with a micro-processor. The growth of silicon oxide films on the TiO_2 surfaces took place in the fused quartz case, annealed at 1000 °C in the electric furnace, although no growth of them in the sapphire case. Thus, silicon monoxide seemed to evaporate from the quartz case, transported and deposited on the TiO_2(110) surface in the quartz case, mentioned later in detail. This indicates that the quartz case act as a vapor source of silicon oxide. The vapor pressure of SiO at about 1000 °C is 10^{-3} Torr, while the same pressure is obtained at 1850 °C for SiO_2 according to Ref. 4.

3.2 X-ray photoemission spectroscopy (XPS) chemical analysis

Over the past few decades X-ray photoelectron spectroscopy (XPS) has developed into a key surface characterization method. Nowadays it is one of the most powerful surface analytical techniques in the area of thin films, capable to provide accurate quantitative elemental information on all elements except hydrogen, from which the quantitative compositions, the chemical states, and the film thickness are drawn [5, 6]. The principle of XPS is based on the photoelectric effect explained by Einstein in 1905; the concept of photon was introduced to describe the ejection of electrons from a surface when photons impinge upon it. This process can be expressed by the following equation:

$$BE = h\nu - KE - \emptyset \qquad (3.1)$$

Here, *BE* is the binding energy of the electron in the atom, and a function of the type of atom and its surrounding environment, $h\nu$ is the photon energy of X-ray source, *KE* is the kinetic energy of the emitted electron, and measured in the XPS spectrometer, and $\emptyset$ is the work

function of the spectrometer. A schematic diagram showing the principle of XPS is depicted in Fig. 3.2.

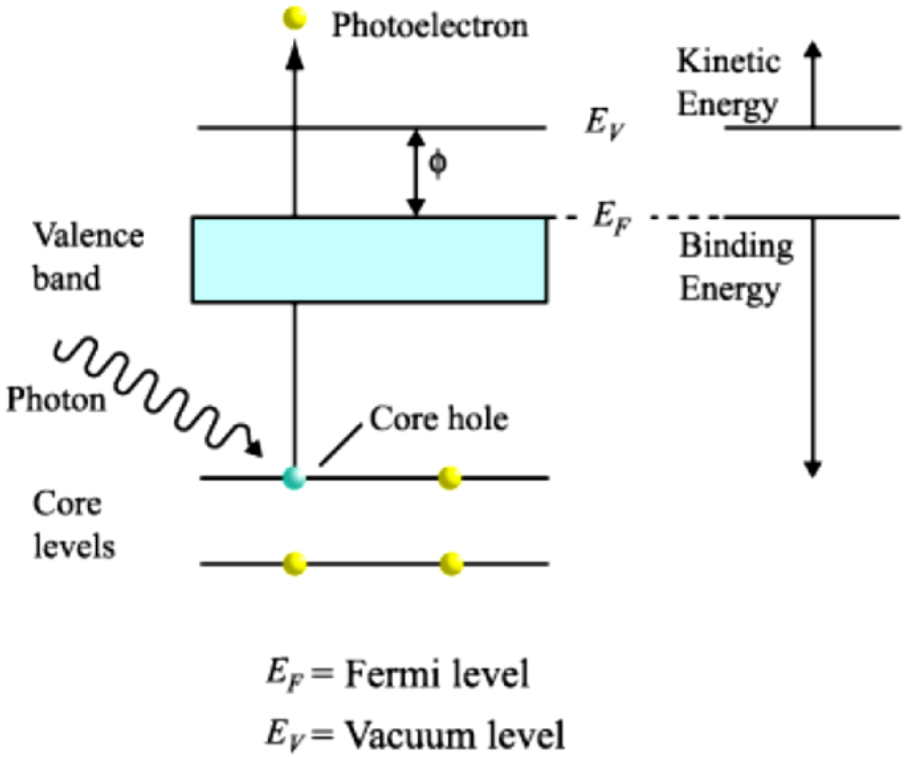

Fig. 3.2: Schematic of the principle of XPS

The XPS counts electrons ejected from a sample surface when irradiated by X-rays; an XPS spectrum represents the number of electrons detected at an energy with a narrow energy window, and the energy is swept over a range. The spectrum includes both a contribution from a background signal and peaks characteristic of the bound states of the electrons in the surface atoms. The peaks prominent from the background are the significant features in an XPS spectrum. XPS spectra are, for the most part, quantified in terms of peak intensities and peak positions. The peak intensities measure how much of a material is at the surface, while the peak positions indicate the elemental species. Other values are useful indicators of chemical state changes and physical influences. For instance, the broadening of

a peak often indicates a change in the number of chemical bonds contributing to the XPS peak, a change in the sample condition (e.g., X-ray damage) and/or differential charging of the surface (e.g., localized differences in the charge state of the surface) [5, 6].

An XPS spectrum with a narrow-range energy scan (termed narrow scan) gives detailed information of each element in a film; the chemical composition in the film can be evaluated from the area value of spectrum integrated over an energy range of the peak shape around the assigned elemental peak, taking into account the sensitivity factor for the element. Subsequently, the film thickness d can be evaluated using Beer-Lambert expression on the assumption that the thin film layer is uniform on the substrate as follows [7]:

$$I_F/I_S = S_F \{1-\exp(-d/ \lambda_F \cos \theta)\}/ S_S \exp(-d/ \lambda_S) \qquad (3.2)$$

Here, I_F and I_S are the peak intensities of the thin film element and substrate element, respectively, λ_F and λ_S are the attenuation lengths of the photo-emitted electrons in the film and the substrate, respectively, and S_F and S_S are the relative sensitivity factors of the thin film element and substrate element, respectively. θ is the photoemission angle with respect to surface normal.

In this study, XPS analysis was conducted using an XPS system (S-probe TM 2803, Fisons Instruments), installed in an UHV chamber with a base pressure of $3x10^{-8}$ Pa with a monochromatic Al Kα X-ray source. The photoemission angle θ with respect to surface normal was set to 35°. We reduced the surface charge of the insulating TiO_2 substrates with a neutralizer installed in the XPS system. The binding energy was referenced to C 1s peak at 284.6 eV. XPS measurements were performed to characterize chemical compositions of TiO_2(110) surfaces after identical cleaning treatment followed by different annealing

processes to reveal the change in contamination as well as absorbed components. In addition, the ultrathin film thicknesses were estimated using the above Beer-Lambert formula.

3.3 Low energy electron diffraction (LEED) structure analysis

Low-energy electrons (i.e., electrons with energies varying from 25 to 600 eV) are ideal probes for surface studies, because they are very easily scattered at surface atoms elastically and inelastically [8]. Hence, if the elastic scattered electrons escape out of the surface without absorption in the top two or three atomic layers, they can provide information on the atomic arrangement at the surface by forming a diffraction pattern owing to periodic ordering between the surface atoms.

In principle, the LEED experiment is rather simple: a mono-energetic electron beam hits the surface; because of the regular periodic arrangement of atoms, electrons are diffracted back in specific directions determined by the lateral periodicity on the surface. With electron energies typically in the range of 25-600 eV the de Broglie wavelength $\lambda = h \Big/ \sqrt{2m_e E}$ (m_e is the electron mass, h is the Planck constant) varies in the range of 2.5-0.5 Å, which is comparable to interatomic distances. This leads to large diffraction angles with usually well-separated diffraction spots on a phosphor screen placed in front of the sample surface [9]. Due to the strong multiple inelastic scattering caused by plasmon excitations the electrons penetrate only a few layers from bulk to the surface. This makes LEED surface sensitive, and consequently provides high precision for determination of the full surface structure such as all atomic coordinates in the surface [10, 11].

For a crystalline surface the diffraction maxima appear at angle α_m according to

$$\sin \alpha_m = m * \lambda/a \quad (3.3)$$

With λ is the wavelength of incident electron, *a* is the lattice constant, and *m* is an integer. The diffraction maintains the incident wave vector of the length $k=2\pi/\lambda$, and a parallel component is expressed as $k_{||} = k * \sin \alpha_m$, which is transformed to the following equation by use of eq. 3.3,

$$k_{||} = m * \frac{2\pi}{a} = m * g \quad (3.4)$$

Here, $g = 2\pi/a$ is the reciprocal lattice constant. For two dimensions the latter becomes vectors $\mathbf{g_1}$ and $\mathbf{g_2}$, the linear combination with multiples of which describe the two-dimensional periodicity of diffraction spots on the screen. They define the so-called reciprocal unit mesh. This is because its size and shape are reciprocal to those of the real space unit mesh of the surface defined by vectors $\mathbf{a_1}$, and $\mathbf{a_2}$. With $\boldsymbol{n}$ the unit vector normal to the surface and $A_g = |\boldsymbol{g_1} \times \boldsymbol{g_2}|$, which is the area of the reciprocal unit mesh, the relations $\boldsymbol{a_1} = 2\pi(\boldsymbol{g_2} \times \boldsymbol{n})/A_g$ and $\boldsymbol{a_2} = 2\pi(\boldsymbol{n} \times \boldsymbol{g_1})/A_g$ hold. Using these relationship and the LEED pattern, the information on the size and the shape of the surface unit mesh can be drawn [7, 9, 10].

In this study, a LEED system (SPECTALEED, Omicron), which is installed in a homemade UHV chamber with a base pressure of 2×10^{-7} Pa, was used to reveal the surface crystalline periodicity of the TiO_2(110)-(1×1) surfaces with/without silicon oxide layers grown on them.

3.4 Frequency-modulation atomic force microscopy (FM-AFM) imaging

So far, atomic force microscopy (AFM) has provided a large number of advantages over conventional microscopy techniques. The AFM probes the force between a sharpened tip and a sample; by keeping the force constant and scanning the tip over the sample surface, it can depict the topography of the sample and measure physical quantities three-dimensionally, i.e., x, y and z direction in a Cartesian coordinate system, over the sample surface. At present the resolution of AFM can achieve ranges of 0.1 to 1.0 nm in the x-y plane and 0.01 nm in the z direction. The AFM requires neither a vacuum environment nor any special sample preparation, and can be used in either an atmospheric or liquid environment. With these advantages the AFM has significantly impacted the fields of materials science, chemistry, biology, and physics [12, 13].

The frequency modulation (FM)-AFM, a highly sensitive AFM technique, is commonly used for atomic resolution imaging. In contrast to a conventional static mode AFM, the FM-AFM is a dynamic technique where the cantilever is used as a mechanical resonator in a self-oscillation circuit so that the cantilever vibrates at its resonance frequency (f) with a constant oscillation amplitude. The frequency shift (Δf) of the cantilever induced by a weak force between the tip and the sample, is detected and used for feedback to control the tip-sample separation to be constant while scanning over the surface, leading to imaging the surface topography. This method is extremely sensitive to a small change in the force, and can stably depict individual atoms on the surface while avoiding tip-sample contact. In addition, the dissipation involved in the tip-sample interaction can also be measured by monitoring the driving voltage needed to keep the oscillation amplitude constant that may damage the tip and

the sample. This approach enables a highly sensitive force feedback control, and separates out the conservative and dissipative components of the interaction force [12].

In this study, FM-AFM imaging to detect a weak force between a tip and a sample was conducted in Milli-Q pure water using a multipurpose scanning probe microscope (SPM) (5500, Agilent) [14]. The photograph and block diagram of this system, which was slightly changed from the standard commercial system in our lab, are shown in Fig.3.3.

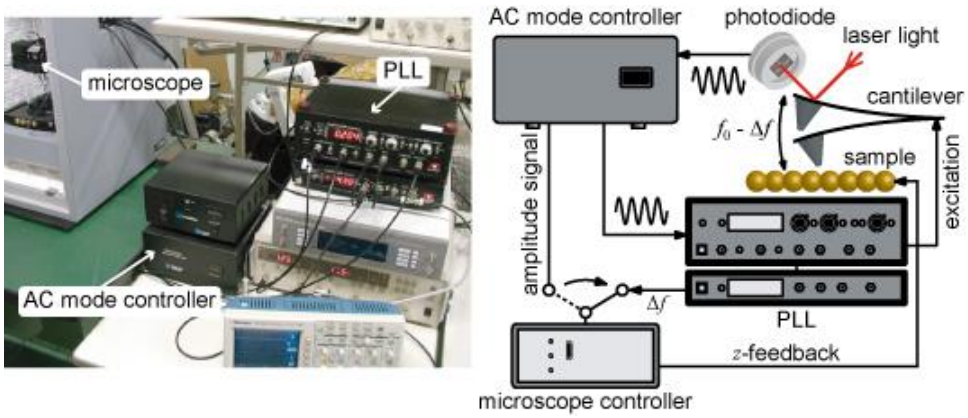

Fig. 3.3: Photograph and schematic diagram of the FM-AFM system

The oscillation of an AFM cantilever was controlled by an FM detector and control system (easyPLL plus Detector and easyPLL plus Controller, Nanosurf); the cantilever was oscillated with its resonant frequency (f_0) and the frequency shift (Δf) signal output from the detector was fed into the input of microscope controller in place of the amplitude signal used in the intermittent contact mode of the SPM. The f_0 and the quality factor Q of a silicon cantilever in pure water were ~70 kHz and ~70, respectively. The oscillation amplitude was estimated to be 4 nm peak to peak. FM-AFM images were processed using a freeware SPM program [15]. In general, the FM-AFM images observed in water supply the surface morphology with

a spatial resolution better than that in air, because the cleanliness of the tip and the sample is probably kept in water much better than that in air.

3.5 Water contact angle measurement

According to the circumstances, in general, a fluid drop on a surface spreads over the surface or forms a truncated spherical ball; if the fluid is water, the nature of fluid is termed hydrophilic or hydrophobic, respectively. The contact angle of a fluid on a solid surface is defined as the angle between the tangent to a profile of the fluid drop and the tangent to the surface at the point of meeting between the atmosphere, the fluid, and the solid [17, 18].

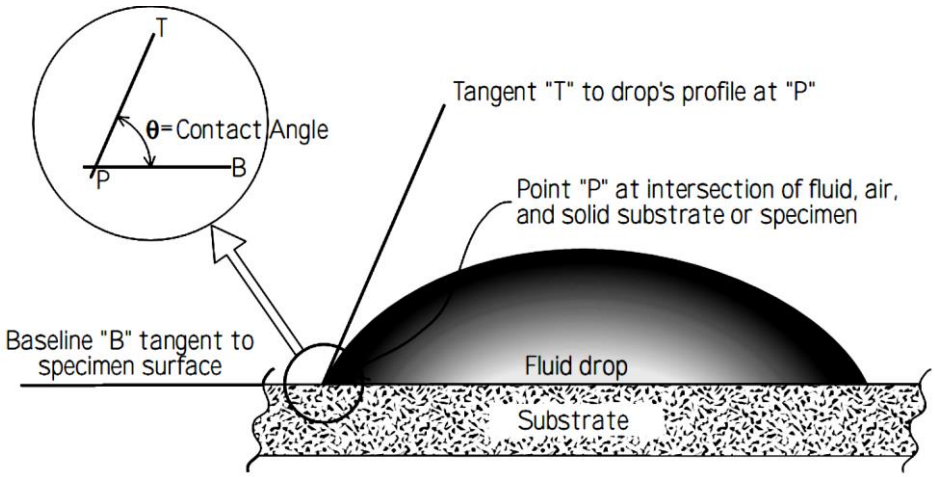

Figure 3.4: Schematic of a contact angle of a fluid drop on a surface [17]

The contact angle is measured under a thermodynamic equilibrium between the three phases: the liquid phase of the fluid drop, the solid phase of the substrate, and the gas/vapor phase of the ambient [16-19]. Under the equilibrium conditions, the chemical potentials in the three phases should be equal. In other words, the contact angle can be regarded as a result of the interface/surface free energies (or surface tension) between the liquid and the solid

surrounded by vapor, and the relationship can be expressed by the Young equation. Physical and chemical properties of interaction between the solid and the liquid concerning wettability, affinity, adhesiveness, and repellency as well as roughness and cleanliness of a solid surface can be evaluated through contact angle measurement. Among some of classifications, contact angle measurement can be categorized to two groups: contact angle goniometry (CAG) and contact angle tensionmetry (CAT). The CAG is to place a drop of water (or other liquid) into contact with the surface, and the angle between the surface and the liquid droplet is measured. In this study, the contact angle measurement was carried out to show the change in surface wettability of TiO_2(110) surfaces after some treatments.

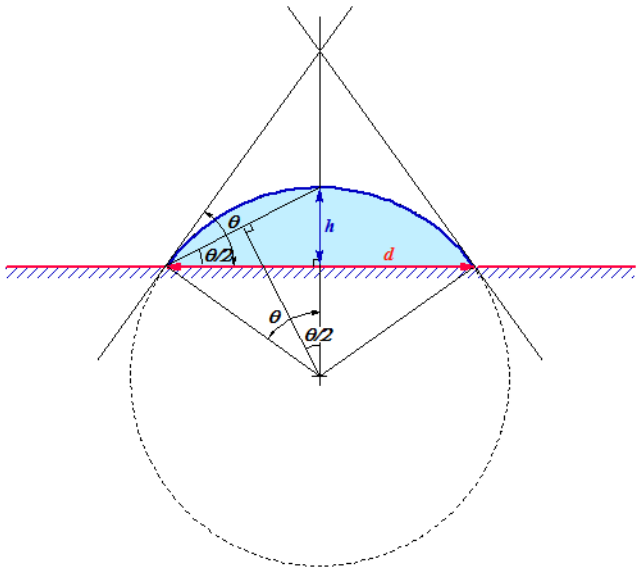

Figure 3.5: Geometry of a contact angle and a truncated spherical droplet

A home-made setup with a three-dimensional mechanical stage, a micro-syringe and a microscope equipped with a compact digital camera was used to measure contact angle, and a half-angle principle given below was adopted to determine the angle [17, 19]:In this method the contact angle θ is given by the following equation:

$$\theta = 2\tan^{-1}(2h/d) \quad (3.5)$$

Where h is the height of a droplet, and d is the diameter of circle of the droplet on the surface. In Fig. 3.5 the contact angle is an angle between a straight line connecting the left and the right ends and a straight line connecting the apex of the droplet and the center of the circle, which is extrapolated from the spherical outline of the truncated drop. The effect of gravitational force can be ignored for a small quantity of droplet; a volume of droplet was 2 µl in this study. The contact angle was measured from a photo of the droplet on the surface using GIMP 2 software [20].

References

[1] K. J. Wynne and R. W. Rice, Ann. Rev. Mater. Sci., 14, 1984, 297.

[2] E. F. Vansant, P. V. D. Voort, K. C. Vrancken, Elsevier Science, Amsterdam, 1995, 450.

[3] S. M. Sze, Semi. Dev., Phys. Technol. B, 3, 1985, 1233.

[4] T. Carlberg, J. Electrochem. Soc.: Solid-State Sci. and Technol., 133, 1986, 1940.

[5] H. M. Choi and S. K. Choi, J. Vac. Sci. & Technol. A, 13, 1995, 2832.

[6] A. Thomson, J. Vac. Sci. & Technol. A, 11, 1974, 666.

[7] P. Mack, R. G. White, J. Wolstenholme, T. Conard, Appl. Surf. Sci., 252, 2006, 8270.

[8] M. A. Van Hove, W. H. Weinberg, C. M. Chan, Springer, 1986, Germany.

[9] H. Luth, Springer, Heidelberg, 1995.

[10] G. M. Gavaza, Z. X. Yu, L. Tsang, C. H. Chan, S. Y. Tong, M. A. Van Hove, Phys. Rev. B, 75, 2007, 014114.

[11] http://en.wikipedia.org/wiki/Low_energy_electron_diffraction.

[12] C. J. Chen, Oxford, New York, 2008.

[13] F. J. Giessibl, Rev. Mod. Phys., 75, 2003, 949.

[14] A. Sasahara and M. Tomitori, J. Vac. Sci. Technol. B, 28, 2010, 3.

[15] I. Horcas et al. Rev. Sci. Instr., 78, 2007, 013705.

[16] Julio Pellicer, Jose A. Manzanares, and Salvador Mafe, Am. J. Phys., 63, 1995, 6.

[17] Robert J. Good, J. Adhe. Sci. Tech., 6, 1992, 12.

[18] D. Y. Kwok, A. W. Neumann, Advances in Col. and Inter. Sci., 81, 3, 1999, 167.

[19] Dory Cwikel, Qi Zhao, Chen Liu, Xueju Su, and Abraham Marmur, Am. Chem. Soc., Langmuir, 26, 2010, 15289.

[20] http://www.gimp.org/

CHAPTER 4

STRUCTURAL AND COMPOSITIONAL ANALYSIS OF SILICON OXIDE LAYERS ON RUTILE TiO_2(110)

Titanium dioxide is a photocatalytic material widely used for many industrial products utilizing its optical, electrical, and chemical properties [1-3]. Among the properties, the super-hydrophilicity of TiO_2 is noticeably attractive, exhibiting a small contact angle ($\theta \leq 5^o$) of a water droplet on the surface. This is an intrinsic property of UHV-annealed TiO_2 [4], and also emerges when TiO_2 is irradiated with UV light. The mechanism of this phenomenon is explained that water molecules adsorb at the oxygen vacancies of the TiO_2 surfaces and dissociate into OH and H, resulting in an increase in the surface hydroxyl groups of the TiO_2 surfaces. In general, the high wettability of TiO_2 surfaces gradually disappears when they are placed in dark [8]. Recently, it was reported that the structure modification of TiO_2 improved its hydrophilic performance; the SiO_2-TiO_2 composite system is the one with the hard and stable SiO_2 layer and catalytic TiO_2 layer to extend the lifetime of super-hydrophilicity even in dark. However, the understanding of the property is insufficient owing to the lack of techniques that fabricate a homogeneous film of SiO_2-TiO_2 on a nano-scale to carry out a control experiment. Thus, we conduct a conventional vapor phase preparation method to deposit a uniform layer of silicon oxide on TiO_2 single crystal and analyze them. FM-AFM observation visualizes surface morphologies at a nano scale. The deposition amounts of Si on the surface are characterized by XPS. LEED patterns are observed to determine the change in surface periodicity.

4.1 Annealing temperature effects of the growth observed by FM-AFM

Initially, FM-AFM operated in water was used to observe the surface morphology of samples. Fig. 4.1 shows typical FM-AFM images of a rutile TiO_2(110) substrate washed in acetone, and etched in HF solution in a wide scanning range with line profiles. The surfaces look flat but covered with some protrusions. From the profiles the roughness of sample etched in HF solution seems higher than that of washed one in acetone. It is likely attributed the erosion of HF solution on the TiO_2(110) surface. The chemical cleaning process is thought to remove most of organic contaminations and metallic purities on the sample. This was also confirmed in XPS analysis as shown later. However, the flatness of surfaces is not enough in atomic scale analyzing after this cleaning process.

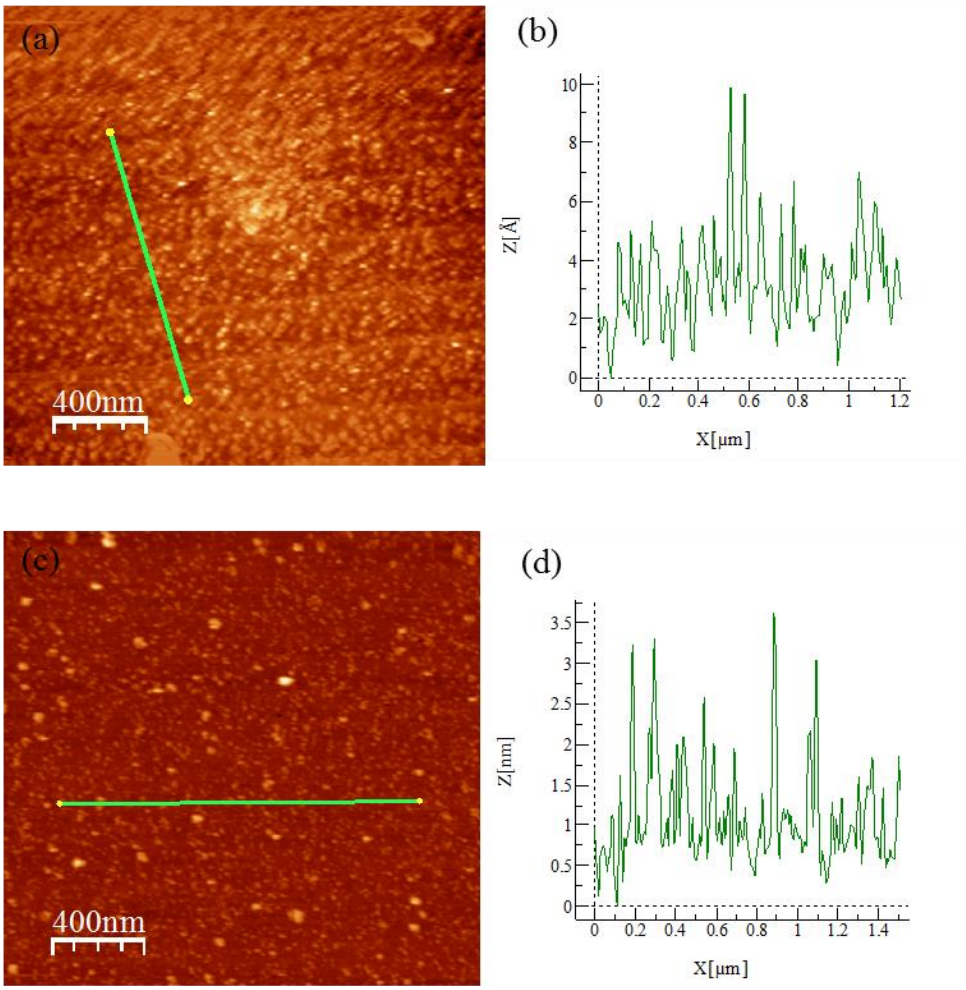

Figure 4.1: FM-AFM images of a rutile TiO_2(110) substrate. (a) After ultrasonically washed in acetone. (b) Cross section along a solid line in (a). (c) After etched in HF solution. (d) Cross section along a solid line in (c).

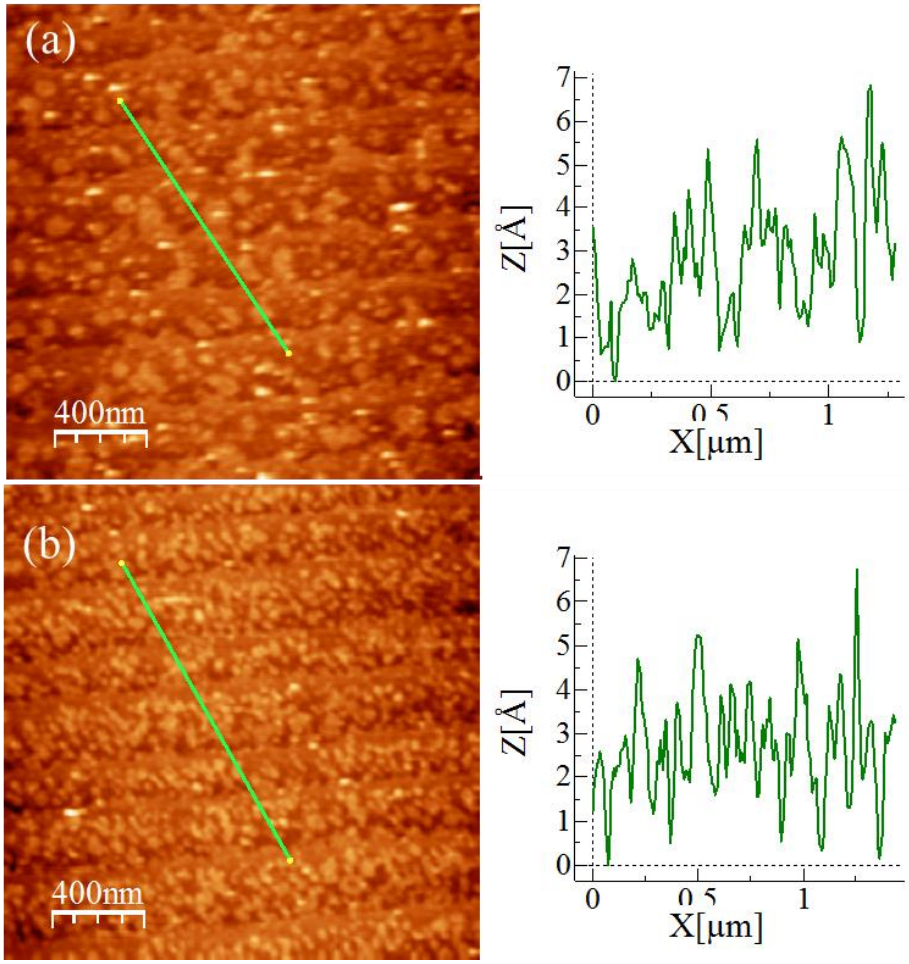
(a)
400nm
Z[Å]
X[μm]
(b)
400nm
Z[Å]
X[μm]

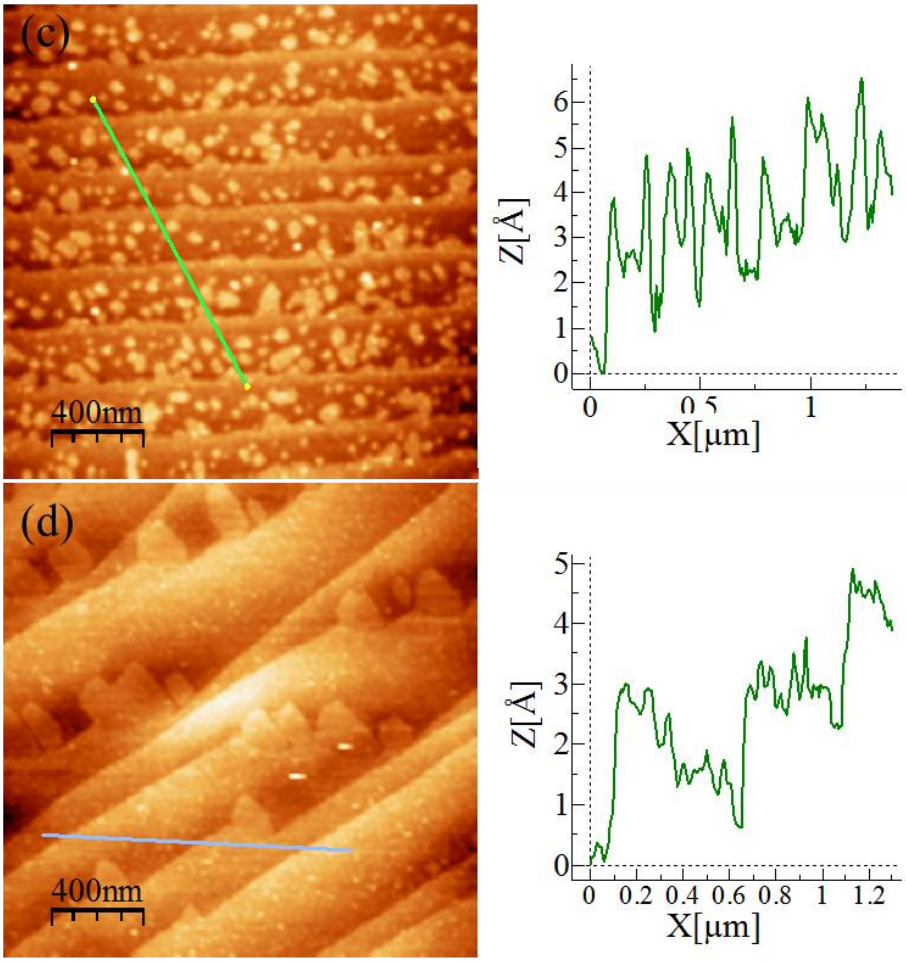

Figure 4.2: FM-AFM images of rutile TiO_2(110) substrates annealed for 6 hours in a quartz container and cross sections along the solid lines in each image. (a) at 600 °C, (b) at 700 °C, (c) at 800 °C, and (d) at 1000 °C.

Next, TiO_2(110) surfaces was analyzed after annealing in a quartz container. The constant frequency shift topography and their profiles of annealed TiO_2 surfaces in the quartz container at different temperatures were shown in Fig. 4.2. After annealing for 6 hours the terrace/step structures were found more clearly with increasing annealing temperature. For samples annealed above 800 °C the step heights were perspicuously observed as around 0.3 nm, e.g., as depicted in Fig. 4.2(c). Since the bright spots increased in number and size, those are

possibly attributed to deposited silicon oxide or contamination segregated from bulk during annealing, as shown in Fig. 4.2 (a) – (c). We estimate that bright spots grown along the step lines on the lower terraces are silicon oxide, because those were grown preferentially from the step edges and increase with increasing annealing temperature. For the sample annealed at 1000 ºC patch structures were found. Those are possibly assigned to silicon oxide, as the XPS analysis shown later. Thus, for the further experiments, we fixed the annealing temperature to 1000 ºC and changed the annealing time. The temperature rising process in this study for comparison of different annealing time was shown below:

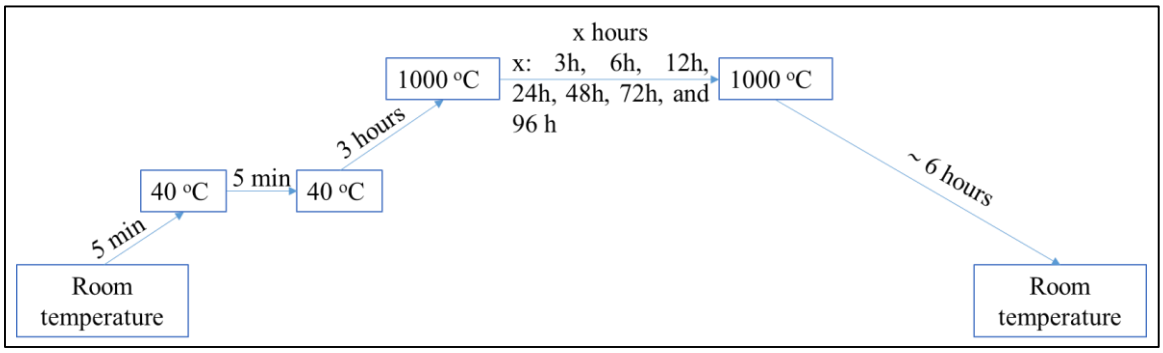

Figure 4.3: A scheme of annealing process in ambient

4.2 XPS analysis results and discussion

To characterize the elemental composition of as-received, chemically cleaned, air-annealed TiO_2(110) surfaces, we performed XPS analysis in wide energy scan ranges as well as in narrow energy scans for Ti 2p, O 1s, and Si 2p core level. The XPS analysis was conducted using an XPS system (S-probe TM 2803, Fisons Instruments), described in chapter 3 in detail.

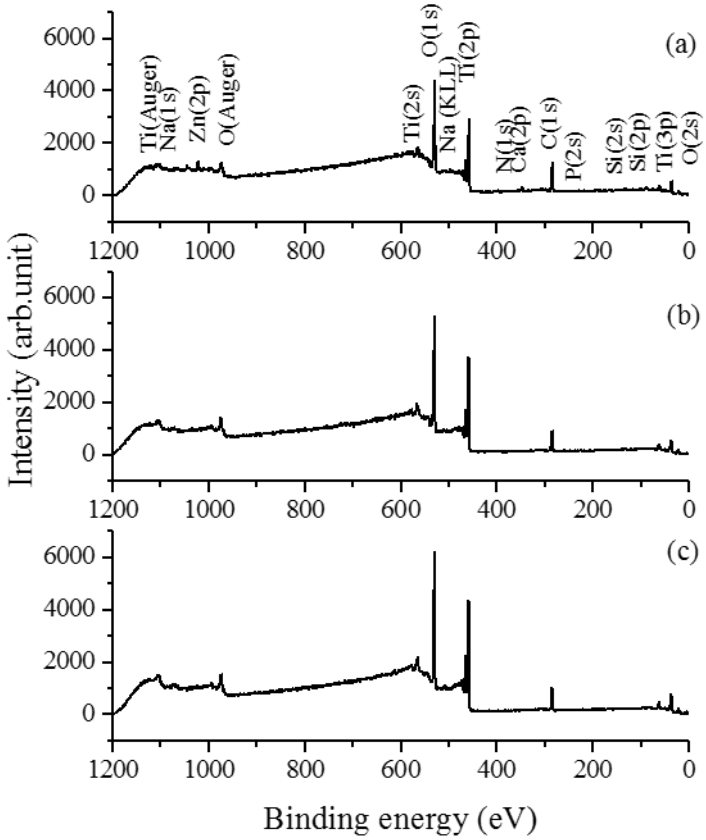

Figure 4.3: Wide-scan XPS spectra of a rutile TiO_2(110) substrate. (a) As-received. Impurity peaks were detected as assigned. (b) After ultrasonically washed in acetone. (c) After etched in HF solution.

A wide-scan XPS spectrum for a rutile TiO_2(110) substrate as received is shown in Fig. 4.3(a). The intense peaks at about 460 eV and 530 eV correspond to Ti 2p and O 1s, respectively. In addition to the Ti 2p and the O 1s peaks, peaks for C, Na, Si, P, Ca, and Zn were observed, as typical impurities contained in TiO_2 crystals. After the substrate was ultrasonically cleaned in acetone and subsequently etched in HF (10 %) solution, the XPS spectra are shown in Fig. 4.1(b) and (c), respectively. The contamination peaks maintained after acetone washing, but disappeared after HF etching. This was reasonable, since acetone

can only remove organic impurities, while HF solution plays a key role in removing most of intrinsic metal contaminations of TiO_2 crystal. The impurities are removed by the HF pretreatment except for C. The presence of C is attributed to organic contaminants from the laboratory air. After chemical cleaning (Fig. 4.3(b) and (c)), O 1s peak increased and C 1s peak decreased, indicating that the surfaces became cleaner than the as-received state.

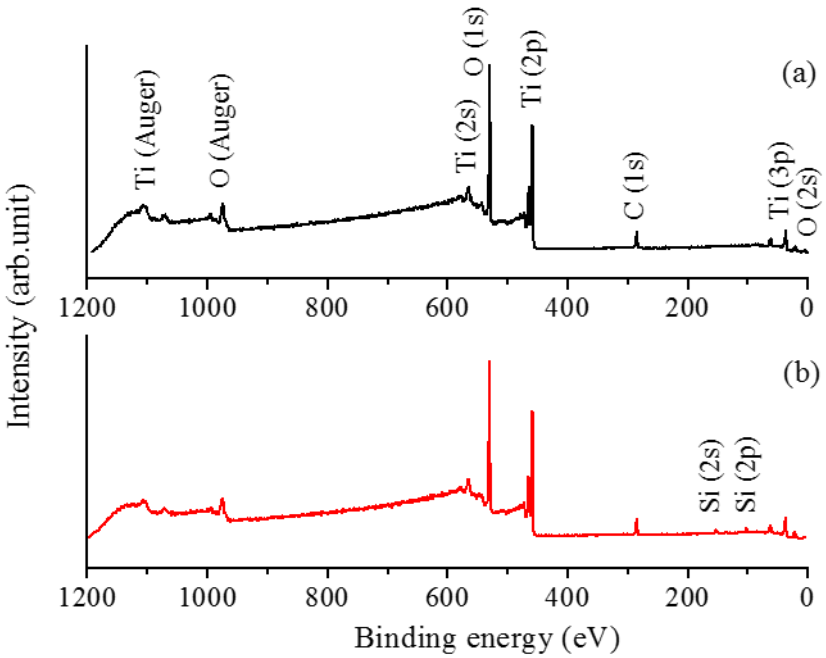

Figure 4.4: Wide-scan XPS spectra of a rutile TiO_2(110) substrate. (a) After annealed in a sapphire container at 1000 °C for 6 hours. (b) After annealed in a quartz container at 1000 °C for 6 hours, where Si peaks were identified.

The TiO_2 substrate was annealed in the sapphire container or in the quartz container at 1000 °C for 6 h, wide-scan XPS spectra were obtained as shown in Fig. 4.4(a) and (b), respectively. In the wide range XPS spectra, we found Si 2p and 2s peaks for the substrate annealed in the quartz container but no Si peaks for that similarly annealed in the sapphire container. Thus, it is drawn that Si evaporates from the quartz container during annealing and adsorbed on the

TiO_2 surface. It means that the quartz container can act as a silicon oxide source of the vapor phase silicon oxide deposition in ambient condition.

Consequently, we further focused on annealed TiO_2(110) surfaces in the quartz container with varying annealing time. We scanned the narrow energy ranges of XPS around Ti 2p, O 1s, and Si 2p peaks on the TiO_2 substrate annealed in the quartz container, as shown in Fig. 4.5(a)-(c) for varying annealing time. In Fig. 4.5(a) for Ti 2p, two peaks were observed at 458.7 eV and 464.6 eV, which correspond to Ti $2p^{3/2}$ and Ti $2p^{1/2}$, respectively [9, 10]. The binding energy and peak shape did not change with increasing annealing time. It is possibly indicated the number of oxygen vacancy in the top layer of annealed TiO_2(110) surfaces is inconsiderable.

The spectra of the O 1s region taken around 530 eV with high binding energy shoulder, as shown in Fig. 4.5(b). The shoulder became more intense with the annealing time. The peak was deconvoluted into three components as shown in Fig. 4.5(c): the major peak from bulk TiO_2 at 529.9 eV (hereinafter denoted by O_{TiO2}), the second component at 530.9 eV, and the third component at 531.9 eV.

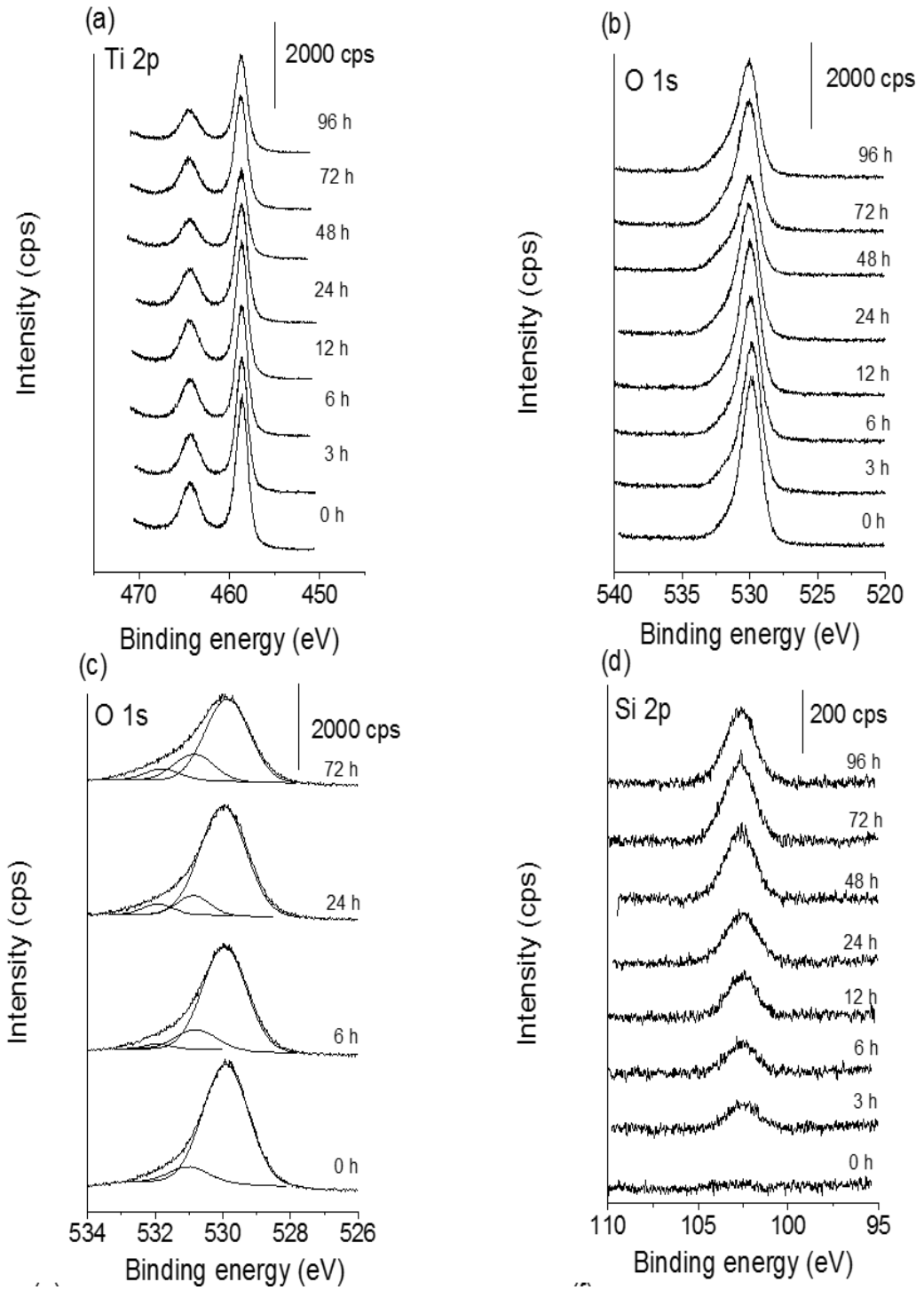

Figure 4.5. Narrow-scan XPS spectra (a) Ti 2p, (b-c) O 1s, and (c) Si 2p regions obtained on the identical TiO_2 surface annealed in the quartz container.

The second and the third components are assigned to OH group [9, 11] and silicon oxide SiO_x ($x \leq 2$), [10-12] respectively. The O giving rise to the peak at 531.9 eV is designated hereafter as O_{SiOx}. The growth of the shoulder indicates the increase of the OH groups and the SiO_x on the surface. The intensity ratio of the component from the OH group with respect to the total O 1s peak was 0.10 on the non-annealed surface and increased to 0.38 on the 72 hours annealed surface. The binding energy of the O_{SiOx} peak was higher than that of the O_{TiO2} peak by 2.0 eV. While the O 1s binding energy of the quartz is higher than that of the rutile TiO_2 by 2.9 eV [13], the O 1s peak of the stishovite SiO_2 (SiO_2 in the rutile structure) appears at the binding energy lower than that of the quartz by 0.8 eV [14]. Therefore, the binding energy of the O_{SiOx} peak is almost identical to that of the O atoms in the stishovite SiO_2, which indicates the formation of the stishovite SiO_2 layer on the TiO_2(110) surface. Note that, in the natural world, under a pressure as high as 10 GPa at temperatures higher than 1273 K, silicon dioxide forms a rutile structure, as stishovite, composed of six-fold coordinated Si, i.e., surrounded with six oxygen atoms.

The peak energy of Si 2p was found around 102.5 eV, as shown in Fig. 4.5(d). The peak height of Si 2p increased with annealing time but remained almost the same after the sample was annealed for 72 hours or more. In comparison to values of Si oxidized states reported in ref. 10, the peak is ascribed to Si^{3+} or Si^{4+} ion. The dependence of the Si/O_{TiO2} atom ratio on the annealing time is shown in Fig. 4.6(a).

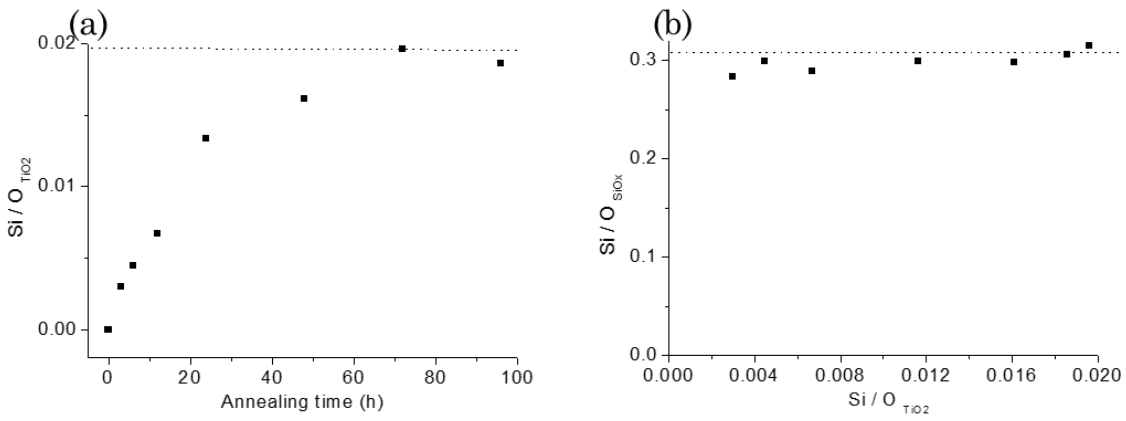

Figure 4.6: (a) Dependence of Si / O_{TiO2} at atom ratio on the annealing time. (b) Si/O_{SiOx} peak atom ratio on TiO_2(110) surfaces with respect to Si /O_{TiO2} ratio ratio.

The Si/O_{TiO2} atom ratio increased with the annealing time, and remained at 0.019 on the surfaces annealed longer than 72 hours. This indicates that the growth of the stishovite SiO_2 layer on the TiO_2(110) surface is self-limited as that on the TiO_2(100) surface [9]. Fig. 4.6(b) shows the plots of the Si/O_{SiOx} atom ratio as a function of the Si/O_{TiO2} atom ratio. The Si/O_{SiOx} atom ratio was 0.31 independently to the Si/O_{TiO2} atom ratio. The Si/O_{SiOx} atom ratio, $I_{Si}/IO_{(SiOx)}$, is related to the density of Si and O_{SiOx} atoms, n_{Si} and n_{SiOx}, by the following equation:

$$\frac{I_{Si}}{I_{O(SiOx)}} = \frac{n_{Si}\sigma_{Si}\lambda_{Si}}{n_{SiOx}\sigma_{O}\lambda_{O}} \quad (4.1)$$

σ_{Si} and σ_O are the photoemission cross sections of Si 2p3/2 and O 1s peaks and are 0.54 and 2.9, respectively [15]. λ_{Si} and λ_O are the inelastic mean free paths (IMFPs) of Si 2p3/2 and O 1s photoelectrons in SiO_2 and are 3.8 and 2.8 nm, respectively [16]. Assuming that the 2/3 of the I_{Si} is from the Si 2p3/2, the Si/O_{SiOx} atom ratio is calculated to be 0.32. The ratio is acceptable for the stishovite SiO_2 at the topmost layer. A part of the O 1s peak assigned to

the OH group is presumably coordinated to Si atoms. Combined with the fact that the binding energy of the O_{SiOx} peak was independent to the Si coverage, the stishovite SiO_2 is formed from the early stage of the SiO_x evaporation.

The thickness of the stishovite SiO_2 layer was estimated on the assumption that the intensity of the photoelectron peak is attenuated in the uniformly grown layer according to the Beer-Lambert law [17]:

$$\frac{I_{Si}}{I_{Ti}} = \frac{I_{0Si}\{1-\exp(-d/\lambda_{Si}\cos\theta)\}}{I_{0Ti}\exp(-d/\lambda_{Ti}\cos\theta)} \quad (4.2)$$

Here, I_{Si} and I_{Ti} are the peak intensities of Si 2p and Ti 2p3/2. I_{0Si} and I_{0Ti} are the intensities of the Si 2p peak from bulk SiO_2 and the Ti 2p3/2 peak from bulk TiO_2. The factory-provided relative sensitivity factors modified by the atom densities and the IMFPs, 1.9 for the Si 2p and 2.1 for the Ti 2p3/2, were used in place of the I_{0Si} and the I_{0Ti}. λ_{Ti} is the IMFP of the Ti 2p3/2 photoelectrons in SiO_2 and is 3.0 nm from Ref. 16. The thickness d of the SiO_2 layer was calculated to be 0.20 nm for the TiO_2 wafer annealed for 72 hours. The single step height on the stishovite SiO_2(110) surface is expected to be 0.30 nm from the crystal structure. Hence, the estimated d indicates that the growth of the stishovite SiO_2 layer is limited to a monolayer.

In conclusion here, using XPS analysis, it is possible that silicon oxide from the quartz container can be adsorbed on TiO_2(110) surface using simply vapor phase deposition method in air.

4.3 Structural analysis by LEED

The LEED analysis was conducted to determine the atomic long range order of chemically cleaned, and annealed TiO_2(110) surface in the sapphire container or in the quartz container. For chemically cleaned surfaces, the LEED image showed only a uniform background, indicating the absence of crystallographic order.

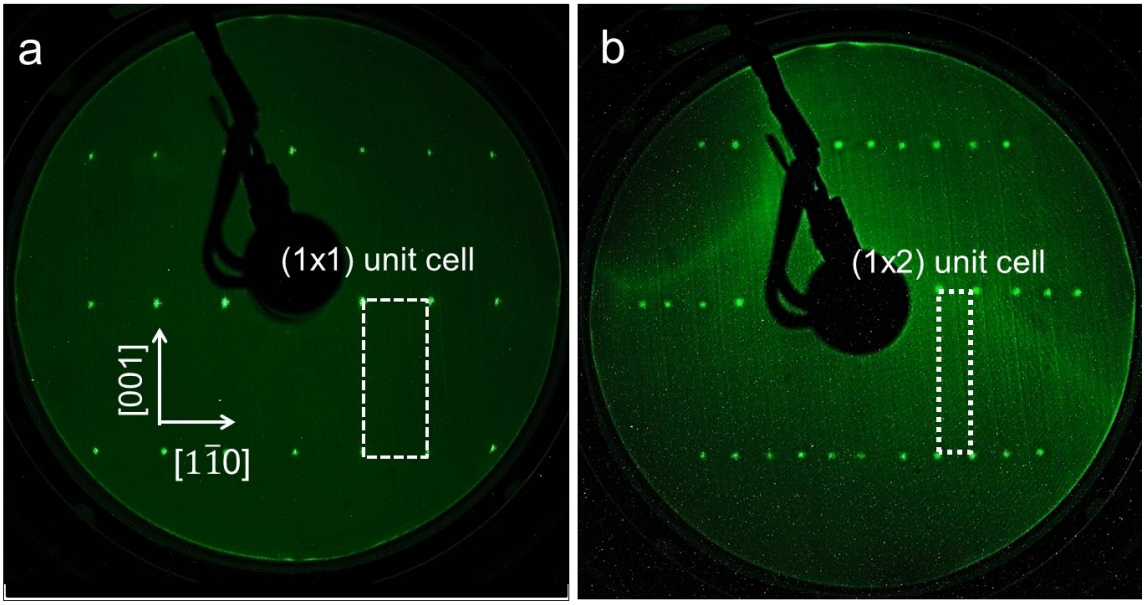

Figure 4.7: LEED patterns of TiO_2(110) surfaces annealed at 1000 °C (a) in the sapphire container for 6 hours, and (b) in the quartz container for 72 hours. Incident electron energy; (a) 120 eV, (b) 140 eV.

It indicated that the erosion of HF solution accelerated the roughness of as-received TiO_2(110) surface. After that, the LEED patterns of the TiO_2 surfaces annealed at 1000 °C in the sapphire container and in the quartz container were observed without any treatments after annealed. Figure 4.7(a) shows a (1×1) pattern for the sample annealed for 6 hours in the sapphire container; the extension of annealing time did not change the LEED pattern. It is noted that the ordered TiO_2(110) surface can be attained by simply annealing in an atmospheric

environment instead of complicated process involved sputtering and annealing in UHV and then re-annealing in oxygen environment [18]. Fig. 4.7(b) shows the LEED pattern observed on the stishovite SiO_2 monolayer prepared by 72 hours annealing of the TiO_2 substrate. A sharp (1×2) pattern was observed, which indicated long range order of the SiO_2 surface atoms with the double periodicity along the $[1\bar{1}0]$ direction of the TiO_2 substrate. The substrate-related periodicity suggests the epitaxial growth of the SiO_2 on the TiO_2(110) surface, which reinforces the formation of the stishovite SiO_2. The length of the Si-O bond in the stishovite is 0.18 nm and is smaller than that of the Ti-O bond in the rutile TiO_2 by 9% [14]. The stishovite SiO_2 layer is probably strained due to the lattice mismatch, which causes the limited growth. The strain may be reduced by a periodic relaxation of the surface atoms in the $[1\bar{1}0]$ direction to show the (1×2) periodicity.

4.4 Surface topography imaged by FM-AFM

According to the LEED patterns of annealed TiO_2(110) surfaces in the sapphire container or the quartz container, the crystalline orders of the TiO_2 and the adsorbed silicon oxide on TiO_2 were displayed. In order to receive the comprehensive surface geometry, FM-AFM was used to observe these surfaces at a nano scale. The FM-AFM was operated in Milli Q-water in air to improve their spatial resolution. Fig. 4.8 shows the typical FM-AFM images of samples annealed in the sapphire container for 6 hours, and in the quartz container with increasing annealing time.

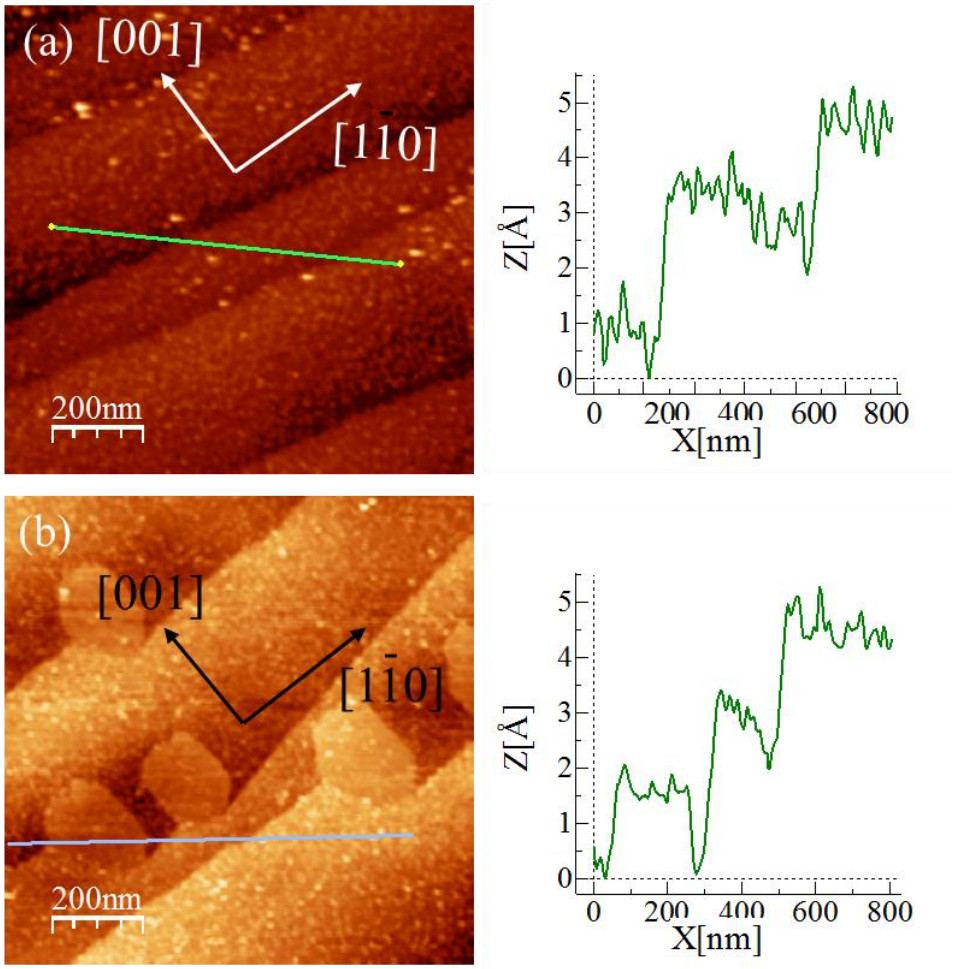
(a) [001]
[1$\bar{1}$0]
200nm
Z[Å]
X[nm]
(b)
[001]
[1$\bar{1}$0]
200nm
Z[Å]
X[nm]

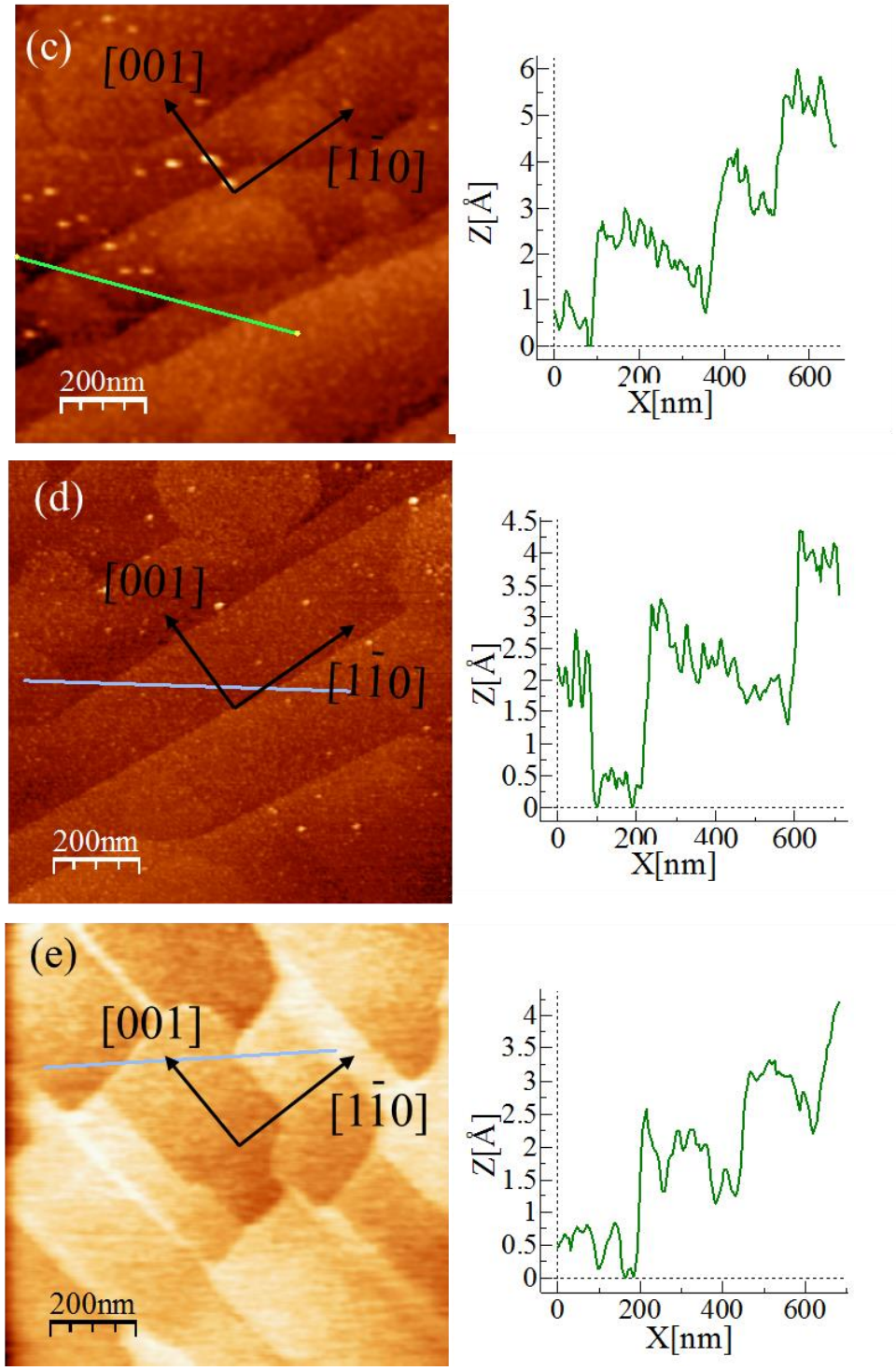

Figure 4.8: FM-AFM images and cross sections along the solid lines in the images of TiO_2(110) surfaces (1000×1000 nm^2) (a) annealed in the sapphire container for 6 hours at a frequency shift (Δf) = +193 Hz, and annealed in the quartz container (b) for 6 hours, Δf = +170 Hz; (c) for 12 hours, Δf = +219 Hz; (d) for 24 hours, Δf = +356 Hz; (e) for 48 hours, Δf = +248 Hz.

The surfaces with consecutive terrace/step structures were observed in all annealed surfaces. The flat surfaces with terrace/step structure could be formed during annealing in air. Fig. 4.8(a) shows the FM-AFM images of the TiO_2(110) surface annealed in the sapphire container for 6 hours. The surface consisted of flat terraces separated by steps nearly parallel to the $[1\bar{1}0]$ direction. The height of the steps was 0.3 nm and was roughly consistent to that of the single step of the (110) surface, 0.32 nm. No appreciable change was observed in surface topography by extending the annealing time up to 48 hours. Fig. 4.8(b-e) shows the FM-AFM images of the TiO_2 surfaces annealed in the quartz container for 6, 12, 24, and 48 hours, respectively. Patches with a height of 0.2 nm appeared after 6 hours annealing as shown in Fig. 4.8(b). The patches were attached to the step edges and appeared growing from the steps. The area of the patches increased after 24 hours annealing as shown in Fig. 4.8(c-d). The surface appeared completely covered by the rectangular patches elongated to the [001] direction after 48 hours annealing as shown in Fig. 4.8(e). The patches are assigned to the stishovite SiO_2 layer grown on the TiO_2 surface. The saturation of the Si/O_{TiO2} XPS atom ratio and the clear (1×2) in LEED pattern were obtained on the patch-covered surfaces. The patch height of 0.2 nm was consistent to the thickness of the stishovite SiO_2 monolayer estimated from the XPS peak intensity.

The constant frequency shift topographies and their profiles of 48 hour annealed TiO_2(110) in the quartz container were focused in more detail. With 48 hour annealing or more, the TiO_2(110) surface was possibly almost covered with silicon oxide. This is illustrated in Fig. 4.8 (e) with the height difference among adjacent rectangular patches of 0.2 nm. The alternating bright and dark lines elongated along the [001] direction in a close-up scanning area of (50x50) nm^2 was likely attributed to atomic rows of bridging oxygen on the topmost

and Si of in-plane layer, which correspond to a new finding well-ordered atomic structure, depicted in Fig 4.9 (a). The height of cross section along the solid line of this image was shown as around 0.2 nm, plausibly supporting the monolayer adsorbed silicon oxide on the subsurface of TiO_2(110)(1x1).

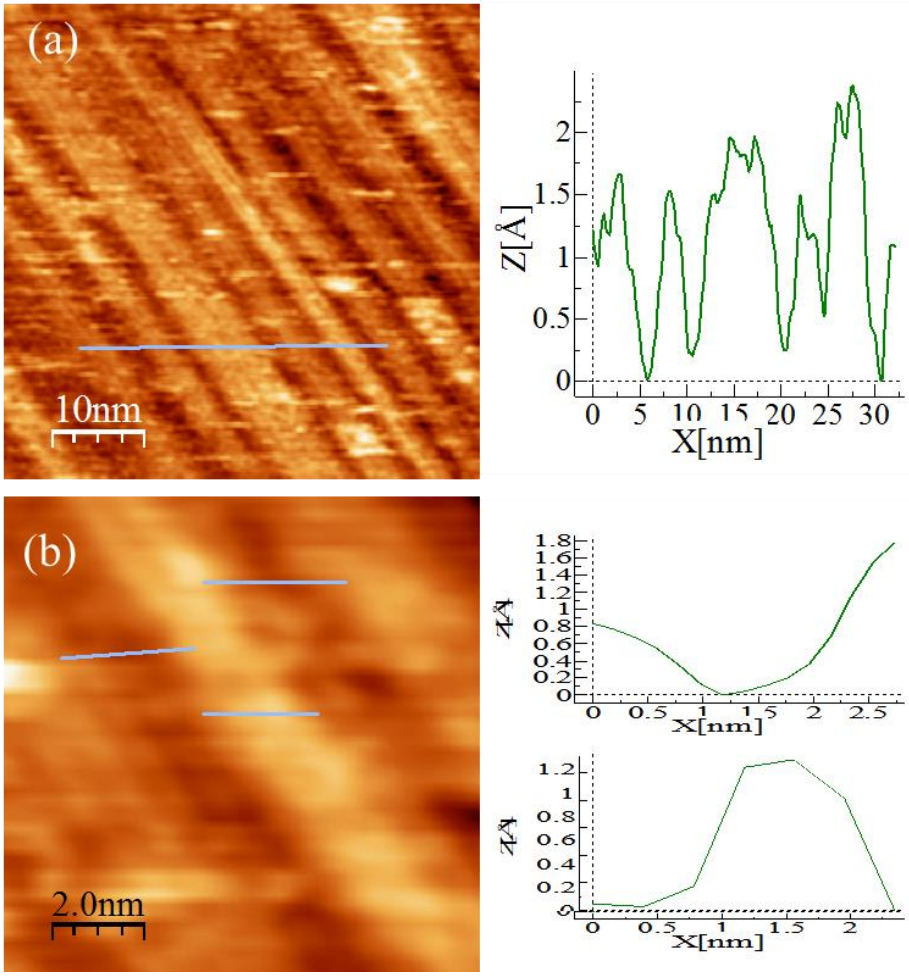

Figure 4.9: FM-AFM images and cross sections along the solid lines in the images of TiO_2(110) surfaces annealed in the quartz container for 48 hours, Δf = +248 Hz. (a) (50x50 nm^2); and (b) the zoom-up of image (a).

However, the width between rows along [001] direction was evaluated around several Angstrom. This large corrugation is not reasonably interpreted until now, but this corrugated structure may be one possibility to enhance the super-hydrophilic characteristics of SiO_2/TiO_2

system. The zoom-up image showed the rows along [001] direction with the width of around 1.2 nm, consistent to the atomic periodicity of TiO_2(110)(1x2) structure in the LEED pattern.

Thus, the stishovite SiO_2 layers are epitaxially grown as rectangular patches on the TiO_2(110) surfaces by vapor transport of the SiO_x from the quartz container. The SiO_x species diffusing on the surface are expected to be stabilized at the step edges. The step edges of the TiO_2(110) surface have the lower-coordinated Ti atoms and act as preferential growth sites for adsorbates [19, 20]

4.5 Model of structures of SiO_2 layers on rutile TiO_2(110)

Hereinafter we discuss an atomic model of the silicon oxide layer on the TiO_2(110) surface to fulfill the results obtained in this study such as the (1×2) reconstruction and the thickness. An intuitive model has been proposed, depicted in Fig. 4.10. We assume that the atomic structure of the TiO_2(110) surface before Si-O adsorption on it is the same with that of TiO_2(110)-(1×1) prepared in ultrahigh vacuum (UHV), but with the existence of perfect bridging oxygen row in the top layers (Fig. 4.10(a)). When the TiO_2 substrate is annealed in the quartz container, Si-O molecules are evaporated from the quartz container, and reach the substrate. They can interact with bridging oxygen atoms of TiO_2 as the most preferential site, as reported in ref. 10 using ab-inito density functional theory calculations for e-beam evaporation of pure Si on a rutile TiO_2(110) surface in UHV. The Si atoms are probably located over the bridging oxygen atoms even in air, as shown in Fig. 4.10(b).

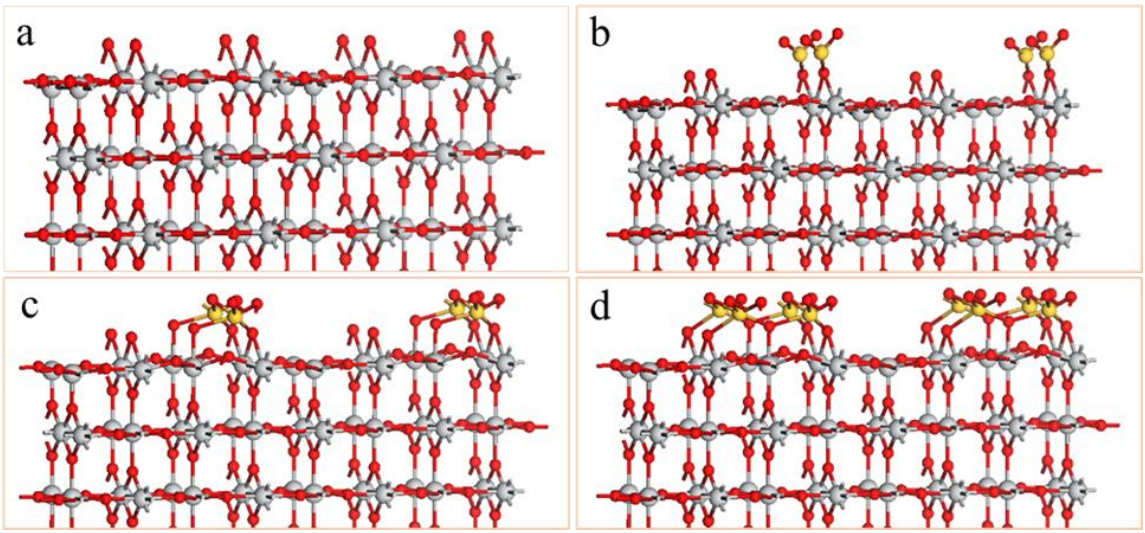

Figure 4.10: Ball and stick atomic models (a) a clean rutile TiO_2(110)-(1×1) surface. Bridging oxygen rows run along the [001] direction on the surface. (b) Si atoms adsorbed on the bridging oxygen row, on which O atoms are bound, (c) relaxed Si-O bounded to Ti atoms with additional O atoms, and forming new bridging oxygen rows above the Si atom rows, and (d) by addition of Si-O rows as to be (1×2), an intuitive model proposed in this study for the silicon oxide layer on the TiO_2(110). The atom positions and inter distances are not optimized. Grey, yellow and red balls represent Ti, Si and O atoms, respectively.

The dangling bonds of the Si atom are terminated with oxygen atoms in air at the high temperature, and the O atom tends to interact with a neighbor fivefold coordinated Ti atom on the surface, accompanied by a lateral and downward position shift of Si atom, as shown in Fig. 4.10(c). A similar preferential atomic configuration was reported for Ti interstitials on the surface of rutile TiO_2(110)-(1×1) [21]. Further silicon oxides reaching the surface also adsorb in the same way, leading to adsorption as a Si_2O_5 added row over the two bridging oxygen rows of the TiO_2. This adsorption can proceed along the bridging oxygen row of TiO_2 substrate, while connecting each other and forming a periodic structure of (1×2) as shown in

Fig. 4.10(d). The arrangement of silicon and oxygen at the top layer is compatible with the height of patch observed by FM-AFM as well as the thickness calculated in the XPS analysis. Since the density of oxygen rows similar to the structure of bridging oxygen row running along the [001] direction, including both sides of the added row, is doubled, the density of the bridging oxygen vacancy possibly increases owing to the lattice mismatch between the silicon oxide and the TiO_2, resulting in a more hydrophilic surface.

It is concluded that silicon oxide was deposited on TiO_2(110) surfaces by vapor phase heteroepitaxial process. The surface periodicity of TiO_2(110) change from (1x1) to (1x2) corresponding adsorbed silicon oxide ultra-thin layers. The existence and increase of Si peaks with annealing time in XPS spectra were consistent with the change in the number and size of patches in FM-AFM images. An atomic model of silicon oxide deposit on a TiO_2(110) surface was proposed to qualitatively elucidate the epitaxial growth of silicon oxide molecules and the change in the atomic periodicity of TiO_2(110)-(1×1) surfaces.

References

[1] A. A. Ashkarran and M. R. Mohammadizadeh, Mater. Res. Bull., 43, 2008, 522.

[2] E. Aubry, V. Demange, A. Billard, Surf. Coat. Technol., 202, 2008, 6120.

[3] P. Novotna, J. Zita, J. Krysa, V. Kalousek, J. Rathousky, Appl. Catal. B, 79, 2008, 179.

[4] A. Fujishima, X. Zhang, D. A. Tryk, Surf. Sci. Rep., 2008, 63515.

[5] A. Kafizas, S. Kellici, J. A. Darr, I. P. Parkin, J. Photochem. Photobiol. A Chem., 204, 2009, 183.

[6] F. Menga and Z. Sun, Appl. Surf. Sci., 255, 2009, 6715.

[7] Y. Taga, Thin Solid Films, 517, 2009, 3167.

[8] M. Takeuchi, K. Sakamoto, G. Martra, S. Coluccia, M. Anpo, J. Phys. Chem. B, 109, 2005, 15422.

[9] A. Sasahara, C. L. Pang, M. Tomitori, J. Phys. Chem. C, 114, 2010, 20189-20194.

[10] J. Abad, et al., *Phys. Rev. B*, 82 (165420), 2010, 1.

[11] M. Machida, K. Norimoto, T. Watanabe, K. Hashimoto, A. Fujishima, J. Mater. Sci., 34, 1999, 2569.

[12] L. Q. Wang, K. F. Ferris, P. X. Skiba, A. N. Shultz, D. R. Baer, M. H. Engelhard, Surf. Sci., 440, 1999, 60.

[13] R. P. Netterfield, P. J. Martin, C. G. Pacey, W. G. Sainty, D. R. McKenzie, G. J. Auchterlonie, J. Appl. Phys., 66, 1989, 1805.

[14] J. Finster, Surf. Inter. Anal., 12, 1988, 309-314.

[15] J. H. Scofield, J. Electron Spectrosc. Relat. Phenomena, 8, 1976, 129.

[16] S. Tanuma, C. J. Powell, D. R. Penn, Surf. Inter. Anal., 17, 1991, 927.

[17] P. Mack, R. G. White, J. Wolstenholme, T. Conard, Appl. Surf. Sci., 252, 2006, 8270.

[18] R. Nakamura et al., J. Phys. Chem. B, 109, 2005, 1648.

[19] W. T. Wallace, B. K. Min, D. W. Goodman, Topics in Catal., 34, 2005, 17.

[20] D. A. Chen, M. C. Bartelt, R. Q. Hwang, K. F. McCarty, Surf. Sci., 450, 2000, 78.

[21] K. T. Park, M. Pan, V. Meunier, E. V. Plummer, Phys. Rev. B, 75, 2007, 245415.

CHAPTER 5

WATER WETTABILITY OF SILICON OXIDE LAYERS ON RUTILE TiO_2(110)

The super-hydrophilicity of the TiO_2 surfaces is significantly valuable in photochemistry, which had already been realized in industrial applications such as self-cleaning and anti-fogging coating [1-6]. It is induced by UV light irradiation to the surface [1, 2]. The fundamental mechanism underlying this phenomenon, however, is still controversial [1-11]. Some authors have reported that TiO_2 is natively hydrophobic with a contact angle around 70^o, and the super-hydrophilicity of UV-irradiated TiO_2 surface was ascribed to the formation of defects, such as surface oxygen vacancies, that promote the dissociation of water molecules into surface OH groups, which are known to enhance the hydrophilicity [1, 2, 7-15]. Others authors reported that native hydrophilicity of TiO_2 was easily deteriorated with the adsorption of hydrocarbon contaminants, and the super-hydrophilic characteristic re-arose by photo-oxidation and decomposition of organic contaminants, leading to the reconstruction of surface OH groups [5, 6, 13-15].

However, the photo-induced superhydrophilicity of TiO_2 rapidly vanishes when the surface is stored in dark, owing to the replacement of hydroxyl groups by oxygen from air [16-19]. When considering practical aspects, a surface cannot permanently be irradiated by UV light. To overcome this drawback, TiO_2-based hyrdophilicity without UV light irradiation has been explored: the treatment of TiO_2 by air plasma [18], or mixing SiO_2 to TiO_2 is promising to extend the lifetime of the hydrophilicity in dark, which is once activated with

UV light irradiation [12, 14, 17-19]. The layers of SiO_2 on TiO_2 substrates have been fabricated using a range of different techniques, including sol-gel dip coating, evaporation induced self-assembly using dip-coating, electrochemical deposition, and ion-milling [17-19]. The mechanism of hydrophilicity of SiO_2 / TiO_2 systems from a scientific point of view, however, has not been fully elucidated.

In this chapter, we characterize the wettability of a fully oxidized TiO_2(110) surface through contact angle measurement, which helps to reveal the relation between the surface structure and the chemical reactivity. In addition, the hydrophobic/hydrophilic conversion on silicon oxide covering TiO_2 surfaces, formed by vapor phase heteroepitaxial deposition in air, is examined. The effects of UV-O_3 as well as intensive UV irradiation on wettability of these surface are also concerned. This gives us a ground for the super-hydrophilic mechanism of SiO_2/TiO_2 systems.

5.1 Water contact angle of TiO_2(110) surfaces

A home-made water contact angle (WCA) measurement system was used to assess the conversion of hydrophobicity/hydrophilicity of TiO_2(110) surface through cleaning treatment and subsequent annealing in a sapphire container. A volume of 2 μL Milli-Q water was dropped on the sample surface in all experiment in ambient condition of room temperature around 20 ^oC and humidity around 60 %. The annealed wafers were cooled in the laboratory air for 6 hours, and a droplet of 2 μL Milli-Q water was placed on horizontal surfaces. The contact angles were determined on the side-view photos.

Initially, we measured the water contact angle (WCA) to evaluate the change in wettability of the TiO_2 surface after cleaning processes. The WCA of an as-received TiO_2(110) surface was about 59°, as shown in Fig. 5.1(a). After acetone washing, the WCA became about 45°, and subsequently about 23° after HF treatment, as depicted in Fig. 5.1(b)-(c), respectively. The WCAs of sample after acetone, HF, and UV-O_3 cleaning process were below 10 º.

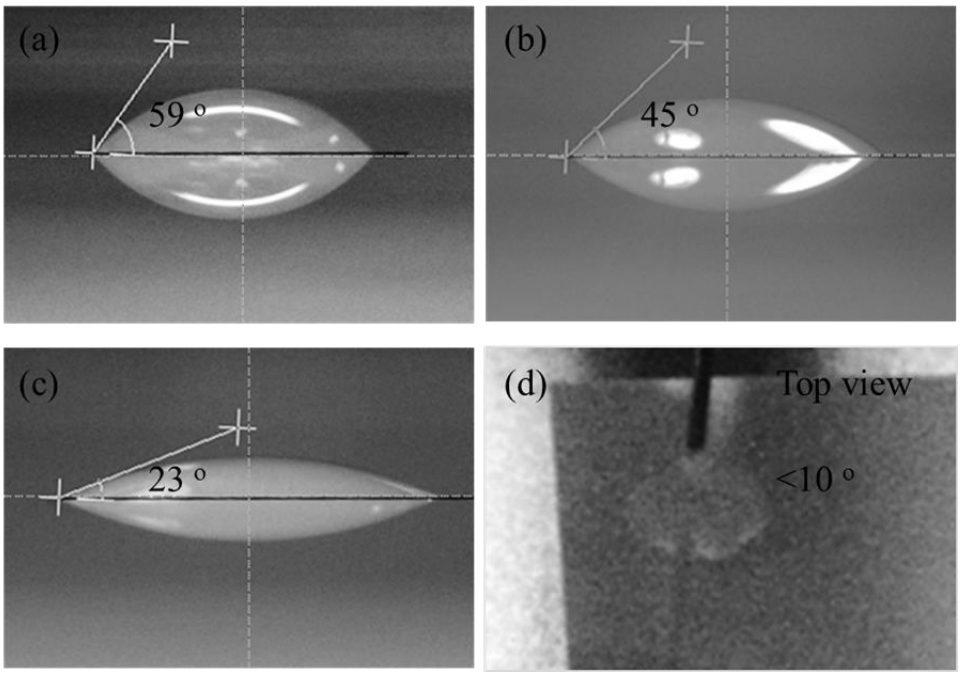

Figure 5.1: WCA measurements of TiO_2(110) surfaces (a) as-received, (b) after acetone cleaning, (c) after acetone and HF treatment, and (d) after acetone, HF and UV-O_3 cleaning(almost top-view).

The as-received sample was probably contaminated with hydrocarbons and other impurities, which were partly removed by the following treatments. According to literature on the hydrophilicity of TiO_2(110) [2, 4, 6, 13, 16, 20, 21] the oxygen vacancies play an important role to provide the super-hydrophilicity under UV light. The HF etching may increase the

number of oxygen vacancies on the surface. After the UV irradiation, however, the TiO_2 surface, was gradually covered with hydrocarbon contamination in ambient, which interacted with oxygen vacancies during experiment. The hydrophilic characteristic of TiO_2 surface in Fig. 5.1(d) was regarded as the hydrocarbon removing effect of UV-O_3.

Fig. 5.2(a)-(c) show the photos of WCA measurements for that annealed at 1000 ^oC in the sapphire container for 6 hours without and with UV-O_3 cleaning as well as intensive UV irradiation. It is noted that the WCA became about 32° for that annealed in the sapphire container after the HF treatment.

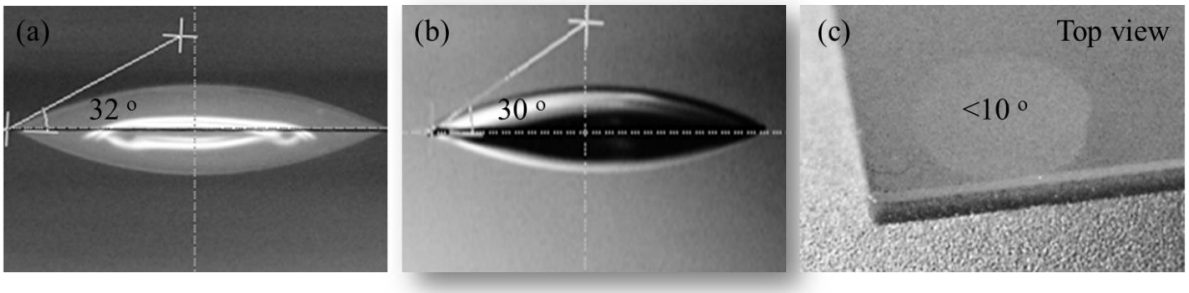

Figure 5.2: WCA measurements of annealed TiO_2(110) surfaces in sapphire container at 1000 ^oC for 6 hours (a)without any treatment more, (b) and UV-O_3 treatment for 1.5 hours, and (c) intensive UV irradiation for 2 minutes.

We firstly tried to treat it by UV-ozone cleaning, because the surface might be covered with hydrocarbons during the annealing and cooling process until the WCA measurement was carried out. However, the WCA of the TiO_2 surface did not change after the UV-ozone cleaning. This implies that the surface after annealed in the sapphire container was not covered perceptibly with hydrocarbons, while it exhibited less hydrophilic. It is likely that the TiO_2 surface annealed in the sapphire container in air is nearly free from bridging oxygen

vacancy. This is agreement with the explanation of interaction between water molecules and TiO_2(110) surfaces. It was reported there are two possibilities for molecules water adsorb on TiO_2(110) surface, one is fivefold coordinated (5f) titanium cation, and another is bridging oxygen anion. Water molecules preferably adsorbed and dissociated to form hydroxyls at bridging oxygen rows in reduced surface with the existence of oxygen vacancies. In contrary, water molecules tend to interact with (5f) titanium rows of fully oxidized surfaces with stoichiometric structure. Different from (100) faces, in rutile TiO_2(110) surface, the distance between bridging oxygen sites and binding sites of water (five-coordinate Ti^{4+} site) is too large to form hydrogen bonding interactions with water that might facilitate O-H bond dissociation [21, 23]. Adsorption of water on rutile (110) is molecular on the stoichiometric surface, leading to a less hydrophilic TiO_2(110) surface. Meanwhile, after the same surface was exposed to intensive UV light (UV source, OMRON) for 2 minutes, Milli-Q water exhibited a contact angle below 10 ^{o} on it. This indicates that UV illumination generates surface defects that are accompanied with electronic charge transfer from oxygen to titanium [24, 25]. As results, the binding energy of titanium decreases, while the binding energy of oxygen increases [26]. Water molecules, therefore, preferably adsorb at oxygen vacancy sites, and dissociate to form hydroxyl group in a hydrophilic manner.

It is plausible that the fully oxidized TiO_2(110) surface, annealed in the sapphire container in atmosphere condition, is nearly free from oxygen vacancy, and more stable with hydrocarbon impurities compared to UHV-annealed ones. This result is consistent with the report of Nakamura et al. using AFM analysis [27]. With its prominent photo-catalytic characteristics, the intense UV irradiation converted it from hydrophobic to hydrophilic. The super-hydrophilicity of TiO_2 surfaces, however, gradually disappeared when UV light turned

off. From these results, SiO_2/TiO_2 water wettability was discussed as one of the supplement candidates for improvement of super-hydrophilicity without UV irradiation. This resulted stimulated the interest in understanding and characterizing the surface wettability, which helps to reveal the relation between wettability and surface structure of SiO_2/TiO_2 systems.

5.2 Water contact angle of silicon oxide layers on rutile TiO_2(110)

Hereinafter we discuss about the hydrophobic/hydrophilic conversion of SiO_2/TiO_2 surface with increasing deposition of silicon oxide. The epitaxially added silicon oxide layer on rutile TiO_2(110) were fabricated in ambient condition, using the quartz container as a silicon oxide vapor source. Fig. 5.3(a)-(d) shows the pictures of the water droplets on the TiO_2(110) surfaces annealed in the quartz container.

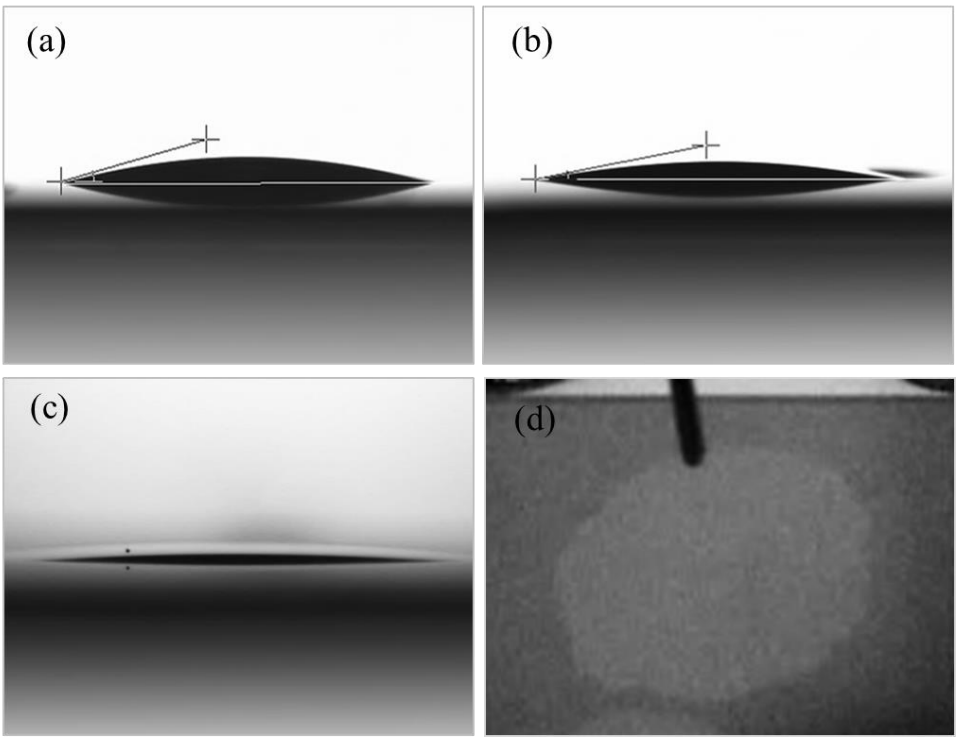

Figure 5.3: WCA measurements of annealed TiO_2(110) surfaces in the quartz container. (a) for 6 hours, (b) for 24 hours, (c) for 48 hours, and (d) for 72 hours(almost top-view).

The WCA was initially 16^{o} for 6-hour annealing, corresponding to the existence of patches grown at the step lines in the FM-AFM image as shown in previous chapter. It is noted that at the same annealing time the WCA of the same surfaces annealed in the quartz container was much smaller than that annealed in the sapphire container. It was plausible that the adsorbed silicon oxide patches changed the wettability of TiO_2(110) surfaces. The WCA of SiO_2/TiO_2 surface moderately decreased with increasing annealing time.

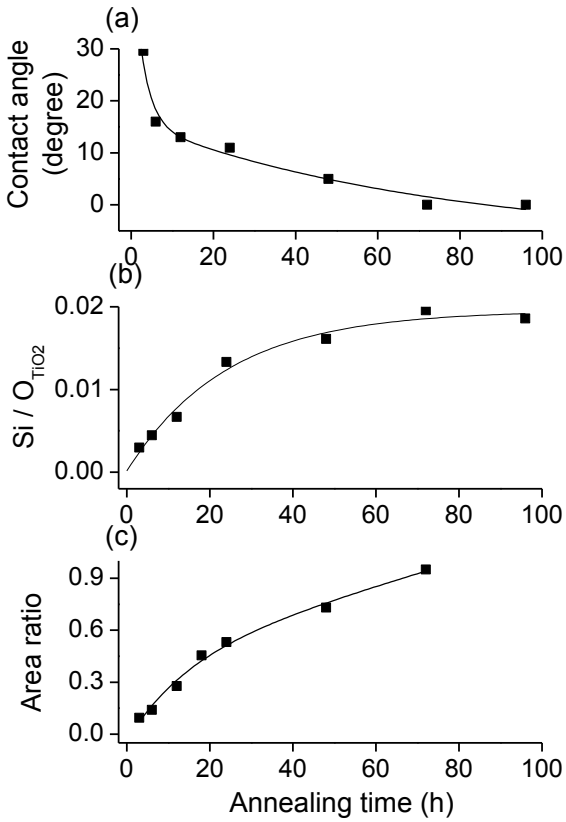

Figure 5.4: Plots of WCA, patch area ratio observed in the AFM images, and XPS atom ratio of Si/O_{TiO2} versus the annealing time.

The water contact angles after 6, 24, and 48, annealing were respectively 16°, 11°, and 5°. Ultimately it approached to 0° after 72-hour annealing in the quartz container, shown in a top-view photo of Fig. 5.3 (d); it is the super-hydrophilicity. Fig. 5.4 shows the dependence of the

water contact angles, the Si/O_{TiO2} XPS atom ratio, and the coverage of the patches on the annealing time. The water contact angles decreased with the increase of the Si/O_{TiO2} atom ratio and the coverage of the patches. The surface became super-hydrophilic after the annealing for 72 hours and above. The hydrophilicity of the surface obviously arises from the stishovite SiO_2 layer, and the stishovite SiO_2 monolayer exhibits super-hydrophilicity. The hydrophilicity is attributed to the OH groups observed in the XPS spectra in Fig. 4.5(c). Thus, the change in surface compositions and long range atomic periodicity are likely the origin of its wettability variation.

A comparison with the bulk SiO_2 surface and the SiO_2-free TiO_2 surface highlights the high wettability of the stishovite SiO_2 monolayer. Fig. 5.5 shows the pictures of the water droplets on the fused SiO_2 surfaces. The WCA of an as-received fused SiO_2 glass plate was 54º, changed to 39º after acetone washing. It was 10° after the HF treatment as shown in Fig. 5.5(b), and increased to 37° after subsequent annealing in the quartz container as shown in Fig. 5.5(c).

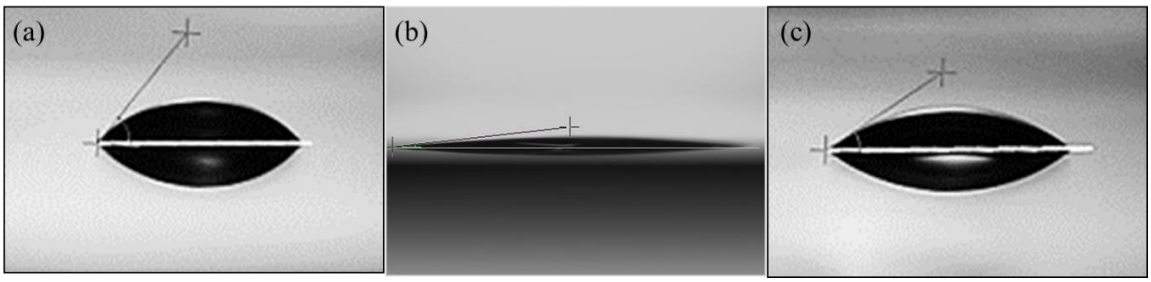

Figure 5.5: WCA measurements of a fused SiO_2 glass plate. (a) as-received, (b) after cleaning with acetone and HF, and (c) after annealed in the quartz container at 1000 °C for 6 hours.

The super-hydrophilicity after the HF treatment is attributed to the increase of silanol groups (-Si-OH) on the top layer of fused SiO_2 glass. When a crystalline quartz surface is fully

hydroxylated, a number of water molecules are able to adsorb by means of hydrogen bonding [17, 19, 22]. On the other hand, after annealed in the quartz container at 1000 ^{o}C for 6 hours, the wettability of a fused SiO_2 glass surface changed from high hydrophilic at a WCA less than 10^{o} to less hydrophilic at a WCA of 37^{o}. This is consistent with experimental results for annealing at higher temperatures than 600 °C in Ref. 22. For crystalline quartz, there are two dehydroxilation processes of the loss of physisorbed water at increasing temperatures, and of the formation of siloxane bonds (-Si-O-Si-) that exhibit hydrophobic. The configuration of siloxane is similar to the bridging oxygen row (-Ti-O-Ti-) on the rutile TiO_2(110), probably leading to the water wettability less hydrophilic than that on the surface covered with hydroxyl groups (-Ti-OH), which are incorporated into the site of bridging oxygen vacancy.

For our experimental results, in spite of the siloxane formation on the fused or crystalline SiO_2 surface annealed over 600 °C, the silicon oxide overlayers on the rutile TiO_2(110)-(1×1) surface exhibited super-hydrophilicity when the annealing time reached 72 hours or more. The acid site derived by the Si-O-Ti linkage is a candidate to explain the increase of the OH groups on the stishovite SiO_2 layer. The positively charged Si-O bonds give rise to Lewis acid sites that promote the molecular and dissociative adsorption of H_2O molecules [30]. Because the SiO_2 is a monolayer, a large number of the acidic sites are exposed to the top surface. For more experimental evidence, the pictures of droplet on rutile TiO_2(110) and SiO_2/TiO_2 surface were observed with two other liquids: Ethylene-glycol, and Diiodo-methane. For SiO_2/TiO_2 surface, while the droplets of two polar liquids (water, Ethylene-glycol) show 0^{o}, it is 29^{o} with Diiodo-methane, a non-polar liquid. Meanwhile, contact angle of water is 32^{o}, of ethylene glycol is 32.5 ^{o}, and of diiodomethane is 30 ^{o} on TiO_2 surface. Following van Oss, Good, and Chaudhury the work of adhesion, W_A, is split

into two components. The Lifshitz-van der Waals (W_A^{LW}) term accounts for van der Waals-London (dispersive), Keesom, and Debye types of interactions. The acid-base (W_A^{AB}) term includes the contribution of Lewis-type acid-base interactions across the interface, including hydrogen bonding. Assuming that nonpolar liquid (diiodomethane) takes a key role to detect the W_A^{LW} component, while polar one (water, or ethylene glycol) is sensitive with W_A^{AB} component. It is obviously only the acid-base term of adhesion work, estimated through contact angles of water and ethylene glycol droplet, dramatically changed with the existence of SiO_2 monolayer, owing the increase of interfacial charge transfer.

Another possible cause of the high density of the OH groups is the surface O vacancies that act as the dissociation sites for H_2O molecules. The bond length of Si-O in the stishovite is 0.18 nm [20, 28-30], which is 9 % smaller than that of Ti-O in the rutile TiO_2. In order to reduce the mismatch between the top most silicon oxide layer and the subsurface of TiO_2, the silicon oxide tends to distort with the relaxation of the top most layer. This mismatch can increase the number of oxygen vacancies where easily accommodate hydroxyl groups forming silanol groups, which strongly interact with the water molecules via hydrogen bonding, leading to enhancement of hydrophilicity [22].

5.3 Ultraviolet irradiation effect on water wettability

As mentioned above, the differences arise from structural variations in relation with hydrophobic/hydrophilic conversion induced by silicon oxide deposition. For more understanding, photo-regenerated super-hydrophilicity was also examined in the container of TiO_2(110) annealed in the sapphire container comparing with SiO_2/TiO_2 surfaces, annealed in the quartz container with varying time. The OMRON, ZUV-C20H system with ZUV-L8H

lens was used as a UV source. The UV illumination power was around 400 mW/cm^2 when the working distance (the distance from cross section of lens to sample) was fixed at 45 mm with a beam diameter of 25 mm. The WCA of these surfaces was examined immediately after each UV irradiation processes. The WCA change of annealed TiO_2 in the sapphire container for 6 hours as well as ones in the quartz container for different time depends on UV irradiation time, depicted in Fig. 5.6. Previously, the WCA of annealed TiO_2(110) surface in the sapphire container did not change much under UV-O_3 cleaning process with power of 15 mW/cm^2 for 1.5 hours. However, it moderately changed under high-intensity UV irradiation. The WCA changed from 32^o to 22^o after 30 seconds UV irradiation, subsequently at 12^o, and finally it shown to 0^o with 150 seconds. It is possibly deduced that UV-O_3 removes almost hydrocarbon contaminations on the TiO_2 surface, while the high intensity UV irradiation took a key role in forming surface oxygen vacancies, which were created through an redox of TiO_2 ($Ti^{4+} + e^- \rightarrow Ti^{3+}$ and $2O^{2-} + 2h^+ \rightarrow O^2$) induced by photo-generated electron-hole pairs. Surface oxygen vacancies can then be saturated by OH groups, which yields a super-hydrophilic surface. The WCA of TiO_2(110) annealed in the quartz container with different time was also affected by intensive UV irradiation. Depending on the initial WCA of each sample, it took from 30 to 90 seconds UV illumination to get super-hydrophilic. The change to super-hydrophilicity of SiO_2/TiO_2 surfaces under UV irradiation is plausibly attributed to the oxygen vacancies formed due to the mismatch between the monolayer SiO_2 and the subsurface of TiO_2. The hydrocarbon possibly adsorbed on these vacancies in ambient was removed by UV light, then water on the top most layer of surface was dissociated to derive the super-hydrophilictity.

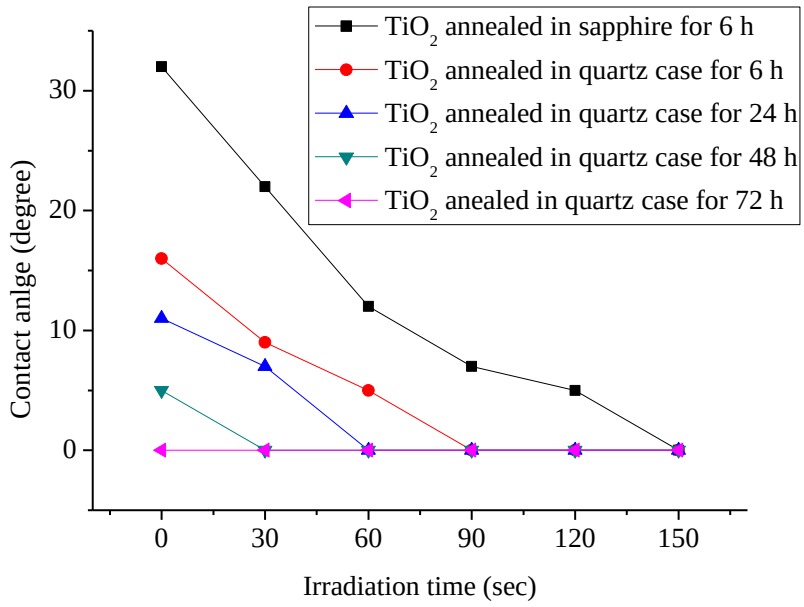

Figure 5.6: The WCA variation versus UV irradiation time of annealed TiO_2(110) at 1000 ^oC in the sapphire container for 6 hours, and in the quartz container at 1000 °C for 6 hours, 24 hours, 48 hours, and 72 hours .

The photo-generated super-hydrophilicity was also elucidated by the photo-catalytic reaction of sub-surface TiO_2 through tunnel effect, permitting the interfacial charge transfer between photo-exited TiO_2 and adsorbates [31]. For comparison, the WCA change of fused SiO_2 after cleaning (un-annealed) and annealing processes under UV irradiation was evaluated, as shown in Fig. 5.7. While the non-annealed SiO_2 under ambient condition with silanol (Si-OH) on the top most layer transit from less hydrophobic to super-hydrophilic under high intensity UV illumination, the wettability of annealed SiO_2 with siloxane in the top most layer nearly unchanged. The former phenomenon plausible deduced that intensive UV irradiation can remove completely hydrocarbon contaminants, which formed in silanol-base surface in ambient. Subsequently, SiO_2 surface shows native hydrophilicity [32].

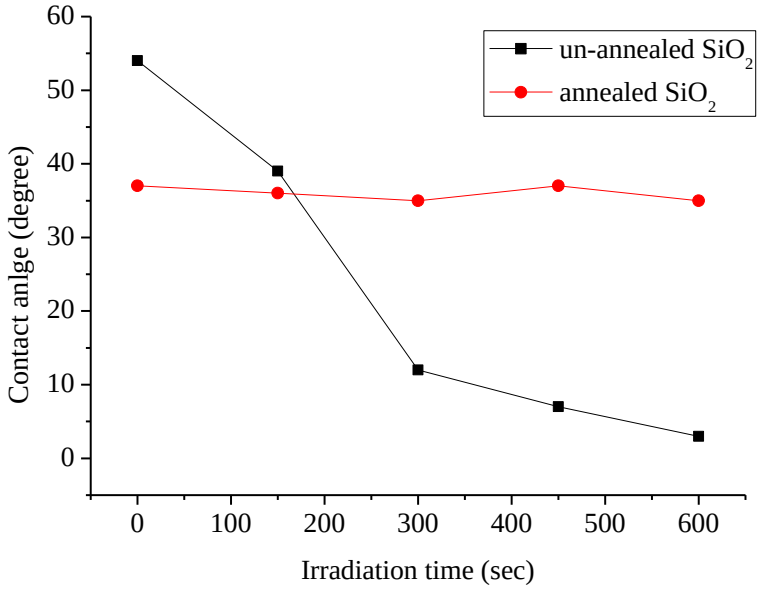

Figure 5.7: The WCA variation versus UV irradiation time of non-annealed SiO_2 in ambient condition and annealed SiO_2 at 1000 ^oC in the quartz container.

Whereas the latter was consistent with that in several studies in literature, indicated the inertness with contaminations and non-photocatalytic activity of dehydroxylated SiO_2 surfaces. It is noted that the UV irradiating time for change SiO_2 surface to super-hydrophilic was much more than that one of TiO_2.

It is likely reported despite the inertness with UV light of annealed SiO_2, the super-hydrophilicity of SiO_2/ TiO_2 surfaces could be approached from photo- catalytic activity of subsurface TiO_2. Another possibility for interpretation of SiO_2/ TiO_2 surfaces in this case is the stishovite (rutile –like) structure of SiO_2 monolayer, which probably formed during epitaxial silicon oxide deposition. Since the density of oxygen rows similar to the structure of bridging oxygen row running along $[1\bar{1}0]$ direction, including both sides of added rows, is

doubled, the density of vacancies at bridging oxygen site possibly increase through mismatch reducing process, resulting in more hydrophilic surfaces.

Consequently, the durability of TiO_2(110), SiO_2/TiO_2 with different composition ratios, and fused SiO_2 surfaces in dark-environment was examined as one of the most significant characteristics for self-cleaning applications. No one has doubted about advantage of photo-catalyst as well as photo-induced wettability of TiO_2 surface. Nevertheless, it was noted that the super-hydrophilicity of TiO_2 surface roughly dismissed under less or without UV light conditions. Through this mention, the change in WCA of TiO_2(110) surface versus keeping time in relationship with UV irradiation was analyzed, as depicted in Fig. 5.8. The WCA of annealed TiO_2(110) in the sapphire container change from 32 ^{o} to 46 ^{o} for 24 hours.

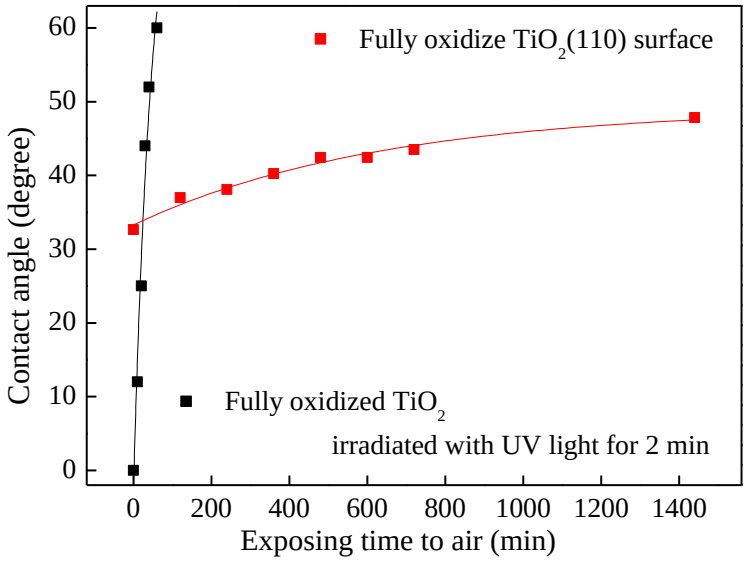

Figure 5.8: The WCA variation versus exposing time of annealed TiO_2 at 1000 ^oC in sapphire container without and with UV irradiation.

In the same sample after irradiated high intensity UV light for 150 seconds, the photo-induced super-hydrophilicity transited to WCA of 60 ^{o} only for 60 minutes. The fully oxidized surface with negligible defects of annealed TiO_2(110) surface in air has been possibly reason for much less hydrocarbon could be adsorbed on original surface. Thus, the conversion hydrophobic/ hydrophilic of this TiO_2 surface lightly occurred. The high intensity UV light has been recognized not only removing hydrocarbon contaminations but also possibly breaking bridging oxygen bonds in the top most layer of TiO_2(110) surface. The super-hydrophilicity of this TiO_2 surface, which is proportional to the number of oxygen vacancies then roughly changed to hydrophobic due to either absorption of organic contaminants or by the release of water molecules, which can be due to adsorption of oxygen molecules. That is the reason why UV irradiated TiO_2 surface easily dismissed its hydrophilic in dark place.

We examined the WCA change of different SiO_2/ TiO_2 surfaces which stored in a dark place in order to evaluate the maintenance of super-hydrophilicity of SiO_2/TiO_2 surfaces in comparison with intrinsic stoichiometric TiO_2(110). After UV illumination, all of surfaces shown super-hydrophilic with WCA of 0 ^{o}. These sample was stored in dark condition of experimental room, and estimated WCA at every two hours. Fig. 5.9 illustrated the variation of wettability of annealed TiO_2 surfaces in quartz container in different time versus exposing time.

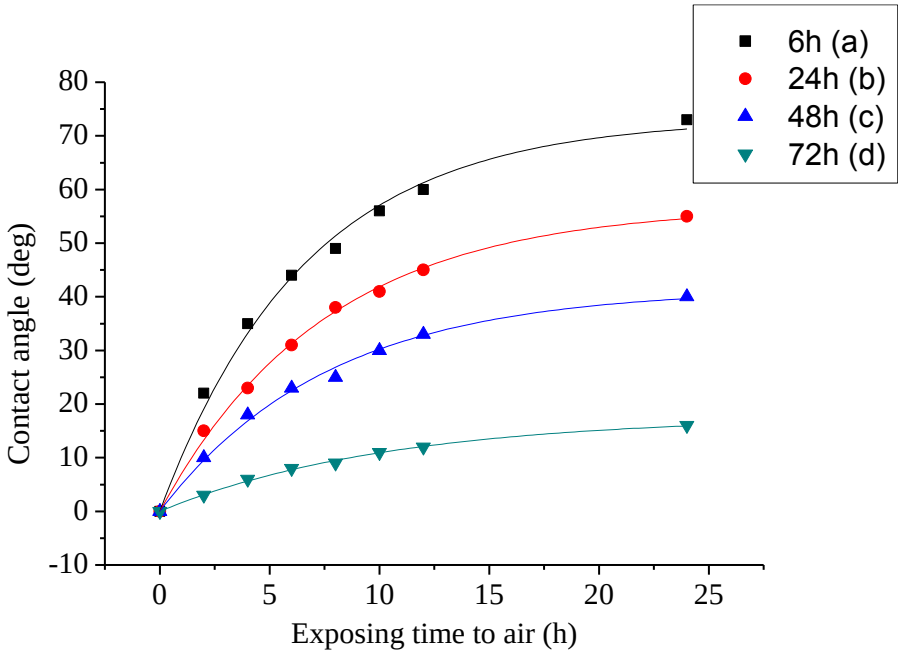

Figure 5.9: The WCA variation versus exposing time after UV irradiation of air-annealed TiO_2 at 1000 ^oC in quartz container (a) for 6 hours, (b) for 24 hours, (c) for 48 hours, and (d) for 72 hours.

The rate of hydrophilic/hydrophobic conversion qualitative decreased with increasing annealing time. Ultimately, for 72 hours annealing, surface displayed the most durable in hydrophilicity, as evidenced by the slightly WCA change from 0^o to 16^o. This is possibly interpreted as the photo-generated electrons in the interfaces of TiO_2 and SiO_2 tend to reduce the Ti^{4+} cations to the Ti^{3+} cations, and the photo-generated holes transmit through the SiO_2 monolayer to uppermost surface. Once going up to the surface, they can dissociate adsorbed water and produce hydroxyl group, which make the hydrophilic surface. It was noticed that the bonding energy of Si-OH bonds is thought to be more stable than that in Ti-OH [34]. The stable hydroxyl groups on the surface can result in the increasing of super-hydrophilcity and the capability of holding absorbed water.

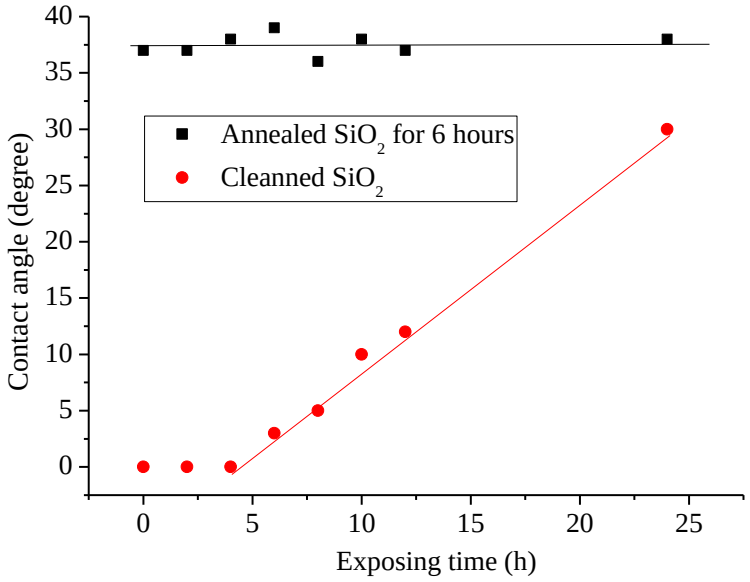

Figure 5.10: The WCA variation versus exposing time after UV irradiation of cleaned fused SiO_2 and annealed SiO_2 at 1000 ^oC in the quartz container for 6 hours.

It likely means that the opportunity for hydrocarbon to adsorb on these surfaces is lower, yielding the improvement of hydrophilicity and persistence of SiO_2/TiO_2 surface stored in dark places.

The change of wettability of fused SiO_2 before and after annealing at 1000 ^oC in the quartz container, as illustrated in Fig. 5.10, supplemented the stand view of hydrophobic/hydrophilic conversion of based TiO_2 surfaces. No change of WCA for SiO_2 annealed during 24 hours likely indicated the difficulty of de-hydroxylation of silica surface at room condition, which is consistent to ref. 22. In the meantime, the WCA of non-annealed SiO_2 surface increased through exposing time in air condition. While the stability of annealed SiO_2 surface was plausible due to the existence of siloxane groups on the top most, the non-annealed SiO_2 with silanol groups in protrusion could be removed by high intensity UV illumination, and formed oxygen vacancies, which are the favorable sites for hydrocarbon to adsorb in ambient, yielding less hydrophilic. Qualitatively, it is also noted that the rate of

hydrophilic/hydrophobic conversion of fused SiO_2 is higher than that of 72 hours annealed SiO_2/TiO_2 surface. It is possible that the adsorbed SiO_2 monolayer on $TiO_2(110)$ enhances the ability to maintain the hydrophilicity of annealed TiO_2 in dark place for a long time.

In conclusion, the annealed $TiO_2(110)$ surface in air, fully oxidized stoichiometric surfaces, displayed native less hydrophilicity with WCA of 32^o. This characteristics different from UHV-annealed (reduced) TiO_2 surfaces, in which the number of oxygen vacancies could not be neglected. Due to photo-catalytic nature, the $TiO_2(110)$ surfaces was also strongly affected by UV irradiation, showing super-hydrophilicity. As the same as many studies in literature, the hydrophilicity quickly disappears when those are stored in dark. The composite SiO_2/TiO_2 surfaces, formed in vapor phase epitaxial deposition in air, displayed more hydrophilic, especially for 72 hours annealing, the SiO_2/TiO_2 surface showed super-hydrophilicity without UV illumination. The change to super-hydrophilicity corresponds to the saturated Si peak height in XPS analysis, the atomic periodicity transition from (1x1) to (1x2) in LEED pattern, and the rectangular formation of silicon oxide along the [001] direction on the subsurface $TiO_2(110)$ as shown in FM-AFM image. This combination of SiO_2/TiO_2 also overcomes the hydrophobicity of annealed SiO_2, due to the formation of siloxane groups. Moreover, the ability of SiO_2/TiO_2 to maintain hydrophilicity was recognized better than that of annealed $TiO_2(110)$ surfaces in air. It was plausible attributed to the hardness and durability of top most silicon oxide layer as well as the maintenance of photo-catalytic of sub-surface $TiO_2(110)$ surface. The atomic model of SiO_2/TiO_2 surface was proposed to elucidate the relation between the change in geometric and electronic characteristics and the hydrophobic/hydrophilic conversion of SiO_2/TiO_2 system.

References

[1] R. Wang, K. Hashimoto, and A. Fujishima, Nature 388, 1997,431.

[2] R. Wang, K. Hashimoto, and A. Fujishima, Adv. Mater. 10, 1998, 135.

[3] K. Hashimoto, H. Irie, and A. Fujishima, Jpn. J. Appl. Phys. 44, 2005, 8269.

[4] A. Fujishima, X. Zhang, and D. A. Tryk, Surf. Sci. Rep., 369, 2008, 63.

[5] T. L. Thompson and J. T. Yates, Jr., Chem. Rev., 106, 2006, 4428.

[6] J. T. Yates, Jr., Surf. Sci., 603, 2009, 1605.

[7] R. Wang, N. Sakai, A. Fujishima, T. Watanabe, and K. Hashimoto, J. Phys. Chem. B, 103, 1999, 2188.

[8] N. Sakai, R. Wang, A. Fujishima, T. Watanabe, and K. Hashimoto, Langmuir, 14, 1998, 5918.

[9] N. Sakai, A. Fujishima, T. Watanabe, and K. Hashimoto, J. Phys. Chem. B, 107, 2003, 1028.

[10] R.-D. Sun, A. Nakajima, A. Fujishima, T. Watanabe, and K. Hashimoto, J. Phys. Chem. B 105, 2001, 1984.

[11] T. Shibata, H. Irie, D. A. Tryk, and K. Hashimoto, Phys. Chem. Chem. Phys. 12, 2010, 7911.

[12] K. Takahashi and H. Yui, J. Phys. Chem. C 113, 2009, 20322.

[13] J. M. White, J. Szanyi, and M. A. Henderson, J. Phys. Chem. B 107, 2003, 9029.

[14] T. Zubkov, D. Stahl, T. L. Thompson, D. Panayotov, O. Diwald, and J. T. Yates, Jr., J. Phys. Chem. B 109, 2005, 15454.

[15] N. Ohtsu, N. Masahashi, Y. Mizukoshi, and K. Wagatsuma, Langmuir 25, 2009, 11586.

[16] N. Ishida, D. Fujita, J. Vac. Sci. Technol. A, 30, 2012, 051402.

[17] M. Machida, K. Norimoto, T. Watanabe, K. Hashimoto, A. Fujishima, J. Mater. Sci., 34, 1999, 2569.

[18] K. Gan, B. Lu, Y. Yin, Sur. & Coat. Tech., 173, 2003, 219.

[19] M. Jarn, Q. Xu, M. Linden, Langmuir, 26, 13, 2010, 11330.

[20] L. Q.Wang, K. F. Ferris, P. X. Skiba, A. N. Shultz, D. R. Baer, M. H. Engelhard, Surf. Sci., 440, 1999, 60.

[21] M. A. Henderson, Langmuir, 12, 1996, 5093.

[22] E. F. Vansant, P. Van der Voort, K. C. Vrancken, Elsevier, Amsterdam, 93, 1995, 59.

[23] V. E. Henrich, G. Dresselhaus, and H. J. Zeiger, Solid State Commun. 24, 1977, 623.

[24] J. G. Highfield, M. J. Gratzel, J. Phys. Chem., 92, 1988, 464.

[25] W. J. Lo, Y. W. Chung, G. A. Somorjai, Surf. Sci., 302, 1994, 329.

[26] W. Gopel, J. A. Anderson, D. Frankel, M. Jaehnig, K. Philips, J. A. Schafer, G. Rocker, Suf. Sci., 139, 1984, 333.

[27] R. Nakamura et al., J. Phys. Chem. B, 109, 2005, 5.

[28] A. Sasahara, C. P. Pang, M. Tomitori, M.; J. Phys. Chem. C, 114, 2010, 20189.

[29] J. Abad, et al., Phys. Rev. B, 82, 2010, 165420.

[30] J. Finster, Surf. Inter. Anal., 12, 1988, 309.

[31] H. Tada, Y. Kubo, M. Akazawa, S. Ito, Langmuir, 14, 1998, 2936.

[32] K. Kajihara et al., Nucl. Instr. And Meth. In Phys. Res. B 218, 2004, 323.

[33] A. Kanta, R. Seved, J. Ralston, Langmuir, 21, 2005, 2400.

[34] M. Nakamura, M. Kobayashi, N. Kuzuya, T. Komatsu, T. Mochizuka, Thin solid films, 502, 2006, 121.

CHAPTER 6

SUMMARY

6.1 Conclusion

In this study, we demonstrated to distinctly fabricate a fully oxidized TiO_2(110)-(1x1) surface and ultra-thin layers of SiO_2 heteroepitaxially grown on a rutile TiO_2(110) surface by annealing in air in different containers, in which the substrate was stored. Their structures and characteristics were analyzed at a nano-scale, and the surface wettability was examined; the correlations between them were discussed to disclose the fascinating properties of titanium dioxide and silicon dioxide composite systems.

First of all, the substrate of a rutile TiO_2(110) wafer was stored in a sapphire container and annealed in air at 1000 °C using a conventional electric furnace after chemically cleaned, resulting in a fully oxidized rutile TiO_2(110)-(1x1) surface. So far, intricate methods, which comprise Ar ion sputtering, annealing in UHV, and re-annealing in oxygen gas, had been conducted to prepare the oxidized surface. On the other hand, our air-annealed method is simple, and a sharp Ti 2p peak in XPS spectra as well as a (1x1) well-ordered LEED pattern can be obtained routinely, indicating that the surface is well-ordered and almost free from vacancies at bridging oxygen sites. In addition, FM-AFM images visualized flat wide terraces with steps running along the $[1\bar{1}0]$ direction with a step height of about 0.3 nm, corresponding to a single step height of the rutile TiO_2(110).

Subsequently, silicon oxide ultra-thin layers were heteroepitaxially grown on a rutile TiO_2(110) surface by vapor phase transport in a quartz container annealed in air, and

characterized using XPS, LEED, FM-AFM operated in water, and water contact angle measurement. The surfaces exhibited patch structures with a (1×2) reconstruction. The layer grew in a self-limited mode at 1000 °C, evidenced by the saturation of the Si/O_{TiO2} XPS peak intensity ratio with deposition time. The surface periodicity changed to a long-range order twice as the primitive unit cell to the $[1\bar{1}0]$ direction as well as prominent features of rectangular patches. The patches partially overlapped and elongated along the [001] direction, and the step height was about 0.2 nm, corresponding to the growth of SiO_2 monolayer. A surface fully covered with the patch layer exhibited super-hydrophilicity without UV light irradiation, while the surface without the layer was less hydrophilic.

Composite SiO_2/TiO_2 materials with hardness and durability of the topmost silicon dioxide layer and with the photocatalytic characteristics of titanium dioxide have the potential to maintain their super-hydrophilicity in dark place for long time. From the results obtained in this study, it is noted that high intensity UV irradiation changed the wettability of fully oxidized and SiO_2 monolayer covered TiO_2(110)-(1x1) surfaces to be super-hydrophilic at different levels. These phenomena were explained by the change of oxygen coordination at the top most layer; oxygen vacancies at bridging oxygen rows accommodate OH groups vertically standing to the surface, leading to super-hydrophilicity, while the less hydrophilicity is brought by the bridging oxygen row without the vacancies, the structure of which is similar to siloxane groups (-O-Si-O-Si-) formed on the SiO_2 annealed in air at 1000 °C.

The atomic structure of the silicon oxide layer was discussed based on the rutile structure of a silicon oxide, that is, stishovite. A model was proposed that the silicon oxide with the stishovite structure is formed as a Si_2O_5 added row over two bridging oxygen rows

of the TiO_2, leading to the periodic structure of (1×2). The density of the bridging oxygen vacancy possibly increases owing to the lattice mismatch between the structures of silicon oxide and the TiO_2, resulting in a more hydrophilic surface.

This study showed the potential of conventional hetero-epitaxial growth of oxides by vapor phase transport in air, and shed light on the mechanism of super-hydrophilicity utilized in commercial products such as anti-fog mirrors of SiO_2-TiO_2 hybrid materials.

6.2 Future prospects

Through this study of a fully oxidized rutile TiO_2(110) surface, and silicon oxide layers on the TiO_2 surfaces using nanoscale analysis together with macro-scale water contact angle measurement, several future prospects and challenging issues are summarized here:

More precise evaluation and understanding of the bridging oxygen sites are necessary to utilize their useful characterization, which are responsible for photocatalytic properties and hydrophilicity, including photo-induced super-hydrophilicity. To reveal the atomic structure of the bridging oxygen row in air and rationalize the proposed model, further elaborated visualization methods are needed. In principle, spectroscopic characterizations and first principle calculation for electronic structures using ultraviolet photoelectron, UV/vis spectroscopies, and for hydroxyl group utilizing infrared spectroscopy will be useful methods. The FM-AFM imaging is also one of the candidates, but the atomic resolution power and stable operation in air should be achieved.

The preparation method used here to form epitaxially grown oxide layers has the potential to the application for other oxide systems. The vapor phase of oxides in air or oxygen

gas environment at high temperatures has advantageous points to remove the contaminants covering the substrate and maintain the surface fully oxidized, though the disadvantageous on the high temperature processes at the substrate. One way to be tried is to separately heat the substrate and the vapor source at different temperatures in a capsulated container. Note that the care should be taken on the vapor from the container.

Research achievement

Paper:

1. Le Tran Uyen Tu, Akira Sasahara, Masahiko Tomitori, Water Wettability of an Ultra-Thin Layer of Silicon Oxide Epitaxial Growth on a Rutile Titanium Dioxide (110) Surface, Journal of Physical Chemistry C, In the press, Publication Date (Web): September 19, 2013, DOI: 10.1021/jp403601m.

2. Le Tran Uyen Tu, Akira Sasahara, Masahiko Tomitori, Photo-induced super-hydrophilicity of a monolayer of SiO_2 epitaxially grown on a rutile TiO_2(110) surface. In preparation.

Conference:

1. Le Tran Uyen Tu, Akira Sasahara, Masahiko Tomitori, AFM and XPS analysis of ultra-thin SiO_2 vapor-deposited rutile TiO_2(110) surfaces with improving hydrophilicity. Oral presentation, in 第32回表面科学学術講演会, Sendai, Nov. 20, 2012.

2. Le Tran Uyen Tu, Akira Sasahara, Masahiko Tomitori, Ultra-thin SiO2 epitaxial heterogeneous growth on rutile TiO_2(110) surfaces with improving hydrophilicity. Oral presentation, in The 60th Japan Society of Applied Physics Spring Meeting 2013, Kanagawa, Mar. 27, 2013.